MINIATURIZING MICROSTRIP PATCH ANTENNAS BY SLOT LOADING

By

Hung Tien Nguyen

A thesis

Submitted to the Faculty of Graduate Studies

in partial fulfillment of the requirement for the degree of

MASTER OF SCIENCE

Department of Electrical and Computer Engineering

The University of Manitoba

THE UNIVERSITY OF MANITOBA

FACULTY OF GRADUATE STUDIES

*****

COPYRIGHT PERMISSION

MINIATURIZING MICROSTRIP PATCH ANTENNAS BY SLOT LOADING

BY

Hung Tien Nguyen

A Thesis/Practicum submitted to the Faculty of Graduate Studies of The University of Manitoba in partial fulfillment of the requirement of the degree

OF

MASTER OF SCIENCE

Table of Contents

Acknowledgements

First and foremost, I would like to express my thankfulness and gratitude to my advisor Professor L. Shafai for his wise advice, valuable guidance, support and continuous encouragement through out the development of this thesis. Without his guidance and support, I would not have been able to complete this thesis project.

In addition, I also would like to thank Professor S. Noghanian for her valuable advice during my research in the master program and serving as a member on my committee.

Special thanks to Ms. S. Girardin, she has made me feel very welcome with her kind smile and willingness to help whenever I shown up at her office to ask for her help. An extended thank to Mr. B. Tabachnick for his patient cooperation while performing experimental measurements.

I also would like to express my appreciation to Professor R. Thomas for serving on my committee.

Finally but not the least, I would like to thank my parents for their great continuous support and encouragement during my study.

Abstract

The demand for low profile, portable and compact size high frequency systems, has increased interest in miniature antennas. The slots loading of microstrip patch antennas for miniaturization is studied in this thesis. These antennas are very compact in size and can perform circular polarization; moreover, wider impedance bandwidth is also achieved. At first, the Koch Island fractal shape is applied to the square patch antenna, which results in reduction of its resonant frequency. The top and bottom slots of the Koch Island patch were removed to create the H-shaped patch, which has a similar resonant frequency. Then the effect of the slot sizes of the H-shaped patch on its resonant frequency is examined. To reduce the resonant frequency of the H-shaped patch further, more slots are embedded in the patch. Furthermore, using 100Ω impedance probe feed will overcome the sensitivity of feed location of these miniaturized antennas. The Koch Island patch antenna then is modified to obtain circular polarization. In order to improve the narrow impedance bandwidth of the miniaturized antennas, slots are loaded on the ground plane. The antenna bandwidth is increased dramatically by using the H-shaped ground plane for linear polarized antennas and Koch Island ground plane for circularly polarized antennas.

List of Figures

List of Tables

Chapter 1

Introduction

Mobile and wireless communications are becoming increasingly important and popular in our lives, and there has been tremendous growth in their applications such as mobile phone, GPS, remote controls, wireless internet, etc. Antennas are an essential part of the wireless communications and make the connection possible. However, the conventional antennas have been too large and sometimes considered as the main impediment in design of small and portable wireless devices. Therefore, the demand for low profile, portable and compact size high frequency systems, has increased interest in miniature antennas.

1.1 Purpose of the Thesis

The purpose of this thesis is to study miniaturized microstrip antennas by slot loading method, which may be used for wireless communication. The conventional antennas are usually considered as the bulky part of wireless communication devices. The microstrip antennas have seemed to meet the requirements for small and low profile antennas, and have been useful in some mobile communications such as radar, missiles guiding systems and telemetry. However, the conventional microstrip patch antennas are still too large for certain applications such as GPS, laptop wireless cards or cell phones. Therefore, miniaturized microstrip patch antennas are greatly desirable in such devices.

To radiate electromagnetic waves from a conventional microstrip patch antenna at a certain frequency, the length of the patch must be about half of its wavelength or larger. There are a number of techniques that can be used to make the microstrip patches smaller

than their conventional sizes. These techniques include using shorts, dielectric loading, lumped element loading, or changing the geometry of antennas. However, the performance of these modified antennas is usually reduced, in terms of the impedance bandwidth, gain, efficiency and sometimes the purity of polarization. This thesis will be dealing with the last technique of size reduction, i.e. changing the antenna geometry.

In this thesis, certain parts of the conducting patch material are removed, so that the surface currents will be redirected to flow a longer path. This will lead to miniaturization of the conventional microstrip patch antennas. However, the miniaturization also means reducing their impedance bandwidth and gain. This thesis will show that if certain parts of the microstrip patch ground plane are removed, its bandwidth will increase. This thesis will not deal with techniques for improving the gain of the miniaturized antennas.

1.2 Organization of the Thesis

This thesis is divided into five chapters. Chapter one gives the objective of the thesis and also delivers an introduction and background of microstrip antennas. In addition, a survey of different techniques to miniaturize microstrip antennas will be provided.

Chapter two provides a detailed study of the miniaturized microstrip antennas by using the slot loading. The effects of various sizes and shapes of the slots on the antenna resonance frequencies, impedance bandwidth and gain will be investigated. Specifically, the effect of the Koch Island, H-shaped and its modifications, on these parameters will be studied. The simulation and experimental results of several slot loaded microstrip

antennas will be given. Furthermore, the Yagi microstrip antennas, using the rectangular, H-shaped and Koch Island patch shapes will also be studied.

Chapter three will be dealing with the circular polarization of the modified Koch Island microstrip antenna. The effects of various lengths and widths of the slots on modified Koch Island patches will be examined.

Chapter four will study a bandwidth enhancement technique, by using the slot loadings in the ground plane. Specifically, the simulation results on impedance bandwidth and gain of the H-shaped and Koch Island ground plane antennas will be provided.

Chapter five will conclude the finding of the thesis and discuss the future work.

1.3 Microstrip Antennas

The first idea of microstrip antennas was introduced in 1953 by Deschamps, but its utilization only started in design from after 1970. The fundamental microstrip antenna contains a conducting patch printed on a thin, grounded dielectric substrate [1]. The patch can be fed by a coaxial probe, transmission line or an aperture coupling. Although the radiating patch can be in various sizes and shapes, the most commonly used are the rectangular (or square) and circular shapes. Below in Fig. 1.1 is the configuration of a conventional rectangular microstrip patch antenna with a coaxial probe feed.

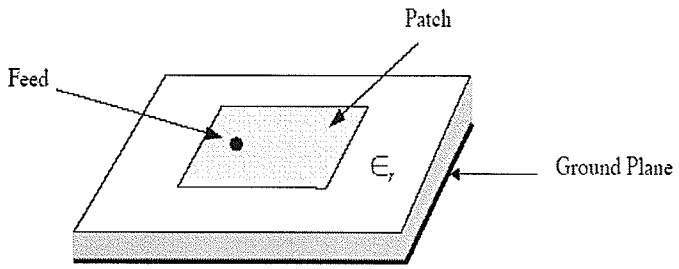

Fig. 1.1: Rectangular microstrip patch antenna with coaxial probe feed [3]

There are a number of parameters that need to be taken into account when designing a rectangular microstrip antenna. Fig. 1.2 shows the parameteric layout of a rectangular microstrip antenna.

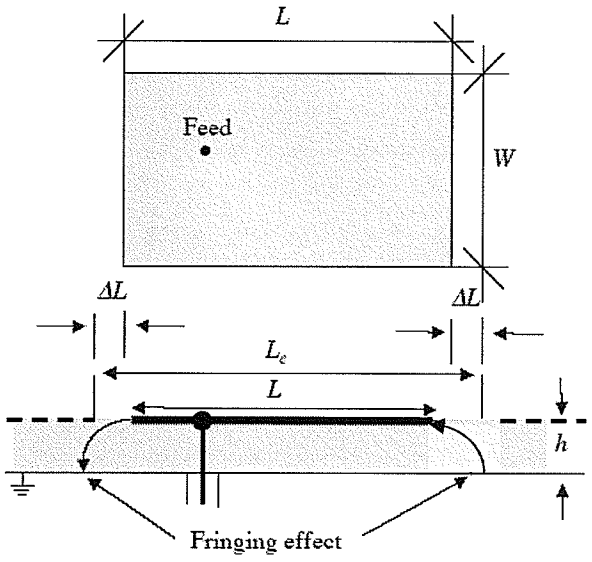

Fig. 1.2: Parameters of a rectangular microstrip antenna [3]

Due to the fringing effects at the open ends of the patch, the patch length appears to be longer than its actual length. To accommodate the fringing effect, small equivalent

lengths ΔL's are added to both ends of the patch, which gives the effective length of the patch as:

$$L_{eff} = L + 2\Delta L \tag{1.1}$$

Thus, the first resonant frequency occurs when the effective length, L_{eff}, of the patch is equal to half of the wavelength in dielectric, λ_d.

$$L_{eff} = \frac{\lambda_d}{2} = \frac{\lambda_0}{2\sqrt{\varepsilon_{eff}}} \tag{1.2}$$

where λ_0 is the wavelength in free space and ε_{eff} is the effective dielectric constant. The effective dielectric constant ε_{eff} is introduced to accommodate the fact that the fringing fields propagate in both dielectric and the air at the patch ends. However, only a small portion of the fringing fields propagates in the air at the patch ends. Therefore, the effective dielectric constant is not very much different from the relative dielectric constant of the substrate, ε_r. The ε_{eff} can be calculated by the following expression [3]:

$$\varepsilon_{eff} = \frac{\varepsilon_r + 1}{2} + \frac{\varepsilon_r - 1}{2}\left(1 + \frac{10h}{W}\right)^{-\frac{1}{2}} \tag{1.3}$$

where h is the height of the substrate and W is the physical width of the patch. The additional length ΔL can be approximately calculated by using the following equation[6]:

$$\Delta L = 0.412h\frac{\left(\varepsilon_{eff} + 0.3\right)\left(\frac{L}{h} + 0.264\right)}{\left(\varepsilon_{eff} - 0.258\right)\left(\frac{L}{h} + 0.8\right)} \tag{1.4}$$

Hence, the first resonant frequency f_{res} is given by:

$$f_{res} = \frac{C}{\lambda_d\sqrt{\varepsilon_{eff}}} = \frac{C}{2L_{eff}\sqrt{\varepsilon_{eff}}} = \frac{C}{2(L + 2\Delta L)\sqrt{\varepsilon_{eff}}} \tag{1.5}$$

An important parameter needing to be known for antennas is the impedance bandwidth of the antennas, BW, which is defined in [2] as the following expression:

$$BW = \frac{VSWR - 1}{Q_t \sqrt{VSWR}} \tag{1.6}$$

where $VSWR$ is the voltage standing wave ratio, which is defined as the ratio of the maximum to minimum of the standing wave voltage, due to the antenna input mismatch. Q_t is the total quality factor representing the losses in the microstrip antenna and is given by:

$$\frac{1}{Q_t} = \frac{1}{Q_{rad}} + \frac{1}{Q_{cu}} + \frac{1}{Q_{di}} + \frac{1}{Q_{sw}} \tag{1.7}$$

where Q_{rad}, Q_{cu}, Q_{sw} and Q_{di} are the quality factors due to radiation loss, conductor loss, surface wave loss and the dielectric loss, respectively.

The far field radiation patterns are the most important parameters of the antenna needing to be specified. In reference [3], the far field expressions for rectangular microstrip antennas are given by using the cavity model representation [3]:

$$E_\theta = \left[\frac{jkWV_0}{\pi} \frac{e^{-jkr}}{r} e^{j(X+Y+Z)} \right] \left[\cos X \frac{\sin Y}{Y} \right] \cos\phi \tag{1.8}$$

$$E_\phi = \left[-\frac{jkWV_0}{\pi} \frac{e^{-jkr}}{r} e^{j(X+Y+Z)} \right] \left[\cos X \frac{\sin Y}{Y} \right] \cos\theta \sin\phi \tag{1.9}$$

in which,

$$Y = \frac{kW}{2} \sin\theta \sin\phi$$

$$X = \frac{kL_{eff}}{2} \sin\theta \cos\phi$$

$$Z = \frac{kh}{2}\cos\theta$$

where V_o is the applied voltage at the feed,

E_θ, E_ϕ are the electric fields in the spherical co-ordinates,

θ and ϕ are elevation and azimuth angles in spherical co-ordinate system,

$k = \omega\sqrt{\mu_0\varepsilon_0}$ is the wave number in the free space,

h is the height of the substrate,

L and W are the length and width of the rectangular patch,

and L_{eff} is the effective length of the rectangular patch, which can be determined by using equations (1.4) at the beginning of this section.

The directivity, D, of the rectangular microstrip patch antennas is given in [6] as follow:

$$D = \frac{\frac{1}{2}\mathrm{Re}\left(E_\theta H_\phi^* - E_\phi H_\theta^*\right)_{\theta=0}}{\frac{P_r}{4\pi r^2}} = \frac{\frac{r^2}{2\eta_0}\left(\left|E_\theta\right|^2 + \left|E_\phi\right|^2\right)_{\theta=0}}{\frac{P_r}{4\pi}} \qquad (1.10)$$

The above equation (1.10) can be simplified by using approximation as below:

$$D \cong \frac{4(kW)^2}{\pi\eta_o G_r} \qquad (1.11)$$

H_θ^*, H_ϕ^* are the complex conjugate of magnetic fields in spherical co-ordinates,

P_r is the radiated power,

W is the width of the rectangular patch,

G_r is the radiation conductance,

and η_o is the free space intrinsic impedance,

The gain, G, of the antennas can be defined as

$$G = e_r D \tag{1.12}$$

where e_r is the radiation efficiency of the antennas

Microstrip antennas have shown a lot of advantages [5] such as low profile, light weight, capabiity of being made conformal to the host surface and having both linear and circular polarizations. However, microstrip antennas have suffered from some disadvantages in comparison to traditional antennas, which are narrow bandwidth, low gain and low power-handling capability. Although conventional microstrip antennas are considered small in volume, they are still too large for some application in personal mobile communication. Therefore, the need for miniaturized and in particular, microstrip antennas has arisen. However, miniaturization means lower gain and narrower bandwidth. The following section will give a brief overview of antenna miniaturization techniques.

1.4 Miniaturized Antennas

"The art of antenna miniaturization is an art of compromise: one has to design the smallest possible antenna that is still suitable for a given application with regard to its radiation characteristics." A. K. Skrivervik [7].

For some applications, the conventional half wavelength antennas can be considered too large. Therefore, interest in research on miniaturized antennas, small antennas that operate in smaller sizes than the conventional half wavelength antennas, has increased during recent years. Hirasawa [8] has stated the definition of small antennas as: "A miniaturized antenna can be defined as one which, for a given frequency, has its linear dimension smaller compared to a similar type of conventional antenna operating at the same frequency". Researchers have proposed several techniques to miniaturize the conventional antennas such as lumped element loaded antennas, antennas loaded with materials, using ground planes and short circuits and modifying antenna geometry [7].

1.4.1 Limitations of Antennas Miniaturization

Miniaturizing an antenna will change its radiation characteristics such as impedance bandwidth, gain efficiency, and polarization purity in some cases [7]. As defined in section 1.3, the bandwidth of antennas is dependent on the quality factor Q_t, which associates with losses of antennas. Thus, higher Q_t means a lower impedance bandwidth. The quality factor of a small antenna can be determined by the following expression [7]:

$$Q_t \cong \frac{1}{(ka)^3} + \frac{1}{ka} \tag{1.13}$$

where k is the wave number and a is the radius of the smallest sphere enclosing the antenna. Miniaturizing the antenna leads to reducing its radius a, which means increasing the quality factor Q. Thus, the fractional bandwidth, FBW, of antenna is decreased due to the following equation:

$$FBW = \frac{\Delta f}{f_0} = \frac{1}{Q} \tag{1.14}$$

There is a very useful and simple formula, which gives a maximum gain that a small antenna can achieve, while still having a reasonable bandwidth [7].

$$G = (ka)^2 + 2ka \tag{1.15}$$

Therefore, reducing the antenna size, decreasing the radius of the enclosing sphere, means lowering its possible peak gain.

When an antenna is miniaturized, there will be a higher surface current density toward one point. Therefore, the antenna efficiency will be decreased as a result of the increased ohmic losses. Moreover, the high density of currents toward one point can increase the cross-polarization of an antenna in some cases.

The last limitation of small antennas is the difficulty in finding a correct feed location. Miniaturizing an antenna makes it closer to a balance structure than an unbalanced one, so a correct feeding method will be an issue from the manufacturing point of view.

1.4.2 Miniaturization Techniques

As stated at the beginning of this section, there are four commonly used techniques to miniaturize an antenna. They are lumped element loaded antennas, antennas loaded with materials, using ground planes and short circuits, and modifying the antenna geometry.

Lumped element loaded antennas is the simplest and most immediate method to make antennas smaller than the resonant size, but still keeping its resonant features. A small antenna has strong reactive input impedance, which can be compensated by loading the antenna with lumped elements. Lumped elements can be resistive, capacitive or inductive components. However, lumped element loading will reduce the antenna radiation efficiency, if the added element has losses. Moreover, if the losses are small, the increments in the antenna quality factor will result in decreasing the impedance bandwidth. Fig. 1.3 shows two different types of lumped element loaded antennas:

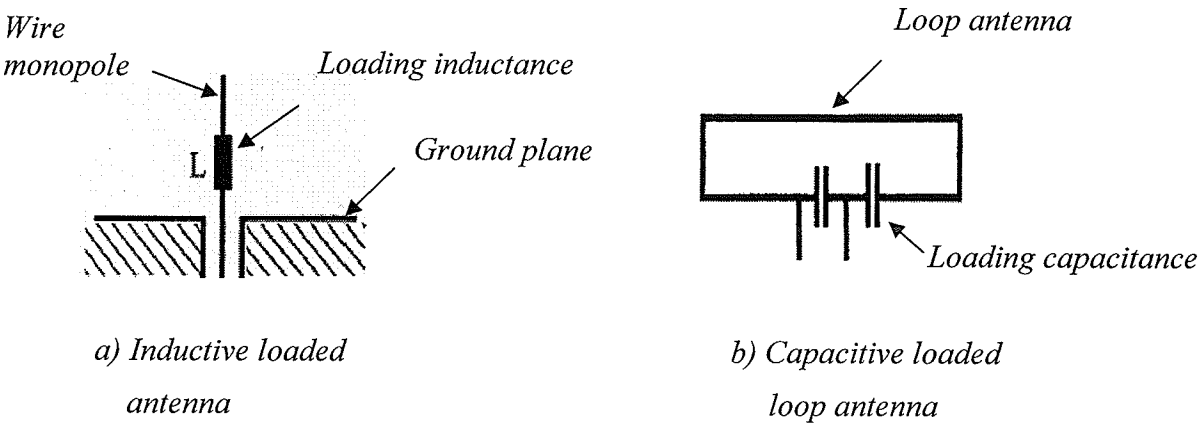

a) Inductive loaded antenna

b) Capacitive loaded loop antenna

Fig. 1.3: Lumped element loading technique [7]

Antenna loaded with materials is the technique that modifies the dielectric or magnetic characteristics of the material surrounding the antennas. In this technique, the wavelength becomes shorter in the higher permittivity material, so the half wave length antennas will be smaller. This loading technique still reduces the bandwidth of the antenna due to the increase in quality factor, under the assumption that there are no added losses. However, electric fields find it more difficult to escape from the high permittivity material. Hence, it is much harder for the antenna to radiate into free space. In addition,

the higher permittivity material leads to a lower gain due to higher dielectric losses. Nevertheless, gain reduction can be compensated for by loading antennas with a superstrate, with the trade off of further bandwidth reduction [9]. Fig. 1.4 shows an example of a material loaded monopole antenna.

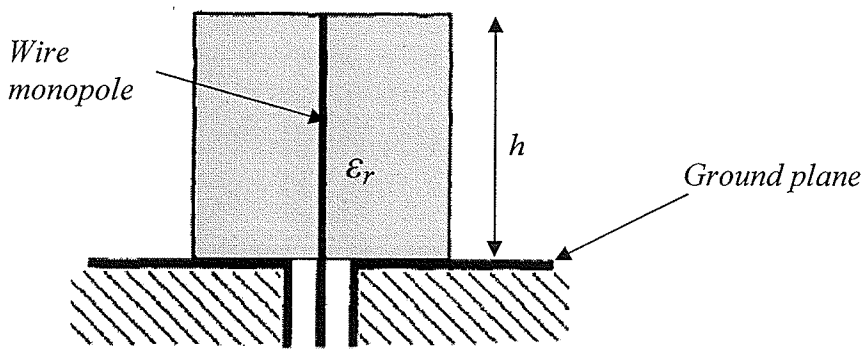

Fig. 1.4: Dielectric loaded monopole [7]

The height h of the loaded monopole will be given as follows:

$$\frac{\lambda_0}{4} \succ h \succ \frac{\lambda_0}{4\sqrt{\varepsilon_r \mu_r}}$$

where λ_o is the wavelength in free space; ε_r and μ_r are relative permittivity and permeability of the loaded dielectric, respectively.

The use of ground planes and short circuits is the most popular technique for miniaturizing the antennas. The principle of this technique is very similar in comparison between a monopole and a dipole antenna. The dipole resonates when its length is approximately half a wavelength. The dipole dimension can be reduced by a half, if one of the dipole arms is replaced by a ground plane, which creates a virtual dipole arm. This

principle can be applied to microstrip antennas by adding short circuits to the ground plane from the patch. For example, inserting a short circuiting strip to the ground at the middle of the patch can reduce patch size by half. Fig. 1.5 shows an example of size reduction using a short circuiting strip.

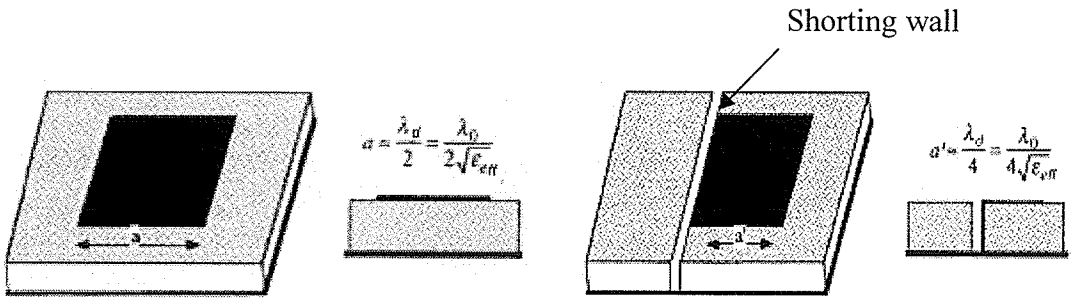

a) Un-shorted microstrip patch *b) Shorted microstrip patch*

Fig. 1.5: An example of short circuiting microstrip antenna [7]

There are some limitations of the above shorted quarter wavelength microstrip antenna. It has a lower gain and efficiency in comparison to the regular un-shorted patch antenna because of its smaller size of radiating element. Other limitations are a narrower bandwidth and difficulty in feeding, due to the high input impedance at its radiating edge.

The patch antenna can be further reduced in size by short-circuiting a portion of the zero potential plane [8]. As shown in Fig. 1.6, the surface currents flow longer paths as the short circuiting strip become smaller. In practice, shorting pins will be used instead of shorting plate.

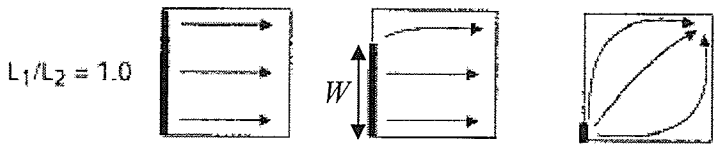

$W = L_1$ $L_1/2<W<L_1$ $W<< L_1$

Fig. 1.6: Variation of surface current flows due to the short circuit plate width (W) variation. L_1 and L_2 are two sides of the shorted patch. [7]

Modifying antennas geometry is a technique that is used to meander the surface current, so that it will flow a longer path. This technique will be used throughout the thesis to miniaturize microstrip patch antennas. A well-known example of this technique is the inverted-L antenna, which can be produced by bending the monopole antenna. Adding a short circuit to the inverted-L antennas will lead to another well-known inverted-F antenna [7]. Fig. 1.7 shows the derivation of above antennas:

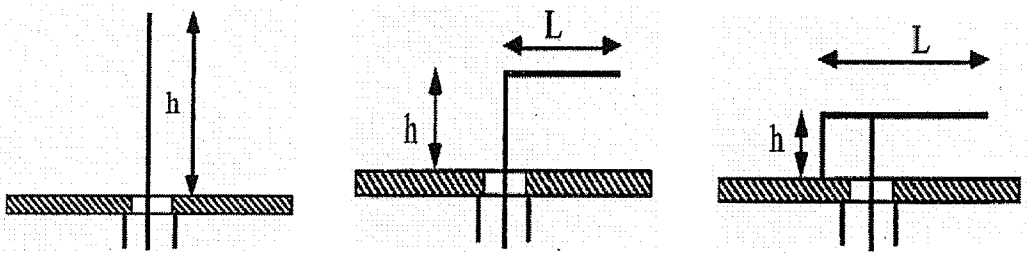

(a) *(b)* *(c)*

Fig. 1.7: a) The monopole antenna, length: $h\approx\lambda_o/4$; (b) the inverted-L antenna, with $h+L\approx\lambda_o/4$; and (c) the inverted-F antenna with $h+L\approx\lambda_o/4$

where λ_o is the free space wavelength [7]

A popular method of miniaturized microstrip antennas is using slot loading of the patch, in order to force the surface currents flow into longer paths. Therefore, the antenna

can operate at lower resonant frequencies. An example of the effect of the slot loading in microstrip antennas is shown in Fig. 1.8 below.

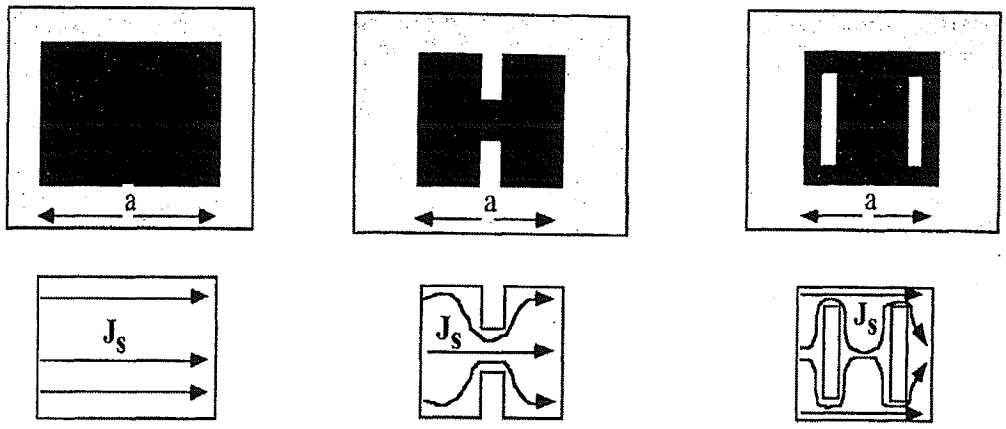

a) Regular patch *b) Patch with notches* *c) Patch with slots*

$a=\lambda_d/2$ $a<\lambda_d/2$ $a<\lambda_d/2$

Fig. 1.8: The effect of slots and notches in a microstrip patch antenna.

λ_d is the wavelength in dielectric [7]

Slot loading of the ground plane of a microstrip antenna also leads to miniaturization, based on the same concept of lengthening the current flow paths. In some cases, the ground slot loading will enhance the impedance bandwidth of the antenna.

1.4.3 Circular Polarization of Microstrip Antennas

There are many applications that require circular polarization antennas such as GPS (Global Positioning System) and mobile phones. The microstrip antenna is a good candidate for such operations. Therefore, it is a good idea to combine both circular polarization and miniaturization of a single microstrip antenna. The circular polarization of microstrip antenna can be achieved by exciting two orthogonal polarizations, which are equal in amplitude but in phase quadrature. It can use either single or dual feed techniques. However, circular polarization microstrip patch antennas suffer from similar

limitations as miniaturized antennas. The limitations are narrow bandwidth and low gain. Therefore, combining both circular polarization and miniaturization on a single microstrip antenna can push those limitations further up, especially bandwidth reduction. Therefore, the demand for bandwidth enhancement in circularly polarized and miniaturized microstrip antennas has occurred.

1.4.4 Bandwidth Enhancement of Miniaturized Microstrip Antennas

There are continuous efforts to overcome the bandwidth limitation of miniaturized microstrip antennas. Some techniques that can be used are increasing the substrate height, chip-resistor loading, using stacked shorted patches, or slot loading of the ground plane [10]. However, each technique has its limitations and trade offs. When raising the substrate height, a longer probe feed will increase the reactance of the antenna, which can cause impedance mismatch. On the other hand, higher losses in the chip-resistor loading technique will affect the quality factor. Stacked shorted patches will also cause the increment in the overall volume of the antenna. The slot loading of the ground plane seems to be a good candidate for both miniaturization and bandwidth enhancement. However, it will affect the overall gain of the antenna. The last technique of bandwidth enhancement will be used to improve the bandwidth limitation of slot loaded microstrip antennas in this thesis.

1.5 Summary

In this chapter, the important design parameters of the simple microstrip patch antennas have been presented. A review of several techniques of antennas miniaturization was also given in details. It also discusses briefly the circularly polarized microstrip antennas and the impedance bandwidth enhancement techniques. The following chapters will give the details of the parametric studies for the slot loading of the microstrip patch antennas for the purpose of miniaturization.

Chapter 2

Slot Loading of Microstrip Antennas for Miniaturization

Slot loading of the patch can reduce the microstrip patch antenna size. One of the methods is the slot loading with fractal shape. The theoretical limitations, however, affect the degree of size reduction. In this chapter, the Koch Island shape slot loading technique is used to design a microstrip antenna for the resonant frequency reduction. The resulting shape is a conventional square patch, with fractal shaped slots removed from its periphery. To understand the effects of these fractal slots, the slots are removed and the resonance frequency is recalculated. Then, the patch is reshaped by introduction of new slots to reduce its resonant frequency further. A novel fractal shaped microstrip patch is introduced, which reduces the resonance frequency to below 60% of that of a square patch. In the process, the input impedance becomes sensitive to the feed location, which is investigated for different slot loaded patch configurations.

2.1 Introduction

The demand for low profile, portable and compact size high frequency systems, has increased interest in miniature antennas. There are different approaches to meet specifications of small size antennas. Recently, in one approach several designs combining fractal geometry and electromagnetic theory have been proposed [11] – [17].

A fractal antenna is a subset of fractal electrodynamics, where electromagnetic theory is applied to fractal geometry in order to create a new class of radiation, propagation and scattering problems. The term *fractal*, which means broken or irregular

fragments, was originally coined by Mandelbrot [18] to describe a family of complex shapes that possess an inherent self-similar or self-affinity in their geometrical structure. Moreover, fractal geometry is a superset of Euclidian geometry, so the geometry based fractal antenna theory is a superset of classical (Euclidian geometry) antenna theory.

2.2 Microstrip Antennas Miniaturization by Fractal Shapes

In reference [12], Koch fractal geometry was applied to microstrip patch antennas to reduce their overall size. This is accomplished by increasing its electrical length, which lowers its resonance frequency, in comparison to conventional type patch antennas. This provides a reduction of mutual coupling between array elements. The Koch island patch is constructed by forming a polygon with a Koch curve at each side of the patch. In [12], a Koch island was constructed from the patch by applying a series of five affine transformations (IFS) to each side of the patch. The curve is characterized by two factors: iteration factor and iteration number. The iteration factor controls the shape of the curve at each time IFS is applied and iteration number controls the number of times IFS is applied to the curve. In [12], it was shown that the antenna resonance frequency doesn't reduce much, after the first iteration.

In this chapter, an extensive parametric study is performed to understand the effect of fractal shape on size reduction of the patch antenna, and the effects of its feed location. A new fractal shape patch is introduced which provides further size reductions.

2.2.1 The Effects of the Slots on Koch Island Microstrip Antenna

A study on the reduction of resonant frequency for Koch Island microstrip antennas has been presented in [12]. It has shown that bigger slot dimensions will reduce the resonant frequency further. In this section, the effects of each slot on the frequency reduction of Koch island fractal microstrip antenna will be investigated. By investigating the Koch Island patch, it was found that the top and bottom slots of the Koch Island patches do not contribute to the frequency reduction. Therefore, mostly frequency reduction was contributed by two slots on the sides of the Koch Island antenna.

In the above studies, a 65.33mm square patch with a substrate thickness of 1.6 mm and relative permittivity of 2.2 has been used. The coaxial probe feed method is used to excite the patches. For the zeroth iteration (square patch), position of the probe is 10 mm from centre of the patch and for the first iteration, it is 6 mm. Figs. 2.1(a) and (b) show the original patch and Koch island patch, after the first iteration with the ratio of 0.25, respectively. Figs. 2.1(c) – (d) show two H-shaped patches, with different slot dimensions. Fig. 2.2 shows the corresponding radiation patterns in the E- and H-planes and their return losses. All antennas are on an infinite ground plane. Table 2.1 summarizes the corresponding resonance frequencies, bandwidth and feed locations. After applying the first iteration, the resonance frequency of the patch is reduced from 1.51GHz to 1.16 GHz. For this type of fractal antenna, as shown in [12], the maximum iteration factor is 1/3, and the resonance frequency cannot be lowered below that of the iteration factor of 1/3. If the iteration factor is greater than 1/3, the patch will be divided into 5 separate ones.

It is evident that the first iteration decreases the resonant frequency to 0.768 of the original frequency (f_0). Furthermore, removing these slots from the up and bottom edges of the patch, like a rotated letter "H", reduces the resonance frequency further to 1.127GHz (0.74 f_0). For a fractal Koch Island patch, if the iteration factor is reduced from 1/4 to 1/6 or 1/10 the resonant frequency increases [12]. However, in the H-shaped patch, the resonant frequency reduces from 1.127GHz to 855MHz, i.e. 0.56f_0 (Fig. 2.2(b)), by reducing the slot width from 16.33mm (1/4 iteration factor) to 8mm. Fig. 2.2(a) also shows that all four antennas give similar far field radiation characteristics. All antennas' cross-polarizations are below -20dB, so they are not shown in the graph.

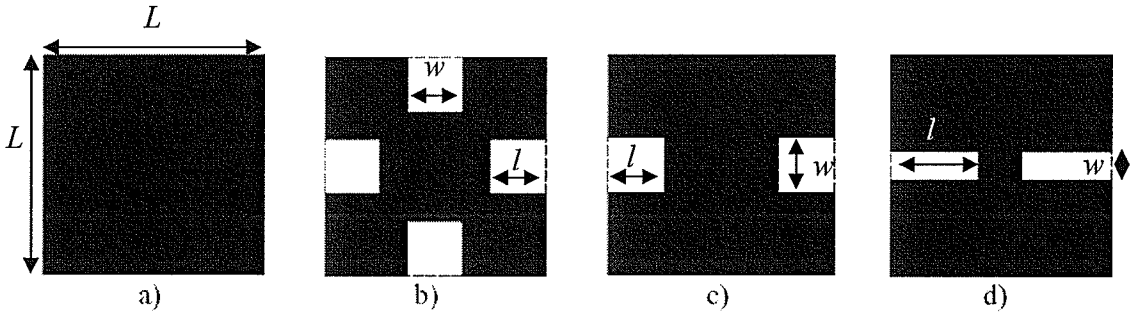

Fig. 2.1: Fractal and H-shaped patch antennas with L = 65.33mm (a) square patch, (b) Koch Island patch with l = w = 16.33mm, (c) H-shaped with thick slots with l = w = 16.33mm, (d) H-shaped with thin slots l =26mm, w = 8mm

Table 2.1: Bandwidth, resonance frequencies and feed locations of antennas shown in Fig. 2.1

Antenna type	a	b	c	d
Bandwidth (%)	1.01	0.35	0.32	0.19
Resonance frequency(GHz)	1.510	1.158	1.127	0.855
Feed location from centre (mm)	10.00	6.00	5.00	2.60

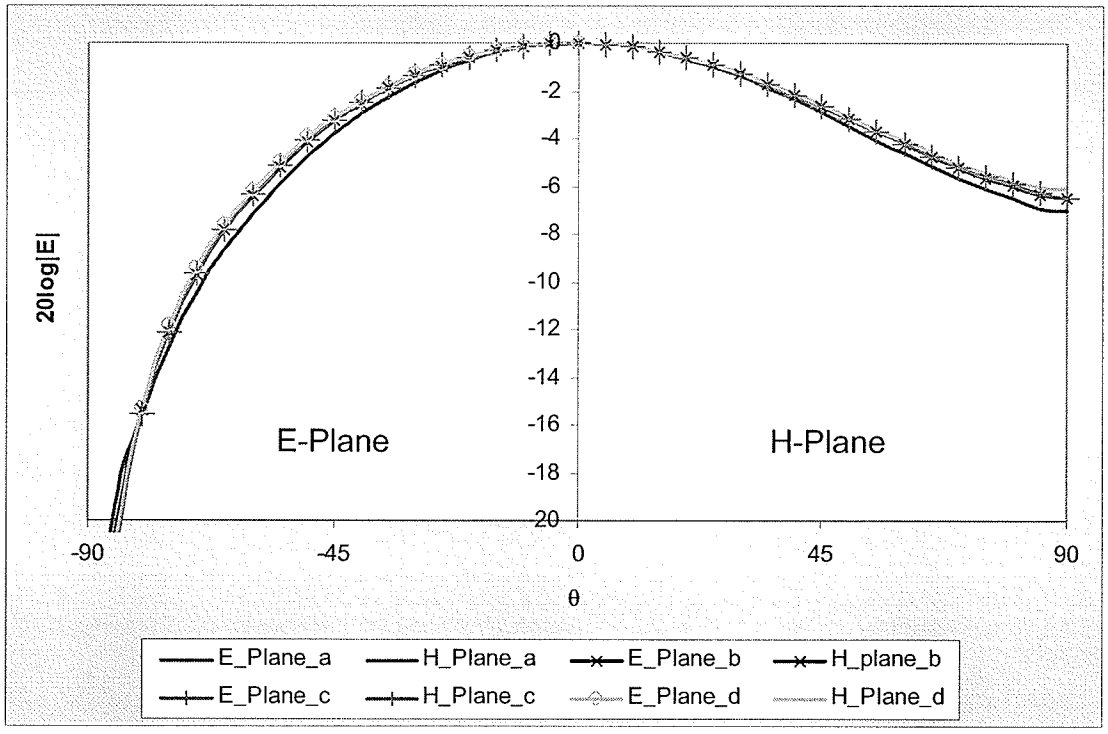

(a)

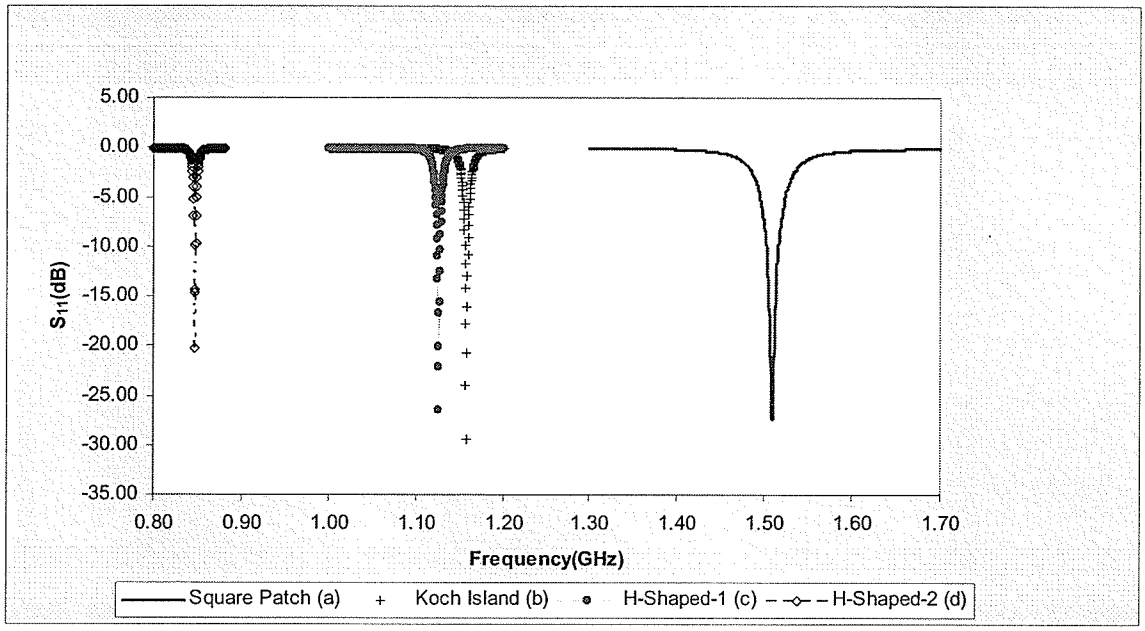

(b)

Fig. 2.2: (a) Radiation patterns with infinite ground plane and (b) Return losses for square, Koch Island and H-shaped microstrip patch antennas in Fig. 2.1

2.2.2 The Effects of Slot Dimensions on H-shaped Patch Antennas

In the above section, the comparison between two H-shaped patch antennas in Fig. 2.1(c) and Fig. 2.1(d) shows that the longer slot length gives lower resonant frequency. This will lead to the full investigation on the effects of slot lengths and widths for H-shaped patch antennas. Fig. 2.3 below is an enlargement of Fig. 2.1(c) with all slot dimension:

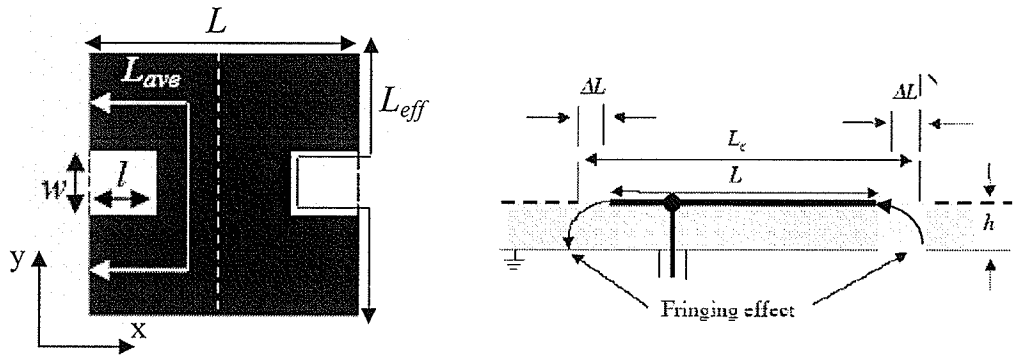

a) Top view *b) Side view*

Fig. 2.3: Dimensions of H-shaped square patch antenna with L = 65.33mm

To investigate the relationship between the slot size and resonant frequency, a parametric study of H-shaped patch antenna is performed. In Fig. 2.3, the slot length and width are shown by l and w, respectively. To relate the resonance frequency to the antenna shape, three length parameters are defined: the length of the square patch L, the effective total edge length $L_{eff} = L+2l+2\Delta L$, the average length between the length of the original square and fractal square $L_{ave} = L+l+w/2+2\Delta L$. The ΔLs are added to compensate for the fringing field effects at the ends of the patch. In the first set of simulations, the slot length is varied from 10mm to 26.33mm, while the slot width is kept at 5mm. The resonance frequency decreases as the slot length increases as shown in Fig. 2.4. Since the ground plane is infinite, the directivity does not change.

In the second set of simulations, the slot length is kept at 26.33mm and its width is varied from 1mm to 20mm. As shown in Fig. 2.5, the narrower slot provides the smaller resonant frequency. Again, since the antenna is on an infinite ground plane, the directivity does not change significantly.

The relations between resonant frequency, effective total edge length (L_{eff}), average length (L_{ave}) and half wavelength λ_d in dielectric are shown in Table 2.2 and Table 2.3. From Table 2.2, it can be seen that as the slot becomes longer, the total effective edge length becomes closer to half wavelength in dielectric. However, if the slot is shorter, the average length (L_{ave}) is closer to half wavelength in dielectric.

In Table 2.3, the effective total edge length (L_{eff}) is unchanged due to its definition, so the ratio between L_{eff} and half wavelength in dielectric becomes smaller as resonant frequency decreasing. The ratio is about one for the slot width of 5mm. On the other hand, the ratio between average length (L_{ave}) and half wavelength in dielectric is also not very close to one. Therefore, further study of this relationship can be carried out later. The above relationship between L_{eff}, L_{ave} and half wavelength in dielectric can be used to define the slot length based on the desirable frequency; the slot width can then be changed to fine tune the resonant frequency.

The following is the calculation for the ΔL in order to determine L_{eff} and L_{ave}

$\varepsilon_r = 2.2$; $h = 1.6mm$; $W = 65.33mm$

$\varepsilon_{eff} = 2.13$ from (1.3); Hence, $\Delta L = 0.8449mm$ from (1.4)

Then ΔL is used to calculate the effective total edge length (L_{eff}) and the average length between the length of the original square and fractal square (L_{ave}).

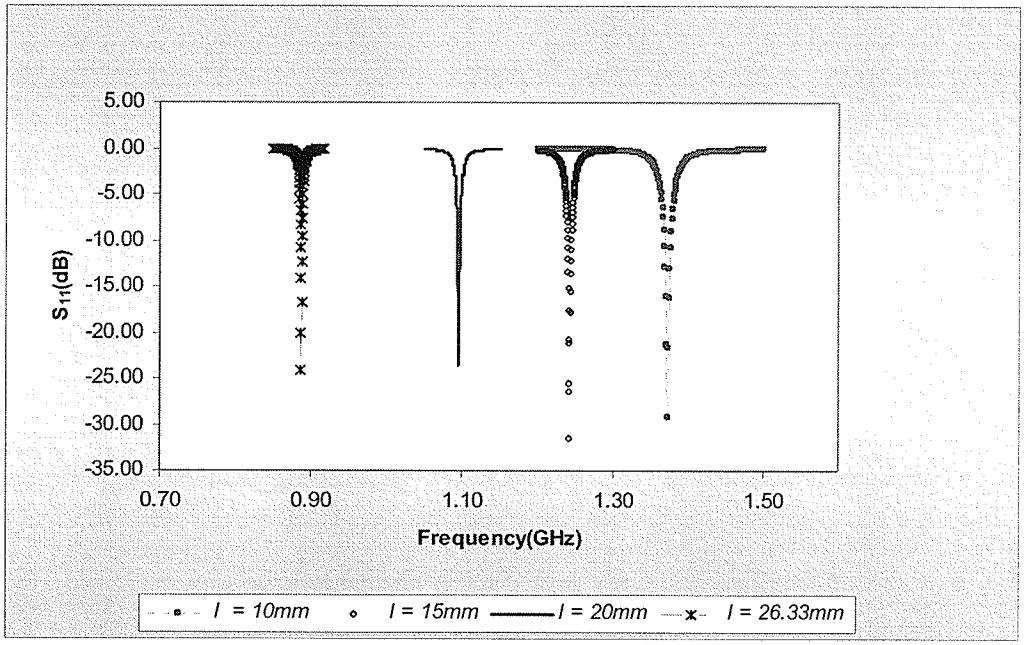

Fig. 2.4: Return loss for H-shaped patch with different slot lengths (l) of 10, 15, 20, 26.33mm, and slot width of w=5mm (Regard to Fig. 2.3)

Table 2.2: The H-shaped patch resonant frequency (f_0), effective patch length (L_{eff}) and average patch length (L_{ave}) for different slot lengths as in Fig. 2.4

l(mm)	f_0 (GHz)	λ (mm)	$L+2l$ (mm)	L_{ave} (mm)	L_{eff} (mm)	$\frac{L_{ave}}{\lambda/2}$	$\frac{L_{eff}}{\lambda/2}$	Directivity (dBi)
10.00	1.37	150.13	85.33	79.52	87.02	1.06	1.16	7.37
15.00	1.24	165.87	95.33	84.52	97.02	1.02	1.17	7.27
20.00	1.10	186.98	105.33	89.52	107.02	0.96	1.14	7.16
26.33	0.89	231.71	118.00	95.85	119.69	0.83	1.03	7.07

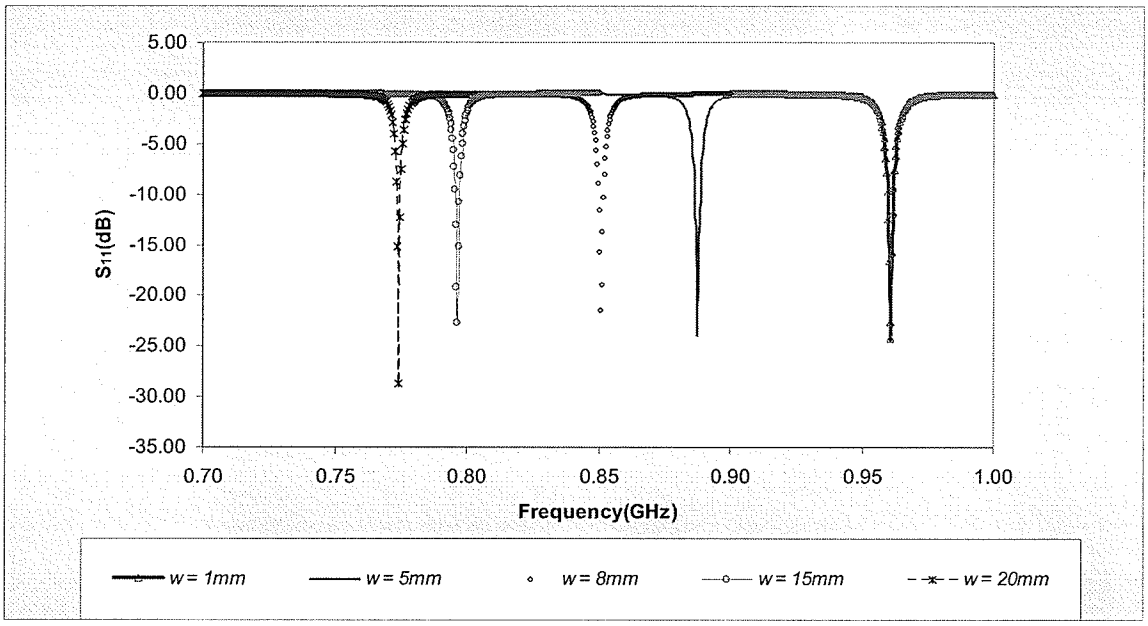

Fig. 2.5: Return loss for H-shaped patch with different slot width (w) of 1, 5, 8, 15, 20mm, and slot length of l=26.33mm (Regard to Fig. 2.3)

Table 2.3: The H-shaped patch resonant frequency (f_0), effective patch length (L_{eff}) and average patch length (L_{ave}) for different slot widths as in Fig. 2.5

w (mm)	f_0 (GHz)	λ (mm)	L_{ave} (mm)	$\frac{L_{ave}}{\lambda/2}$	$\frac{L_{eff}}{\lambda/2}$	Directivity (dB)
1.00	0.96	214.25	93.85	0.88	1.12	7.11
5.00	0.87	231.71	95.85	0.83	1.03	7.07
8.00	0.85	241.79	97.35	0.81	0.99	7.08
15.00	0.80	258.18	100.85	0.78	0.93	6.93
20.00	0.77	265.57	103.35	0.78	0.90	7.06

In order to have a closer look at the dependency of the slot dimensions and the resonant frequency, the same H-shaped patch antenna is varied in term of the substrate height and permitivity. At first, the same set of simulations are performed when varying the substrate permitivity (1.01, 2.2 and 9.8) while keeping its height constant at 1.6mm (Table 2.4 and Table 2.5). The relationships between resonant frequency of these H-shaped patchs and slot length (l), average patch length (L_{ave}), and effective patch length (L_{eff}), while changing the slot length (l), are shown in Figs. 2.6, 2.7 and 2.8, respectively (From Table 2.4). It shows that the resonant frequency of the H-shaped patch antenna is linearly dependent on its slot length, average patch length, or effective patch length. On the other hand, the slot width (w) and the average patch length (L_{ave}) do not seem to be linearly dependent on the resonant frequency of the H-shaped patch in Fig. 2.9 and Fig. 2.10 (data from Table 2.5).

The second set of simulations is dealing with the change of substrate height (0.78mm, 1.6mm and 3.2mm) while its permittivity is constant at 2.2 (Table 2.6 and Table 2.7). Once again, it is shown that the slot length (l), average patch length (L_{ave}), and effective patch length (L_{eff}) are reversed proportional to the the resonant frequency of the antenna in Figs. 2.11, 2.12 and 2.13, respectively (with the data from Table 2.6). However, Fig. 2.14 and Fig. 2.15 clearly show that the slot width (w) and the average patch length (L_{ave}) are not linearly dependent with the H-shaped patch resonant frequency (data from Table 2.7).

Table 2.4: Resonant frequency (f_0) and -10dB impedance bandwidth (BW) of the H-shaped patch antennas for different substrate permitivity (ε_r = 1.01, 2.2 and 9.8) but same substrate height h = 1.6mm and slot width w = 5mm with the variations of slot length l (same patch sizes as in Table 2.2)

Slot length	ε_r = 1.01		ε_r = 2.2		ε_r = 9.8	
l(mm)	f_0 (GHz)	BW (%)	f_0 (GHz)	BW (%)	f_0 (MHz)	BW (%)
10.00	1.963	0.92	1.370	0.73	669.8	0.39
15.00	1.776	0.56	1.240	0.48	611.9	0.31
20.00	1.562	0.32	1.100	0.36	539.8	0.30
26.33	1.263	0.32	0.890	0.22	440.8	0.32

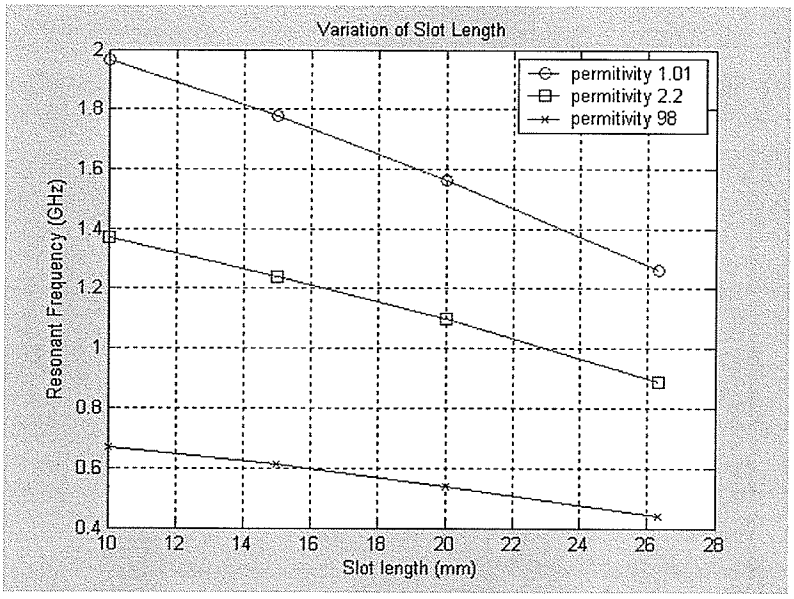

Fig. 2.6: Resonant frequency versus slot length (l) with different ε_r = 1.01, 2.2, 9.8, while keeping substrate height constant at h = 1.6mm in regard to Table 2.4

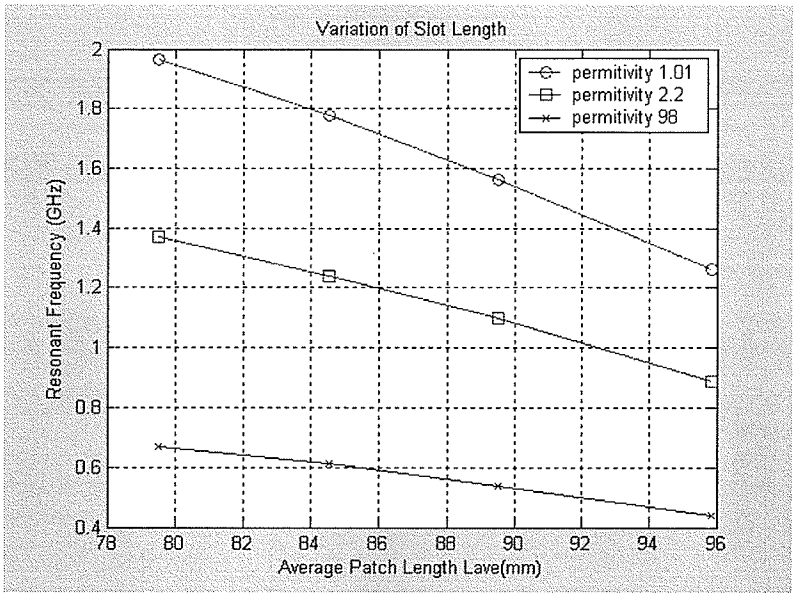

Fig. 2.7: Resonant frequency versus the average length (L_{ave}) of the H-shaped patch with different ε_r = 1.01, 2.2, 9.8, while keeping substrate height constant at h = 1.6mm and varying slot length (l) in regard to Table 2.4

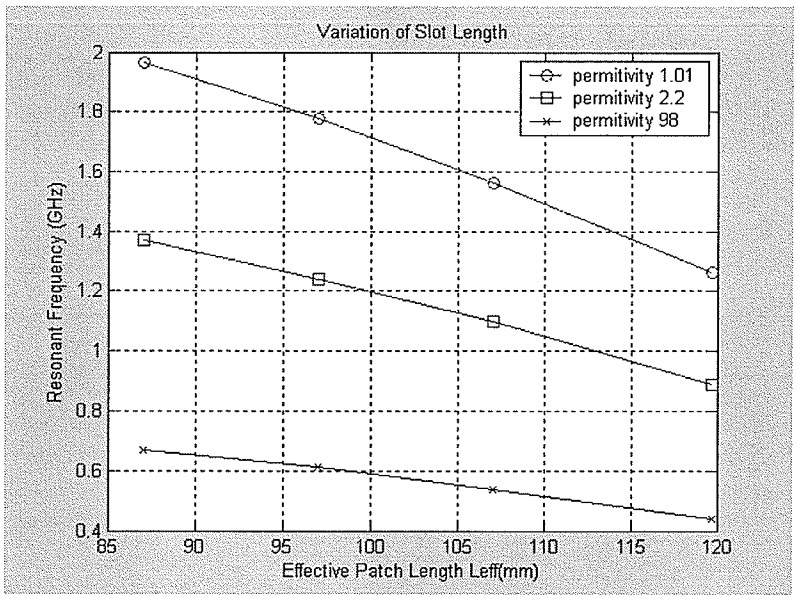

Fig. 2.8: Resonant frequency versus the effective length (L_{eff}) of the H-shaped patch with different ε_r = 1.01, 2.2, 9.8, while keeping substrate height constant at h = 1.6mm and varying slot length (l)) in regard to Table 2.4

Table 2.5: Resonant frequency (f_0) and impedance bandwidth (BW) of the H-shaped patch antennas for different substrate permitivity (ε_r = 1.01, 2.2 and 9.8) but same substrate height h = 1.6mm and slot length l = 26.33mm with the variations of slot width *w* (same patch sizes as in Table 2.3)

Slot width	$\varepsilon_r = 1.01$		$\varepsilon_r = 2.2$		$\varepsilon_r = 9.8$	
w(mm)	f_0 (GHz)	BW (%)	f_0 (GHz)	BW (%)	f_0 (MHz)	BW (%)
1	1.382	0.22	0.96	0.31	487.5	0.35
5	1.263	0.16	0.87	0.22	440.8	0.32
8	1.213	0.16	0.85	0.23	422.1	0.28
15	1.133	0.18	0.80	0.19	396.3	0.38
20	1.101	0.18	0.77	0.19	382.6	0.31

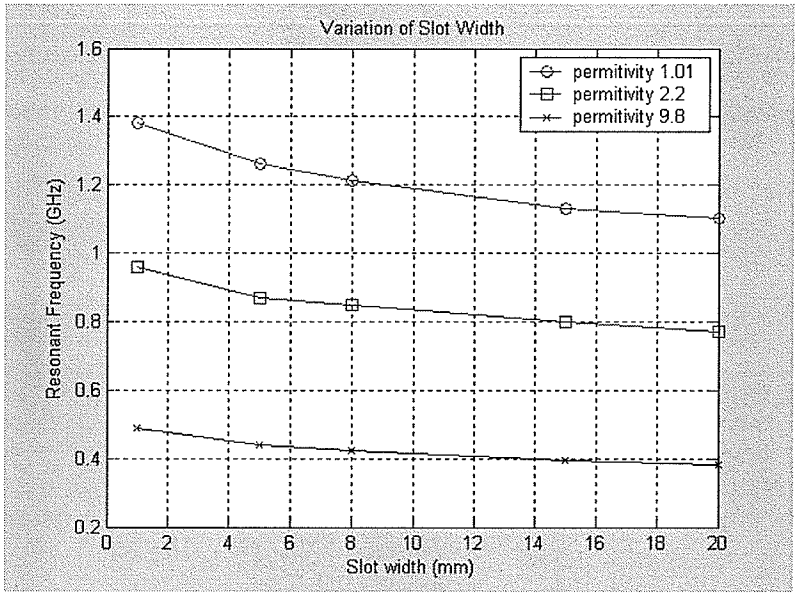

Fig. 2.9: Resonant frequency versus slot width (w) with different ε_r = 1.01, 2.2, 9.8, while keeping substrate height constant at h = 1.6mm and varying slot width (w) in regard to Table 2.5

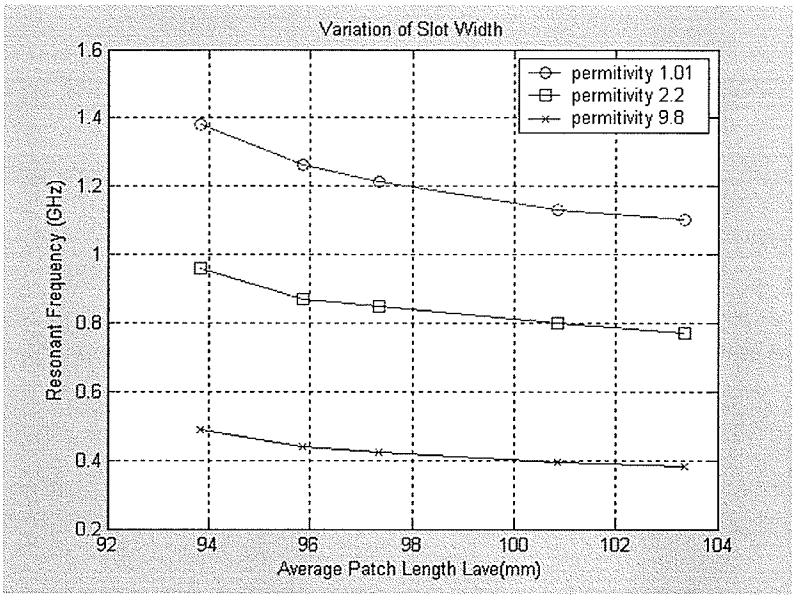

Fig. 2.10: Resonant frequency versus the average length (L_{ave}) of the H-shaped patch with different ε_r = 1.01, 2.2, 9.8, while keeping substrate height constant at h = 1.6mm and varying slot width (w)) in regard to Table 2.5

Table 2.6: Resonant frequency (f_0) and impedance bandwidth (BW) of the H-shaped patch antennas for different substrate height (h = 0.78, 1.6, and 3.2mm) but same ε_r = 2.2 with the variations of slot length *l* (same patch sizes as in Table 2.2)

Slot length	h = 0.78mm		h = 1.6mm		h = 3.2mm	
l(mm)	f_0 (GHz)	BW (%)	f_0 (GHz)	BW (%)	f_0 (GHz)	BW (%)
10.00	1.373	0.44	1.37	0.73	1.366	1.10
15.00	1.235	0.32	1.24	0.48	1.256	0.80
20.00	1.078	0.28	1.10	0.36	1.124	0.53
26.33	0.861	0.23	0.89	0.22	0.937	0.21

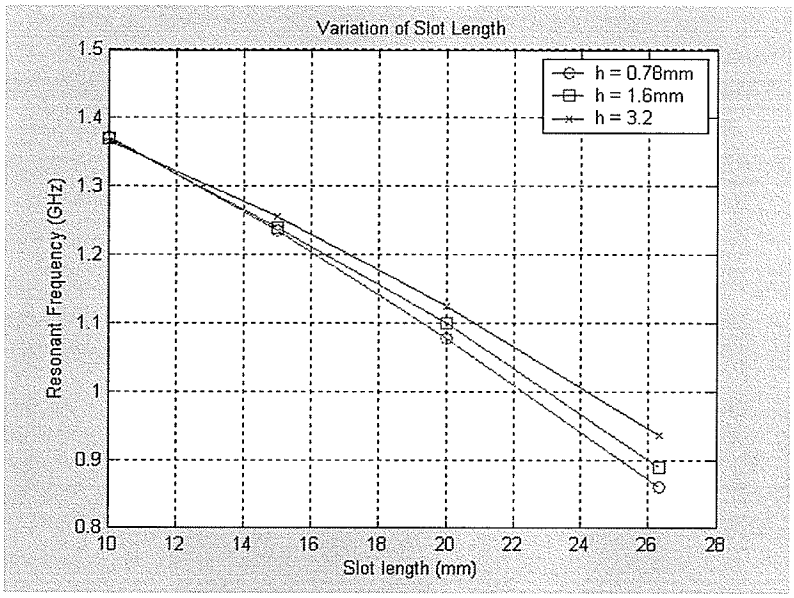

Fig. 2.11: Resonant frequency versus slot length (l) with different h = 0.78, 1.6, 3.2mm, while keeping permitivity constant at ε_r = 2.2 and varying slot length (l) in regard to Table 2.6

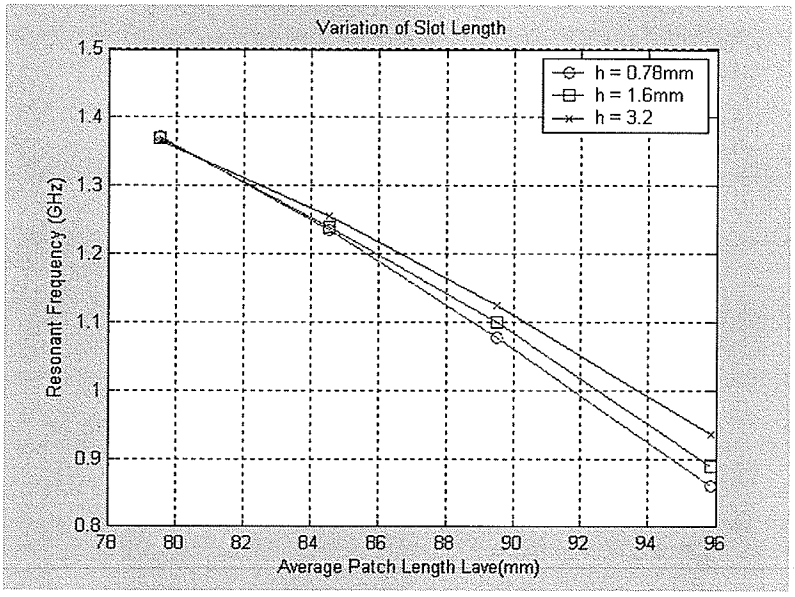

Fig. 2.12: Resonant frequency versus the average length (L_{ave}) of the H-shaped patch) with different h = 0.78, 1.6, 3.2mm, while keeping permitivity constant at ε_r = 2.2 and varying slot length (l) in regard to Table 2.6

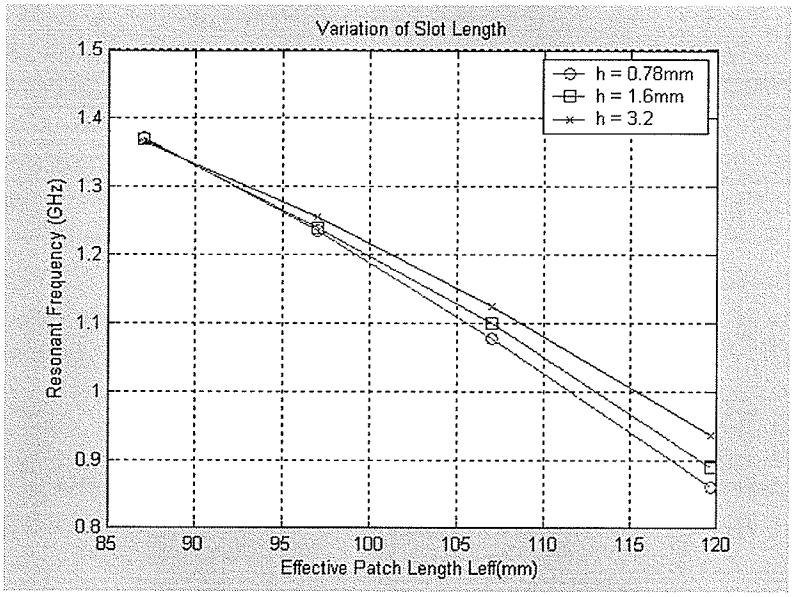

Fig. 2.13: Resonant frequency versus the effective length (L_{eff}) of the H-shaped patch with different different h = 0.78, 1.6, 3.2mm, while keeping permitivity constant at ε_r = 2.2 and varying slot length (l) in regard to Table 2.6

Table 2.7: Resonant frequency (f_0) and impedance bandwidth (BW) of the H-shaped patch antennas for different substrate height (h = 0.78, 1.6, and 3.2mm) but same ε_r = 2.2 with the variations of slot width *w* (same patch sizes as in Table 2.3)

Slot width	h = 0.78mm		h = 1.6mm		h = 3.2mm	
w(mm)	f_0 (MHz)	BW (%)	f_0 (MHz)	BW (%)	f_0 (MHz)	BW (%)
1	939.5	0.32	960	0.28	1037	0.34
5	863.0	0.35	870	0.22	937	0.32
8	824.5	0.30	850	0.23	895	0.22
15	771.7	0.32	800	0.19	835	0.24
20	753.0	0.33	770	0.19	810	0.25

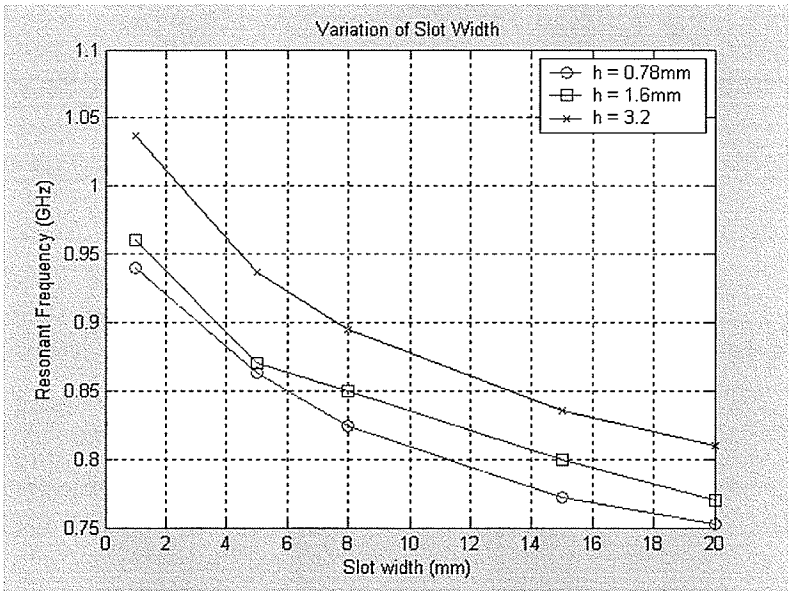

Fig. 2.14: Resonant frequency versus slot width (w) with different h = 0.78, 1.6, 3.2mm, while keeping permitivity constant at ε_r = 2.2 and varying slot width (w) in regard to Table 2.7

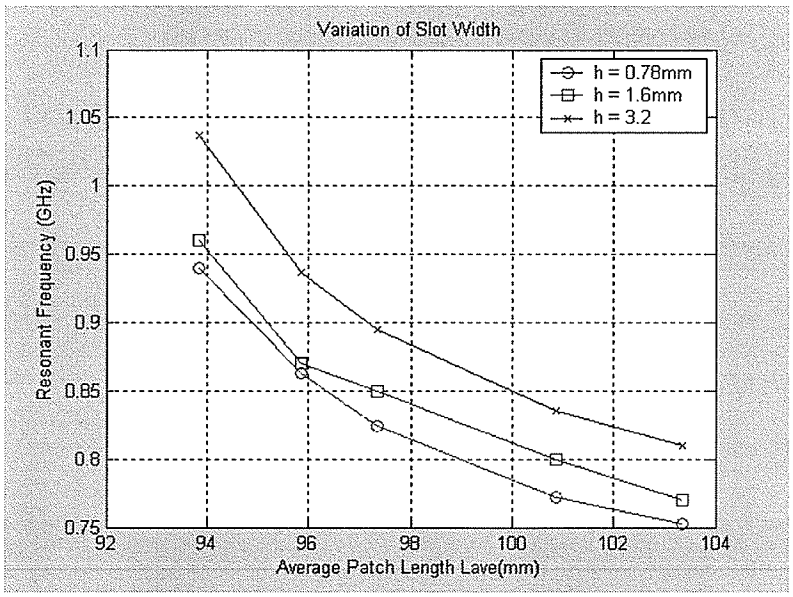

Fig. 2.15: Resonant frequency versus the average length (L_{ave}) of the H-shaped patch) with different h = 0.78, 1.6, 3.2mm, while keeping permitivity constant at ε_r = 2.2 and varying slot width (w) in regard to Table 2.7

Fig. 2.16 compares the current distributions for w=5mm and 20mm. It can be seen that the surface current around the edge of the slot has larger normal component to the edge for w=20mm, while for the narrow slot the surface current is almost tangential to the edge. This is in agreement with the ratio $L_{eff}/(\lambda/2)$ greater than one.

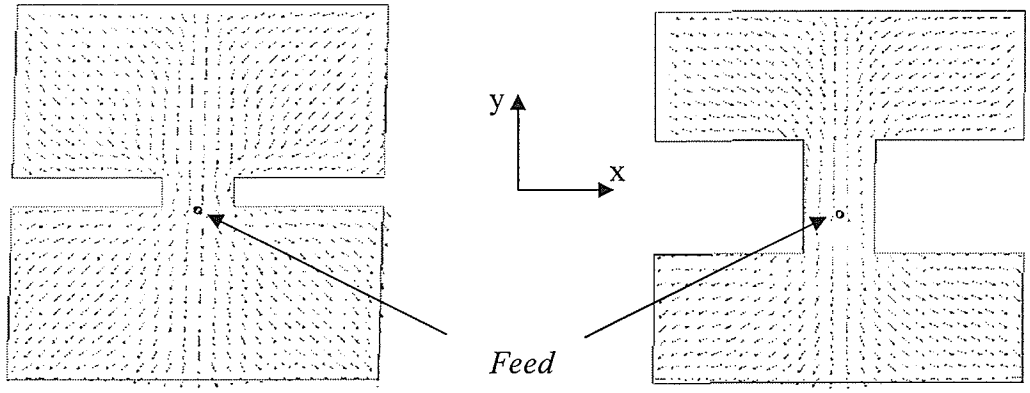

(a) Thin slot *(b) Thick slot*

Fig. 2.16: The current distributions of thin and thick slot H-shaped square patch antennas with L = 65.33mm, l = 26.33mm and slot width (a) w=5mm, (b) w=20mm in regard to Fig. 2.3

2.2.3 The Effects of Slot Dimensions on Modified H-shaped Antennas

In the previous section, the parametric study of H-shaped microstrip patch antennas was given. It showed that the wavelength of the antenna becomes longer as the physical edge length increases. However, the slot length increment will reach its limit as the slot approach the middle of the patch. Therefore, if the physical edge length of the patch can somehow be longer, the resonant frequency of the antenna will be reduced further. In this

section, the technique of modifying the original H-shaped patch to increase the physical edge length is presented.

In order to increase the physical edge length, smaller slots were added to the main slots. These modifications are shown in Fig. 2.17. Fig. 2.16(a) shows the previous H-shaped patch with w=5mm and l=26.33m. In Fig. 2.17(b) two additional vertical slots of length 10mm and width of 5mm are inserted, while in Fig. 2.17(c) four more horizontal slots with widths of 5mm and lengths of 15mm are added, to form slots with a shape of letter T, and finally, in Fig. 2.17(d) eight vertical slots of widths 3mm and lengths 10mm are included to form the shape of a rotated letter T. One can interpret Fig. 2.17(b) as the zero order, Fig. 2.17(c) as the first order, and Fig. 2.17(d) as the second order iterations of a fractal shape. As expected, the additional slots reduce the resonance frequencies further from 888MHz for (a) to 847MHz, 769MHz and 570MHz for configurations (b), (c) and (d), respectively. The multi-slot configuration of Fig. 2.17(d) shows the frequency reduction of $0.38f_0$. The return losses for these patches are shown in Fig. 2.18. Their radiation patterns are similar to those of the original patch. Since the ground plane is infinite the radiation patterns do not change with the changes in the slot shape. Table 2.4 summarizes the resonance frequencies, bandwidths and feed locations for these antennas.

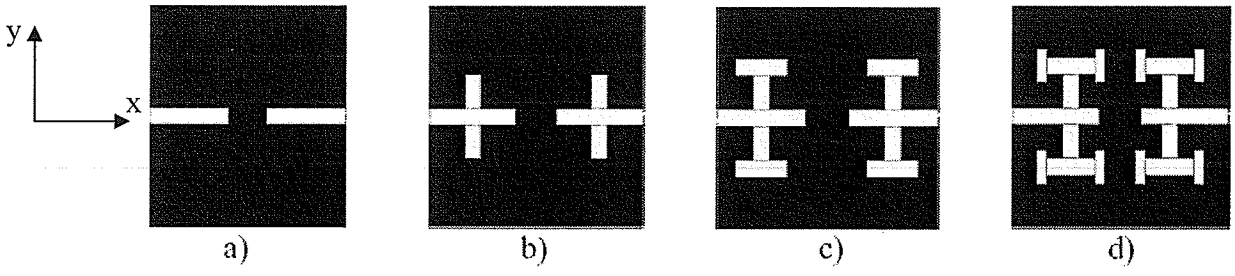

Fig. 2.17: Slot modification of H-shaped antenna to reduce its resonant frequency

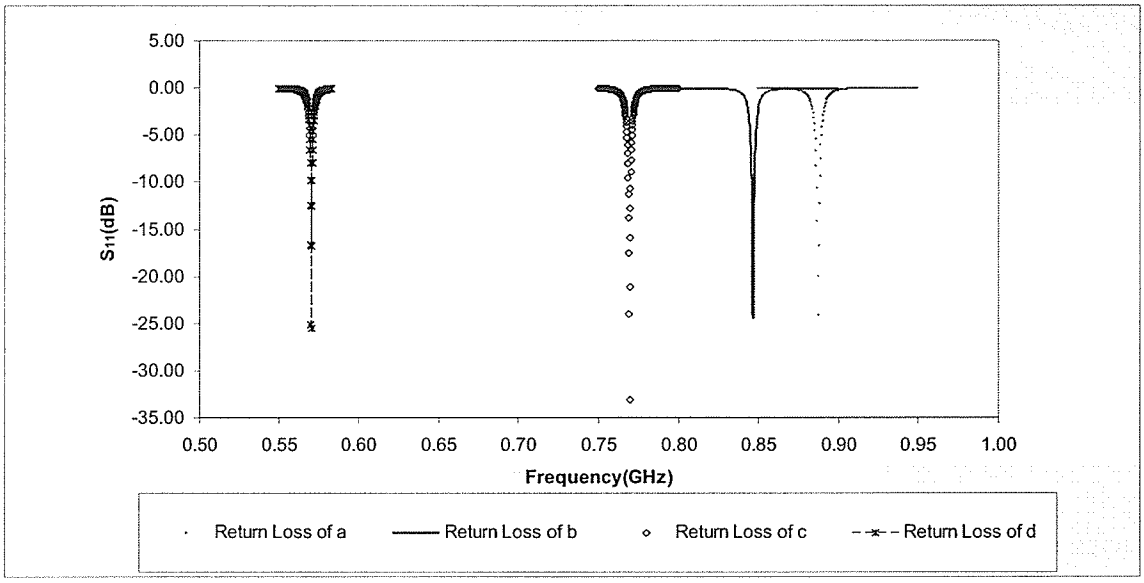

Fig. 2.18: Return losses for different patch configurations shown in Fig. 2.17

Table 2.8: Bandwidths, resonance frequencies and feed locations of antennas shown in Fig. 2.17

Antenna	a	b	c	d
Bandwidth (%)	0.225	0.197	0.196	0.205
Resonance Frequency (MHZ)	887.0	847.0	769.5	570.3
Feed distance from patch centre (mm)	3.0	3.0	3.5	4.7

It can be seen from Table 2.8 that all antennas have very small impedance bandwidth of about 0.2%. Therefore, these antennas are only suitable for applications with small bandwidth requirement. For other applications that require wider bandwidth, some improvements have to be made to enhance these antennas impedance bandwidth.

2.3 Feed Positions of the H-shaped and Multi-slots Antennas

As stated earlier, one of limitations in miniaturized antennas is choosing their exact feeding location, and it is the case for the H-shaped and multi-slot patch antennas. In this section, the sensitivity of feed locations on the above patch antennas will be studied. It will be shown that if 100Ω input impedance is used instead of conventional 50Ω, the feed locations are less sensitive; therefore, easier to fabricate.

To investigate the effects of feed location for the H-shaped and the multi-slot antennas in Fig. 2.19 and Fig. 2.20, the probe feed distance from the patches' centre was varied from 1mm-31mm, in separated simulations, along the vertical symmetrical axis of the patches. The resonant frequency, return loss, input impedance at each feed location will be recorded and reported in Table 2.9 – Table 2.12. Slot dimensions are given in the titles of Table 2.9 and Table 2.11. For these feed locations, the changes in the resonant frequency and return loss, for 50Ω and 100Ω line characteristic impedances, are shown in Table 2.9 – Table 2.12.

Table 2.13 is the summary of all the best cases in Tables 2.9 – 2.12. All cases provide similar frequency bandwidths of about 0.2%. Fig. 2.21 shows the sensitivity of return loss to the feed location for the cases discussed. One can see that the impedance of multi-slot antenna is less sensitive to the feed location and can be matched over a wider range.

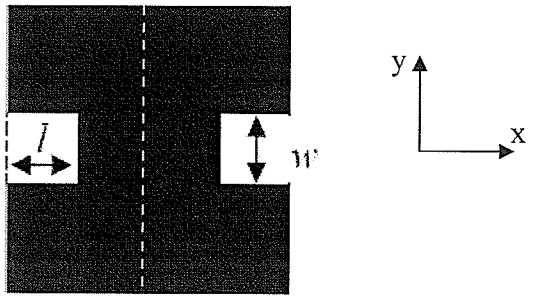

Fig. 2.19: H-shaped patch for feed location investigation

Table 2.9: Effect of feed location on input impedance of a H-shaped antenna fed by a 50Ω probe, *L=65.33mm, l=26.33mm, w=5mm,* feed location measured from the patch centre.

Feed Location (mm)	Frequency (MHz)	S_{11}(dB)	Real(Z) (Ω)	Imag(Z) (Ω)
1.0	883.00	-2.35	6.76	4.03
2.0	883.68	-10.29	26.69	2.61
2.3	884.24	-15.52	35.75	1.85
2.5	881.92	-23.72	44.09	1.61
2.6	881.92	-30.20	47.43	1.57
2.7	881.92	-40.71	50.70	0.60
3.0	885.24	-22.33	57.22	-3.91
3.3	881.64	-14.67	72.35	-3.40
3.6	881.64	-11.60	85.38	-2.42
4.0	881.60	-9.23	103.38	-2.91
4.5	882.56	-7.25	127.45	-1.51

Table 2.10: Effect of feed location on input impedance of a H-shaped antenna fed by a 100Ω probe, dimensions the same as Table 2.9

Feed Location (mm)	Frequency (MHz)	S_{11}(dB)	Real(Z) (Ω)	Imag(Z) (Ω)
1.0	882.80	-1.17	6.74	5.00
2.0	883.84	-4.75	25.96	-0.25
3.0	885.20	-11.58	57.73	-1.94
3.5	881.60	-19.70	81.60	-1.57
4.0	881.60	-32.89	102.99	-3.49
4.5	882.56	-18.31	127.66	0.51
5.0	882.80	-13.44	153.34	1.25
6.0	883.40	-9.12	207.62	-4.41
7.0	881.80	-6.86	266.41	1.31

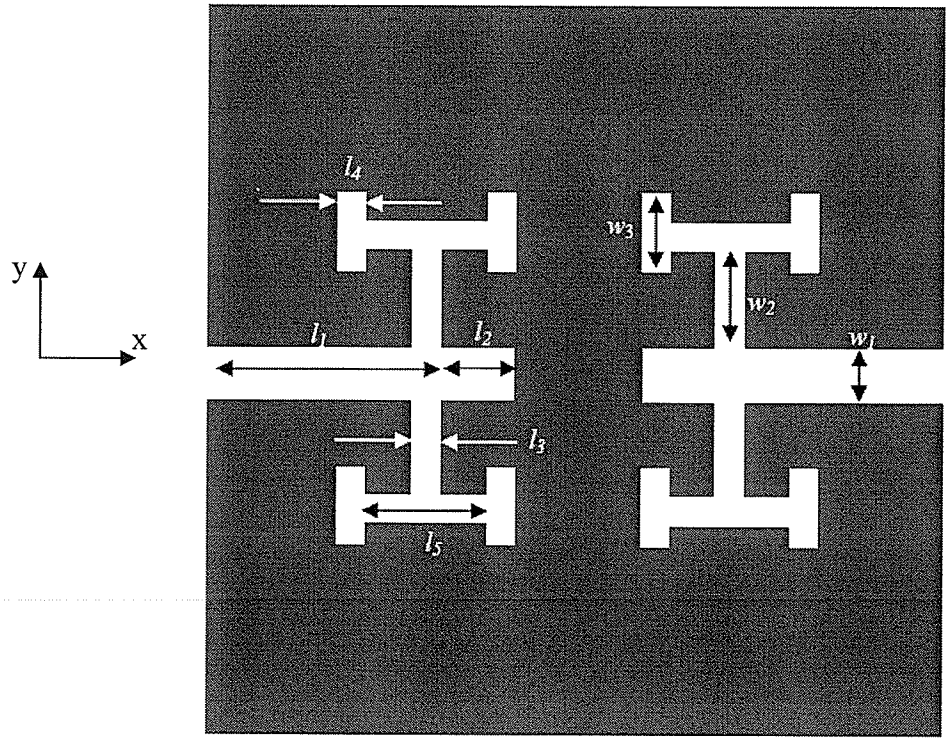

Fig. 2.20: Multi-slot patch for feed location investigation

Table 2.11: Effect of feed location on input impedance of a multi-slot antenna fed by a 50Ω probe, *L=65.33mm, l_1 +l_2=26.33mm, l_3=5mm, l_4=3mm, l_5=15mm, w_1=5mm, w_2=10mm, w_3=10mm (Regard to Fig. 2.20)*

Feed Location (mm)	Frequency (MHz)	S_{11}(dB)	Real(Z) (Ω)	Imag(Z) (Ω)
1.0	571.70	-0.5	1.49	2.42
2.0	574.00	-2.62	7.49	1.56
3.0	571.80	-5.99	16.60	1.67
4.0	572.20	-12.60	31.01	0.04
4.3	572.40	-12.69	31.16	-0.11
4.5	572.32	-18.64	39.54	-0.62
4.8	572.38	-19.18	40.11	0.57
5.0	571.74	-35.03	48.38	0.65
5.2	572.96	-34.79	51.82	-0.37
5.5	573.10	-21.88	58.62	-1.49
5.7	574.08	-16.03	68.39	-3.49
6.0	571.72	-16.22	67.75	-4.07
6.5	572.36	-13.07	77.85	-5.61
7.0	571.80	-9.91	96.51	-5.62

Table 2.12: Effect of feed location on input impedance of a multi-slot antenna fed by a 100Ω probe, dimensions the same as Table 2.11

Feed Location (mm)	Frequency (MHz)	S_{11}(dB)	Real(Z) (Ω)	Imag(Z) (Ω)
4.00	572.04	-5.49	30.38	0.25
5.00	571.80	-9.20	48.38	-0.32
6.00	571.64	-14.51	68.20	-1.23
6.50	572.48	-18.12	77.91	-0.31
7.00	571.79	-36.72	97.11	0.39
7.50	573.88	-22.69	115.82	-0.13
8.00	574.80	-14.89	143.99	1.62
9.00	574.51	-11.82	168.93	1.41
10.00	574.18	-8.20	227.41	-1.48

Table 2.13: Frequency bandwidth of best matched cases that were shown in Tables 2.9 - 2.12

Case	Feed location (mm)	f_0 (MHz)	Δf (MHz)	BW (%)	S_{11} (dB)
H-shaped 50Ω	2.7	881.94	1.90	0.22	-40.71
H-shaped 100Ω	4.0	881.60	1.96	0.22	-32.89
Multi-slot 50Ω	5.0	571.74	1.04	0.18	-35.03
Multi-slot 100Ω	7.0	571.79	1.11	0.19	-36.72

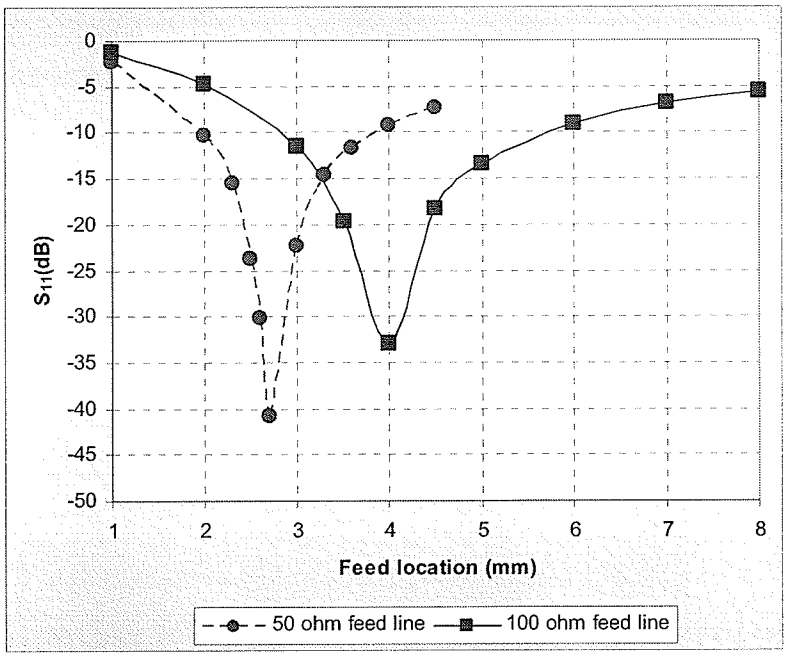

(a)

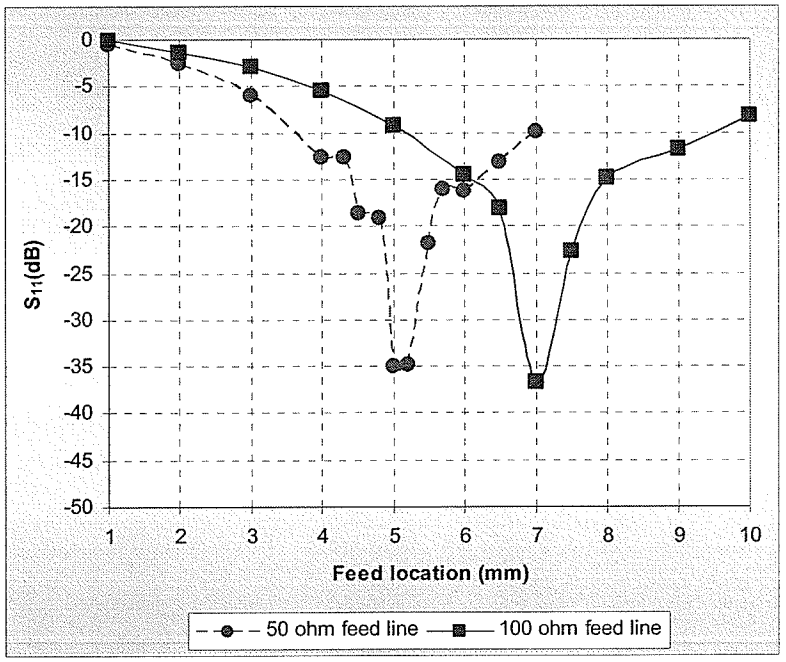

(b)

Fig. 2.21: Feed location effects on the return loss (a) H-shaped antennas in Table 2.9 and 2.10, (b) multi-slot antennas in Table 2.11 and 2.12

2.4 Experimental Results

To validate the simulation results, two sets of experiments were performed. In the first set two equal size patch antennas were fabricated on a substrate with dielectric constant of 2.5 and a square area of 65.33mm by 65.33mm. They were the H-shaped patch and the multi-slot patch configurations, as shown in Fig 2.22. The feed locations for the H-shaped and multi-slot patch were 3mm and 5mm from the centre, respectively. The resonant frequencies were measured using an Anritsu Network Analyzer ME7808A, and the results are compared with numerical simulation in Fig. 2.23. For the H-shaped patch the error in the resonance frequency is 1.8%, and for the multi-slot it is 2%. Both antennas were fed using a 50Ω impedance coaxial cable.

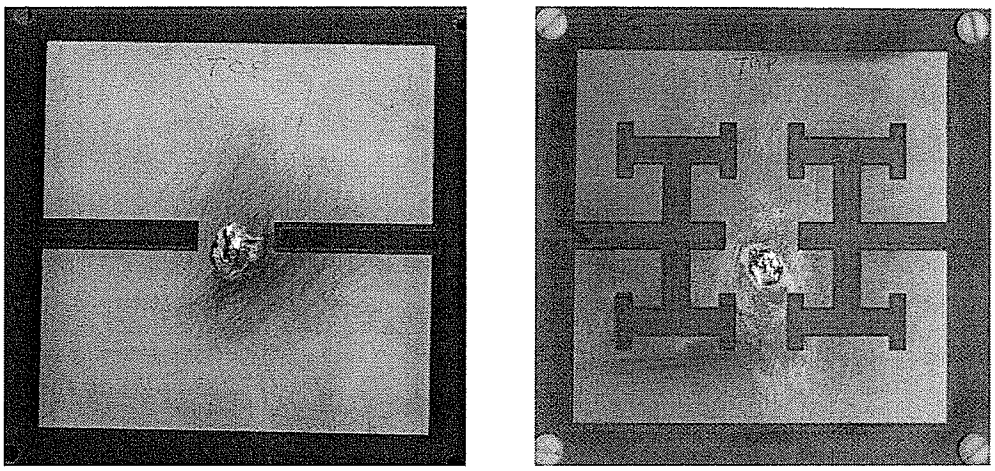

(a) *(b)*

Fig. 2.22: Fabricated patch antennas (a) H-shaped with l=26.33mm and w=5mm (b) multi-slot with l_1 +l_2=26.33mm, l_3=5mm, l_4=3mm, l_5=15mm, w_1=5mm, and w_2=w_3=10mm (Regard to Fig. 2.20)

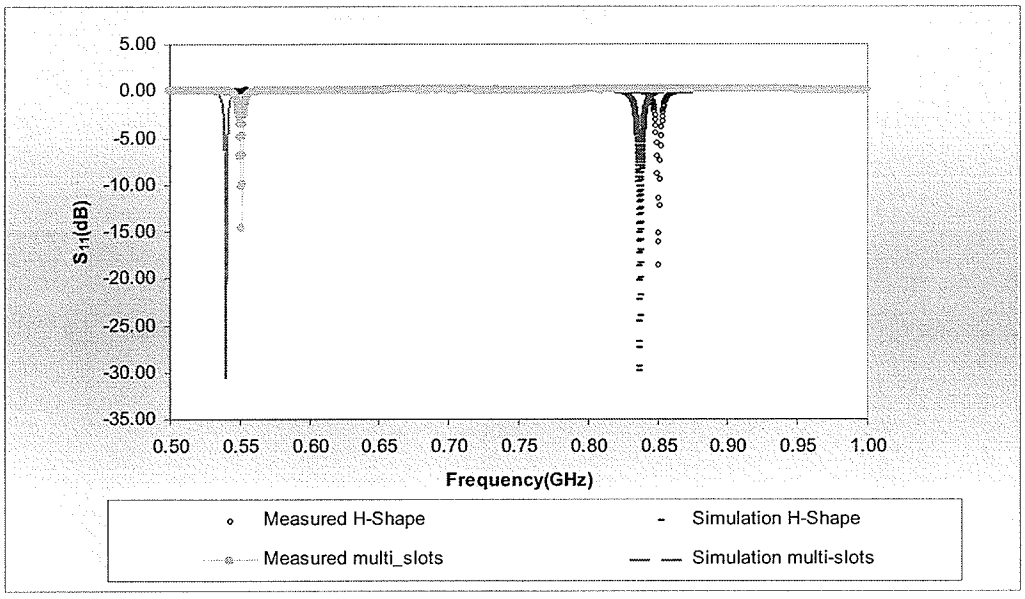

Fig. 2.23: Measured and simulated resonant frequencies for H-shaped and multi-slot antennas

In the second set of experiments, three different size patch antennas were designed for the same resonant frequency of around 2GHz (Fig. 2.24). The patch areas were 45mm by 45 mm for the square patch, 30mm by 31mm for H-shaped patch and 20mm by 21mm for multi-slot patch. These antennas were fabricated on a substrate with a dielectric constant of ε_r=2.5 and height of h=1.6mm, with a ground plane of 80mm by 80mm. Their feeds were located at 6mm for square patch, 2.5mm for H-shaped and 0.8mm for multi-slot antenna, from the centre of the patch. The slot dimensions are shown in Fig. 2.24, and the measured return losses are shown in Fig. 2.25. Their resonance frequencies and bandwidths are summarized in Table 2.14. Gains of these three antennas were measured and compared, in Table 2.15, with the simulation results obtained using Ansoft Designer. Table 2.15 also shows the measured gains, directivities calculated using the radiation patterns, and gains given in the cases of no dielectric losses (perfect dielectric) or no

conductor losses (perfect conductor). One can see that, although the directivity for the three antennas is almost the same, there is a gain reduction for the H-shaped and multi-slot antennas. If only the dielectric losses are added, with the use of perfect conductors for the patch and its ground plane, the calculated gain becomes closer to the measurement. This means that the main contribution for the gain reduction in the H-shaped and multi-slot patch antennas are from the conductor losses, which are ohmic losses. Fig. 2.26 and Fig. 2.27 show measured radiation patterns at the resonance frequencies for the three antennas. The cross-polarizations are relatively low, in compare to the co-polarizations for these manufactured antennas.

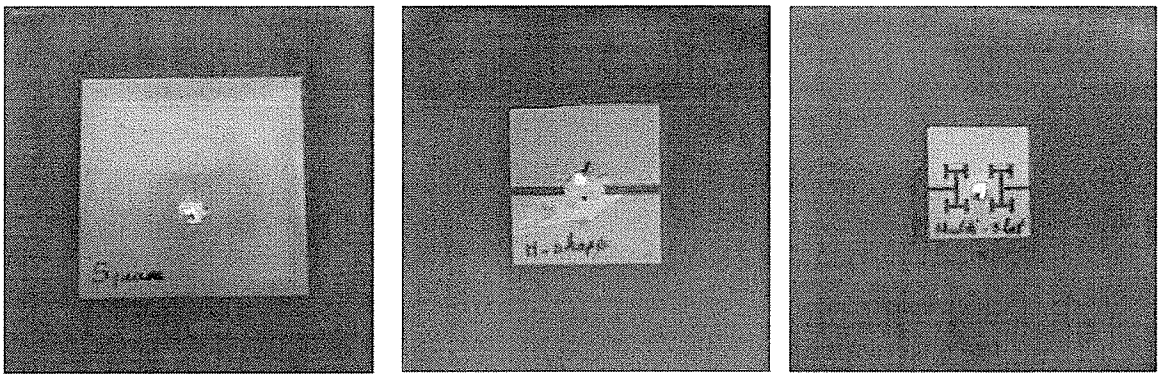

(a) (b) (c)

Fig. 2.24: Fabricated antennas for 2GHz resonance frequency, (a) square patch L=45mm by 45mm (b), H-shaped with L=30mm by 31mm, l=11mm and w=2mm, and (c) multi-slot with L=20mm by 21mm, l_1=6mm, l_2=0, l_3=l_4=1mm, l_5=5mm, w_1=1mm, w_2=2.5mm and w_3=3mm (Regard to Fig. 2.20)

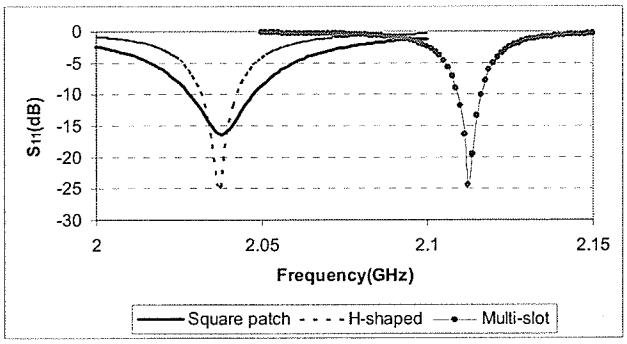

Fig. 2.25: Measured return losses for antennas in Fig. 2.24

Table 2.14: Frequency bandwidths and resonance frequencies for fabricated antennas shown in Fig. 2.23

Antenna Type	Square patch	H-shaped	Multi-slot
Bandwidth (%)	0.98	0.55	0.35
f_0 (GHz)	2.0375	2.0375	2.1125
Simulated f_0 (GHz)	2.0480	2.0580	2.0660

Table 2.15: Gain and directivities of antennas shown in Fig. 2.23 with ground plane sizes of 80 by 80mm

Antenna Type	Directivity (dBi)	Measured Gain (dBi	Simulated Gain (dBi)		
			All losses	*Perfect conductors*	*Perfect dielectric*
Square patch	7.20	7.48	7.54	6.44	6.70
H-Shaped	6.85	4.38	4.98	4.45	5.24
Multi-slots	6.82	0.63	0.47	-0.16	1.38

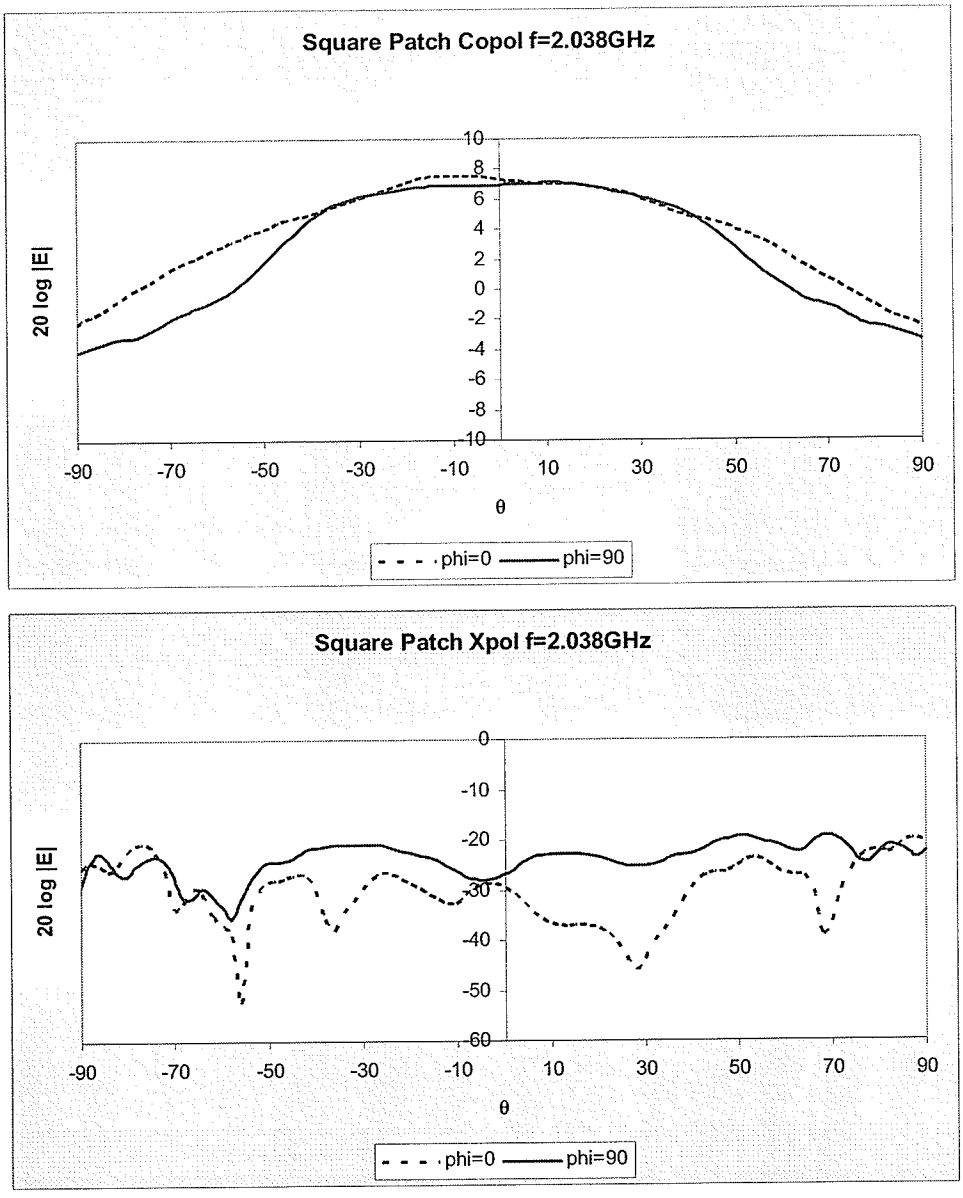

Fig. 2.26: Radiation patterns for square patch shown in Fig. 2.23

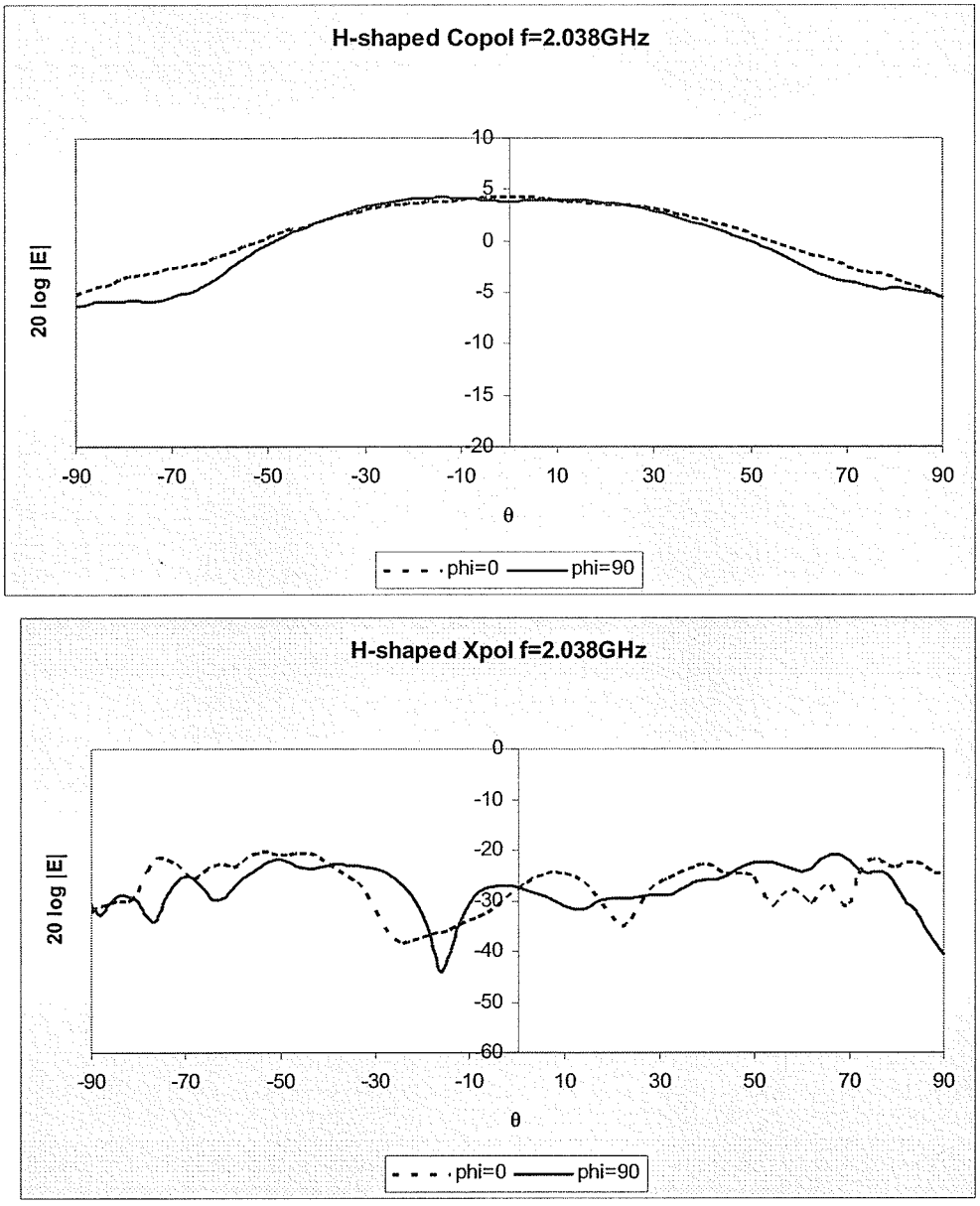

Fig. 2.27: Radiation patterns for H-shaped shown in Fig. 2.23

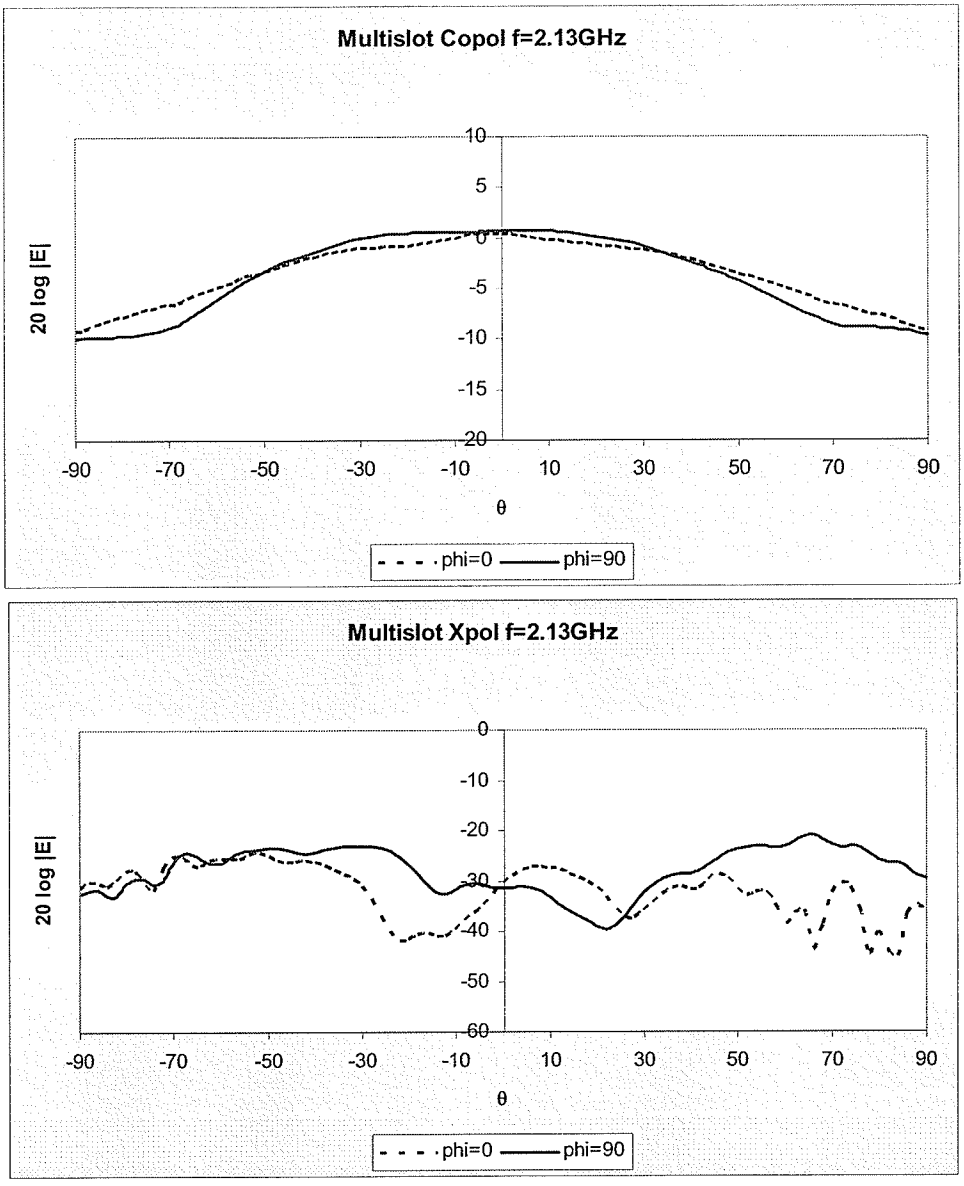

Fig. 2.28: Radiation patterns multi-slot shown in Fig. 2.23

2.5 Yagi Configurations

A Yagi microstrip square patch was designed to provide the main beam with a 45 degree tilt from the broadside. The patch width for the driven element and two directors were chosen to be 65.33mm, 62.33mm and 60.33mm, respectively. The antenna configuration is shown in Fig. 2.29(a). The same widths were used for fractal Koch Island, as shown in Fig. 2.29(b). The radiation patterns in both E- and H-planes are shown in Fig. 2.30. The fractal Koch Island Yagi antenna does not show any coupling from the driven patch to the directors, and as a result the main beam is not tilted in the E-plane. This could have happened because of large differences in the resonant frequencies of driven patch and directors, and due to larger effective spacing of the elements, caused by the central slot. To resolve this problem, another set of microstrip Yagi antennas were designed, where driven patch and directors had the same width (65.33mm). Fig. 2.31 shows four different designs. The antenna shown in Fig. 2.31(a) is a square patch Yagi, the second one shown in Fig. 2.31(b) is a fractal patch Yagi, and the third and fourth are the modified fractal shapes. Fig. 2.32 shows their return losses. Table 2.16 summarizes the resonance frequencies, tilt angles and gains for these four antennas. The H-shaped Yagi provides $0.75f_0$ frequency reduction and the same tilt angle as square patch Yagi. However, a reduction of 2.73dB in its gain is observed.

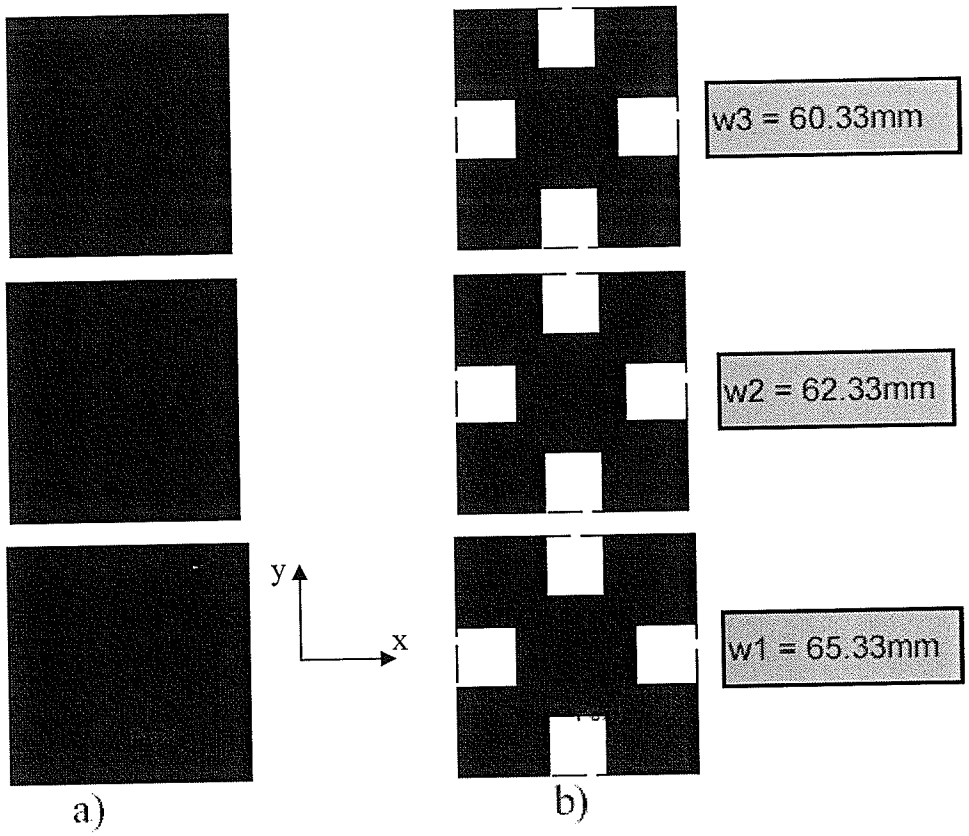

Fig. 2.29: Yagi square and fractal patch with different widths.

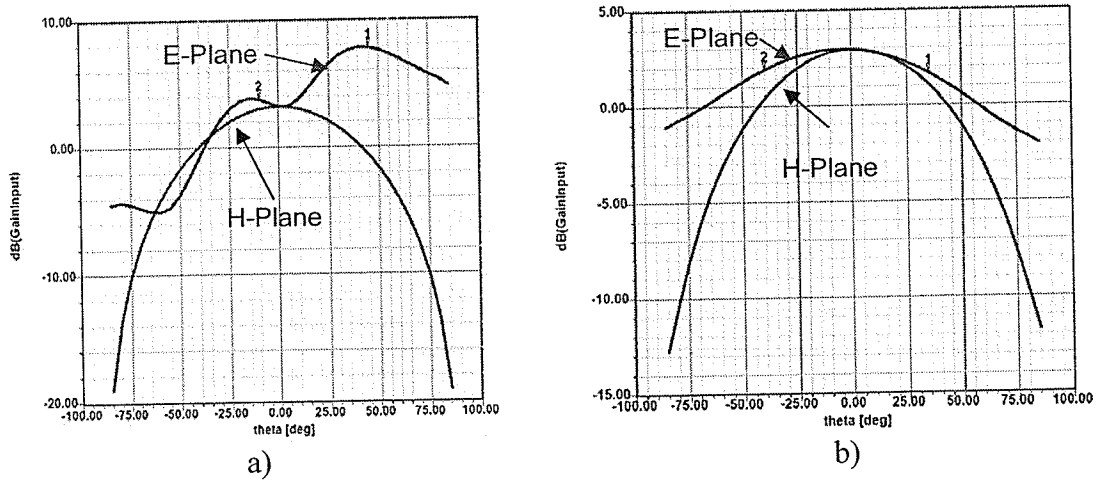

Fig. 2.30: Radiation patterns for a) Square patch Yagi; and (b) Fractal Yagi

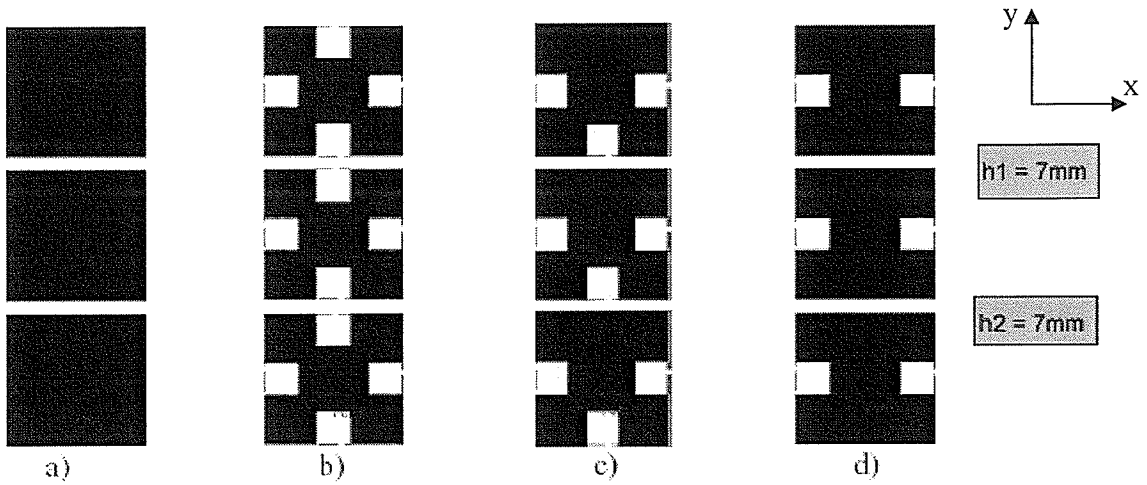

Fig. 2.31: Yagi patch antennas width same widths but different patch shapes

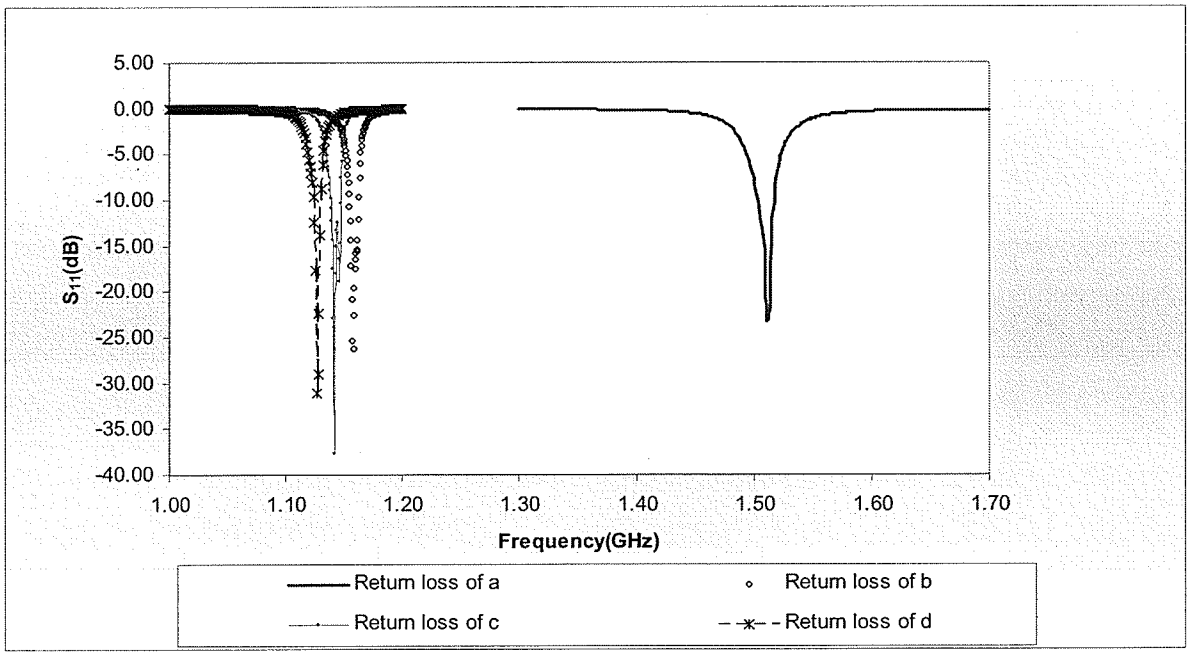

Fig. 2.32: Return loss for different Yagi patch antenna

Table 2.16: Resonant frequencies, tilt angles and directivities of different Yagi patch shapes with (ε_r=2.2, *tan* δ=0.001) shown in Fig. 2.30

Yagi type	f(GHz)	Tilt angle (degrees)	Gain (dBi)
a	1.512	50	7.50
b	1.150	10	2.93
c	1.142	40	5.68
d	1.128	50	4.77

2.6 Different Slot Shapes for Slot Loading Patch Antennas

In the previous sections, the slot loading method used only rectangular slot to create the H-shaped patch antennas. In this section, further study for the effect of slot shape on the resonance frequency reduction is carried out. Fig. 2.33 shows three different slot shapes of triangular, T-shaped and rectangular for loading of the square patch antenna (same properties as in section 2.2). For all slot shapes, the slot's width is 5mm. The antennas' parameters are shown in Table 2.17. Comparing the resonance frequencies in Table 2.17 it becomes evident that, the triangular shape seems shorter (equivalent to 17mm H-slot) and the T-shape is longer (equivalent to 23.5mm).

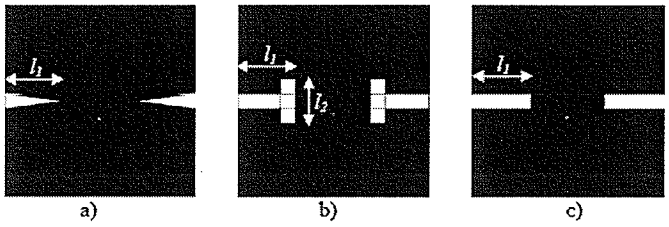

Fig. 2.33: Different slot shapes for slot loading patch antennas: a) Triangular slot with l_1 = 20mm; b) T-shaped slot with l_1 = 20mm, l_2 = 15mm; c) Rectangular slot for H-shaped patch with l_1 = 20mm and l_1 = 23.5mm

Table 2.17: Resonance frequency (f_0), minimum return loss (S_{11min}), -10dB impedance bandwidth (BW), and directivity of the three antennas in Fig. 2.33

	f_0(MHz)	S_{11min}(dB)	BW (%)	Directivity (dBi)
Triagular Slot l_1 = 20mm	1192	-29	0.42	4.66
T-shaped Slot l_1 = 20mm l_2 = 15mm	984	-32	0.24	2.24
H-shaped l_1 = 20mm	1009	-26	0.36	4.00
H-shaped l_1 = 23.5mm	990	-27	0.24	2.51

2.7 Slot Loading for Rectangular Patch Antenna

In section 2.2, slots loaded square patch antennas were studied, and it was shown that the resonant frequency of the H-shaped patch is inversely proportional to its slot length. Therefore, if the slot length is increased, the resonant frequency will be reduced further. A reasonable approach is to increase the patch width so that the loaded slots have more room to extent. Fig. 2.32 shows the rectangular H-shaped patch antenna with the same length L = 65.33mm but W = 105.33mm (40mm bigger than L), ε_r of 2.2, and substrate thickness h = 1.6mm. With the antenna configuration in Fig. 2.32, the resonant frequency can be reduced further in comparison to the H-shaped square patch antenna, due to the fact that each slot has 20mm more in which to extend. Table 2.17 shows the

resonant frequency (f_0) and -10dB impedance bandwidth of the rectangular H-shaped patch antenna in Fig. 2.32 with the variation of slot length (l) and slot width (w).

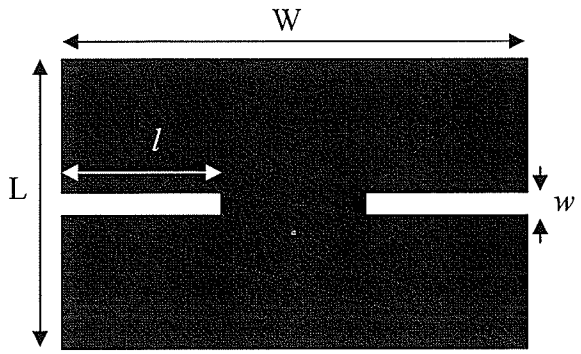

Fig. 2.34: Slot loaded rectangular microstrip patch antenna with L = 65.33mm and W = 105.33mm

Table 2.17: Resonant frequency (f_0) and -10dB impedance bandwidth of the rectangular H-shaped patch antenna in Fig. 2.32

w = 5mm			l = 40mm		
l(mm)	f_0 (MHz)	BW (%)	*w(mm)*	f_0 (MHz)	BW (%)
0	1502	1.20	NA	NA	NA
26	1070	0.28	1	841.0	0.20
30	985.0	0.30	5	784.7	0.23
36	865.0	0.23	10	752.5	0.21
40	784.8	0.23	15	733.0	0.19
46	659.1	0.23	20	721.3	0.21

2.6 Summary

In this chapter, different methods for miniaturization of a square microstrip patch were studied and a novel fractal patch with multi-slots was introduced. The new patch can provide a resonance frequency of $0.38f_0$, where f_0 is the resonance frequency of the square patch. A parametric study of the H-shaped slots showed that, increasing the slot length and increasing the slot width can reduce the resonant frequency. The resonant frequency of the patch is linearly dependent on the slot length (l). Two sets of sample antennas were built and measurement results showed excellent agreements with numerical results.

Also, the Yagi configuration of Koch Island and H-shaped patch were investigated. Both Koch Island and H-shaped Yagi can provide reduction in the resonant frequency. However, Koch Island Yagi does not show a good coupling to its directors, and consequently, it does not provide adequate beam tilt angle and directivity. The H-shaped patch provides good tilt angles, but with the price of reduced directivity.

Chapter 3

Modified Koch Island Microstrip Antenna for Circular Polarization

3.1 Introduction

The Koch Island microstrip antenna has been presented in the previous chapter as a miniaturized antenna. However, this miniaturized antenna only operated at linear polarization. In many wireless applications such as GPS, the antenna system has to be able to operate with circular polarization. In this chapter, the Koch Island microstrip patch antenna will be modified so that it can radiate a circular polarizated waves in order to meet the demands of such systems.

3.1.1 Antenna Polarization

The polarization of antenna in a given direction is the polarization of the electromagnetic wave transmitted by the antenna [19]. The polarization of a radiated wave is defined as the direction of its electric field [20]. In other words, the polarization of an electromagnetic wave is defined by the shape and orientation of the tip of the electric field vector as it varies with time [21].

In the far field region, the spherical wave radiated from the antenna is considered as a plane wave at the point of investigation. The method to calculate the polarization of an antenna is using vector operations on a two-dimensional space using the far field vector as the normal to the plane. Polarization of an antenna can be linear, circular, or elliptical.

If the electric field vector, which is a function of time, is always directed along a line, the antenna radiating a linearly polarized field. On the other hand, if the electric field vector traces an ellipse, the elliptical polarization is achieved. The circular polarization is a special case of the elliptical polarization, when the ellipse becomes a circle. Therefore, the linear polarization is also a special case of the elliptical polarization when ellipse shrinks to a straight line. When the electric field vector has clockwise rotation, it is assigned as right-hand polarization. Similarly, the left-hand polarization associates with counter clockwise rotation.

The polarization pattern [19] represents polarization characteristics of an antenna which defines as the spatial distribution of the polarization of a vector field excited (radiated) by an antenna taken over its radiation sphere. Reference lines of the radiation sphere must be specified when describing its polarizations. At each point on the radiation sphere, the polarization is usually broken down into a pair of orthogonal polarizations, co-polarization and cross-polarization. To accomplish this, the co-polarization must be specified at each point on the radiation sphere.

In reference [22], Ludwig has provided three alternative definitions that can be used to define the polarizations at a point on the radiation sphere of an antenna. All three definitions are represented in Fig. 3.1. The first definition uses a rectangular coordinate system: one vector is given as the reference polarization direction (co-polarization) and another as cross-polarization direction. The second definition uses the spherical coordinate system unit tangential vectors at the point on the spherical surface as co-polarization and cross-polarization directions. In the last definition, "reference and cross polarization are defined to be what one measures when antenna pattern are taken in the

usual manner". In this thesis, the first and second definitions are used to describe polarizations of the antennas.

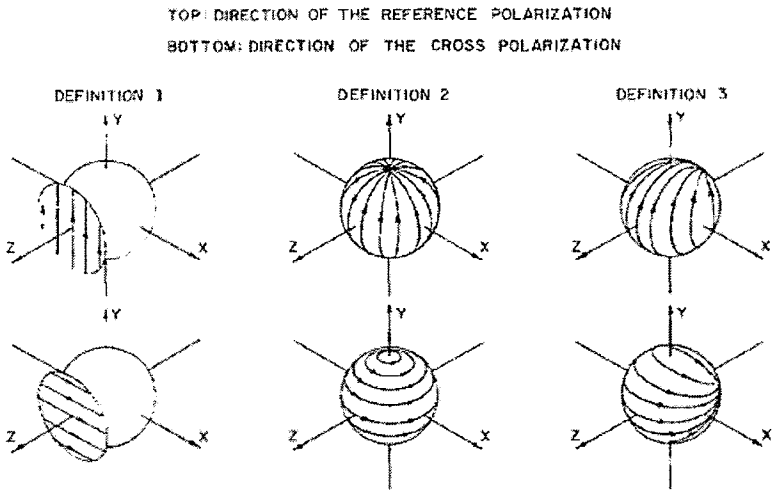

Fig. 3.1: Alternate polarization definition [22]

The following calculations are the procedure for obtaining polarization pattern of an antenna [20]. In the far field region, the spherical wave contains only θ and ϕ components of the electric field.

$$\mathrm{E} = E_\theta \hat{\theta} + E_\phi \hat{\phi} \tag{3.1}$$

where E_θ and E_ϕ are the phasor components in the direction of the unit vector $\hat{\theta}$ and $\hat{\phi}$.

The equation (3.1) can be rewritten as

$$\mathrm{E} = E_\theta \left(\hat{\theta} + \hat{\rho}_L \hat{\phi} \right) \tag{3.2}$$

with $\hat{\rho}_L = \dfrac{E_\phi}{E_\theta}$

where $\hat{\rho}_L$ is the linear polarization ratio, a complex constant.

As the time varies, the tip of the electric field traced in space over time. It occurs as an ellipse with the electric field rotating in either clockwise or counter clockwise (Fig. 3.2). τ is the tilt angle of the polarization ellipse measured from the x-axis and the angle of maximum response. The ratio between maximum and minimum linearly polarized responses on the ellipse is defined as axial ratio (AR).

$$AR(dB) = 20\log\frac{E_{\max}}{E_{\min}} \tag{3.3}$$

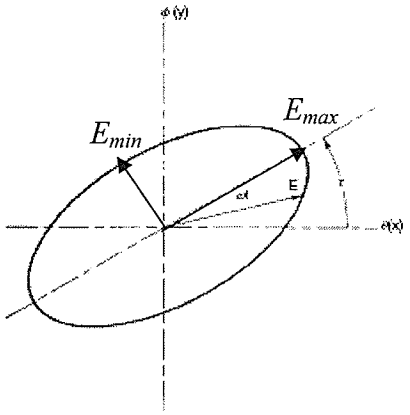

Fig. 3.2: Polarization ellipse [20]

If $\hat{\rho}_L = e^{\pm j\pi/2}$, the ellipse becomes a circle and the special case of circular polarization has appeared. On the other hand, when $\hat{\rho}_L$ = a constant number, the response will be pure linear polarization.

3.1.2 Circularly Polarized Microstrip Antennas

As stated earlier, the microstrip antenna is one of the low profile candidates for circular polarized applications. Thus, researchers have proposed many different configurations for microstrip antenna that radiate circularly polarized waves. Circularly

polarized waves are achieved when two orthogonal field components with equal amplitude but in phase quadrature are radiated. There are two types of circularly polarized microstrip antennas: the traveling-wave and the resonator types [6].

The traveling-wave antennas which radiate circularly polarized waves can be in single element or in an array form. The following Fig. 3.3 shows examples of some different approaches for single element traveling wave circularly polarized antennas. Fig. 3.4 shows an example of traveling-wave printed arrays for circular polarization (dipole and slot arrays).

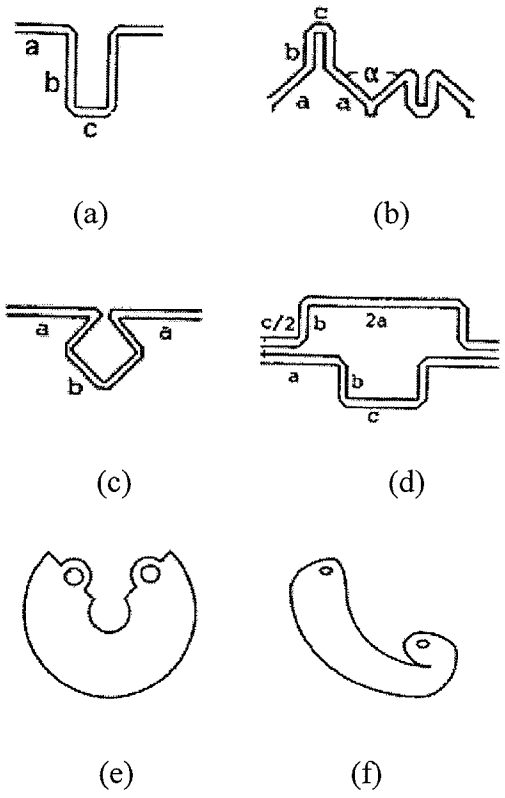

Fig. 3.3: Fundamental elements circular polarized curved microstrip line antenna: (a) rampart line antenna; (b) chain antenna; (c) square-loop microstrip line antenna; (d) crank-type microstrip line antenna; (e) sector of circular microstrip transmission line and (f) spiral microstrip line antenna [6]

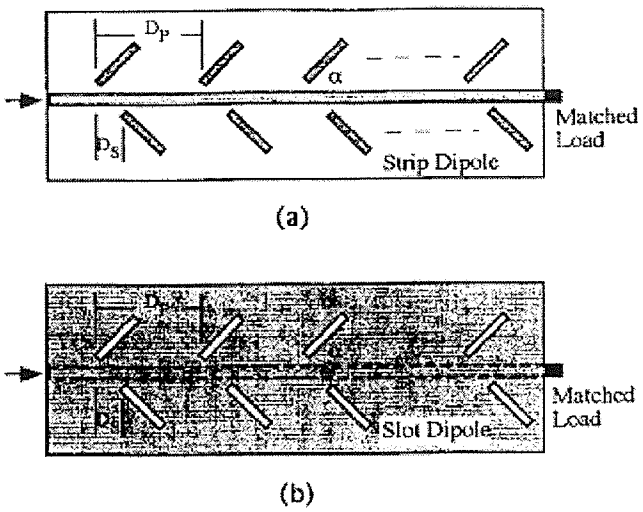

Fig. 3.4: Traveling-wave printed arrays for circular polarization: (a) dipole array and (b) slot array [6]

Microstrip patch antennas as a resonator-type are normally designed for linear polarization. In order to support circular polarization, a microstrip patch must radiate two orthogonal fields of equal amplitude but in phase quadrature. The approaches can be a single patch with proper excitations or an array of patches with certain arrangement and phasing. Single patch circular polarization can be achieved by using single feed or dual-orthogonal feed. The dual-orthogonal feed excites two orthogonal modes which have equal in amplitude but in phase quadrature. Fig. 3.5 shows typical configurations of dual-fed circularly polarized antennas. The single fed patch can radiate circular polarization by slightly perturbing a patch at appropriate locations with respect to the feed [6]. Fig. 3.6 gives typical configurations of single fed circularly polarized antennas.

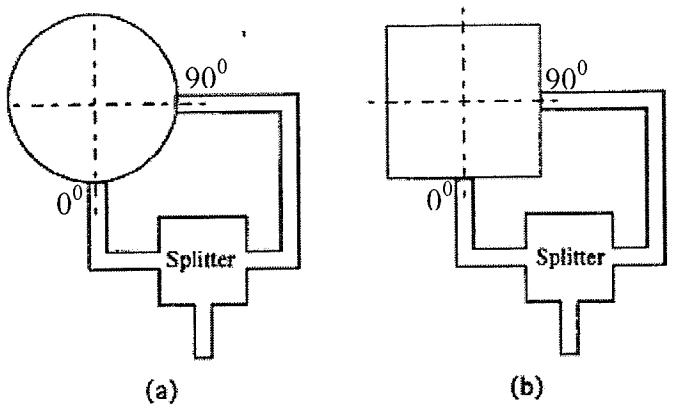

Fig. 3.5: Typical configurations of dual-fed circular polarized microstrip antennas: (a) circular patch and (b) square patch [6]

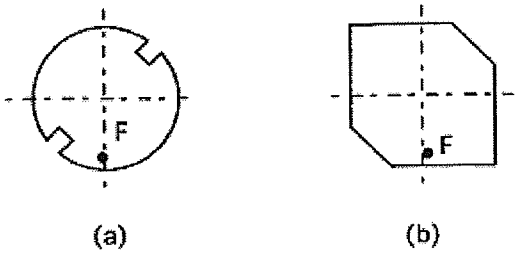

Fig. 3.6: Typical configurations of single fed circular polarized microstrip antennas: (a) circular patch and (b) square patch [6]

Due to simplification in manufacturing, many approaches for single feed circular polarized microstrip patches have been proposed. Fig. 3.6 and 3.7 show two types of single fed circular polarized patch antennas, which are differentiated by feeding location. Type A associates with the feed location on the x or y axis and type B is when feed location lies on the diagonal axis of the patch.

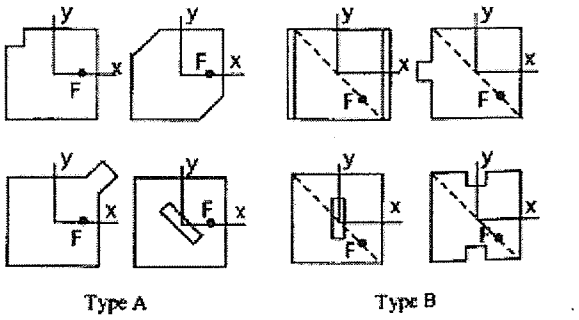

Fig. 3.7: Various types of microstrip antenna perturbations for circular polarization generation [6]

In [23], it has been shown that if an array of linearly polarized elements is placed in certain arrangement and phasing, it can also generate circularly polarized waves (Fig. 3.8). The advantage of this configuration is the wider axial ratio in comparison to single circularly polarized and dual-fed patch. However, the drawback of this technique is the requirement for a larger space volume for the antennas.

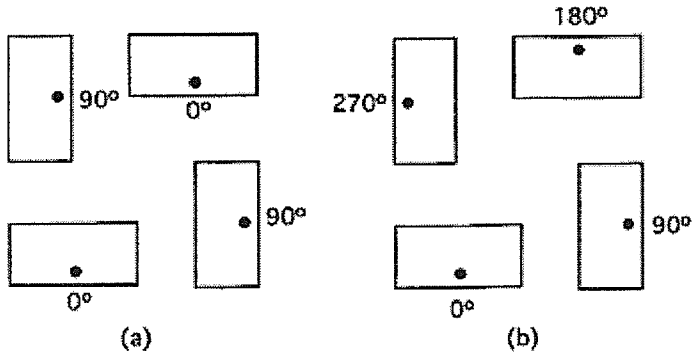

Fig. 3.8: 2x2 microstrip arrays with LP element for CP generation: (a) narrow-band arrangement and (b) wide-band arrangement [6]

3.2 Modified Koch Island Microstrip Antenna for Circular Polarization

In 1987, Wong [24] proposed a single-fed small circularly polarized square microstrip antenna, which is very similar to the Koch Island microstrip antenna (Fig. 3.9). The original, from previous chapter, Koch Island patch antenna can achieve circular polarization by slightly extending the length of the top and bottom slots. Moreover, the probe feed should be placed on the proper position along the diagonal axis of the patch. The feed will excite two orthogonal near-degenerate modes on the patch, which creates the circular polarization. The feed position point C gives left hand circular polarization (LHCP) and D is for right hand circular polarization (RHCP). In this section, a parametric study on the effect of slot sizes on resonant frequency, impedance bandwidth, and axial ratio bandwidth will be presented.

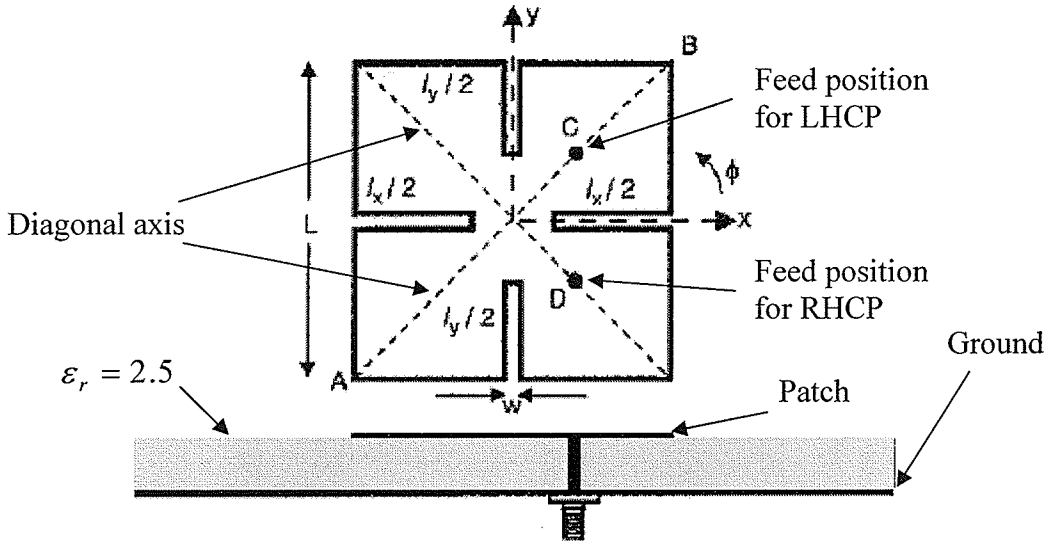

Fig. 3.9: Geometry of single feed small circularly polarized square microstrip antenna (modified Koch Island patch) with patch sizes of 40mm by 40mm, ground plane sizes of 80m by 80mm, dielectric constant $\varepsilon_r = 2.5$ *and substrate thickness* $h = 1.6mm$

In order to investigate the effect of slots on antenna operation, a microstrip patch antenna of size 40mm by 40 mm, dielectric constant $\varepsilon_r = 2.5$ and substrate thickness $h = 1.6mm$ was used. The ground plane was chosen at the size of 80mm by 80mm. All simulations were run on Ansoft Designer version 2.0 software package. In the first set of simulation, the slots width was fixed at $w = 2mm$, and then the slot lengths $l_x/2$ and $l_y/2$ were varied from 3 to 15 mm. The second set of simulation dealt with the variations of slots width w from 1 to 12 mm while the slot's length $l_x/2$ is fixed. However, the slot's length $l_y/2$ changes slightly in each case in order to get better circular polarized operation. The return loss, axial ratio versus frequency and angle were recorded and reported.

3.2.1 Effect of Slot Length

In this section, length of the slots of the proposed patch antenna is varied, while keeping the slot's width w constant. The slots lengths are given as $l_x/2$ = 3, 5, 7, 9, 11, 13, 15 mm. The slot widths is constant at w = 2mm. Fig. 3.10 shows the return loss graphs of the modified Koch Island patches, when varying the slot length. As the slot length is extended, the resonant frequency reduced dramatically but still maintained reasonable circularly polarized operation. The resonant frequency decreased from 2.247GHz for $l_x/2$ of 3mm to 1.559GHz for $l_x/2$ of 15mm (31% reduction). The return loss plots also show that the frequency reduction is more effective for longer slots lengths. With the same slot length increment longer slots give more dramatic changes in comparison to shorter slots (referred to Table 3.1). In other words, the slot's length is more sensitive to frequency reduction, when slot's length is longer. Fig. 3.11 shows the relationship between axial ratio and frequency of the same modified Koch Island patches at boresight. The response

is very similar to the return loss plots. The minimum axial ratio frequency is reduced, as the slots length decreased. Fig. 3.12 shows the relationship between the axial ratio and angle θ of the modified Koch Island patches at the frequencies that gave lowest axial ratio response and ϕ is set at 0 degree. The response for $\phi = 90$ degrees is very similar to the plots when $\phi = 0$. Therefore, only plots for $\phi = 0$ are shown. The 3dB beamwidths of all antennas for reasonable circular polarization are around 165 degrees; so these are very broad beamwidth antennas for circular polarized operation.

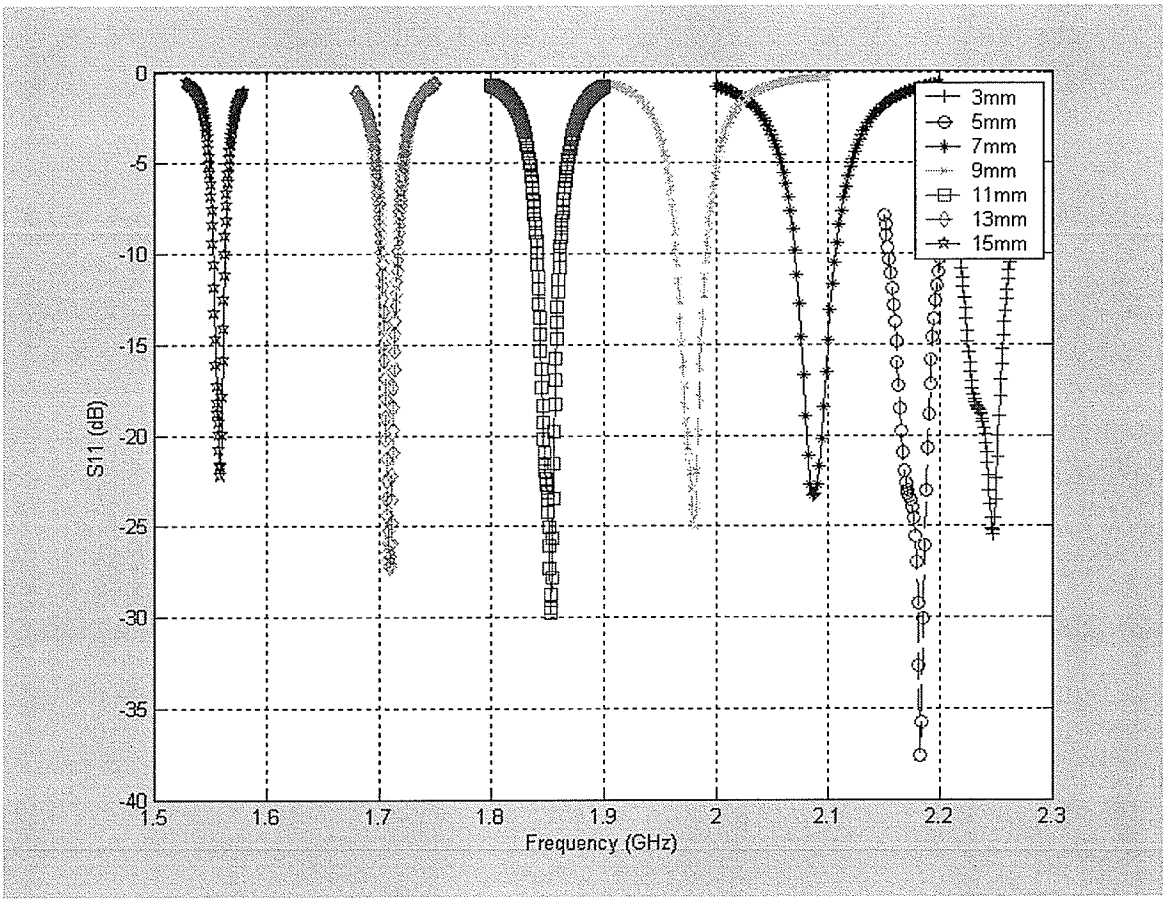

Fig. 3.10: Return losses of modified Koch Island patches at $l_x/2$ = 3, 5, 7, 9, 11, 13, 15mm, while keeping w = 2mm (in regard to Fig. 3.9)

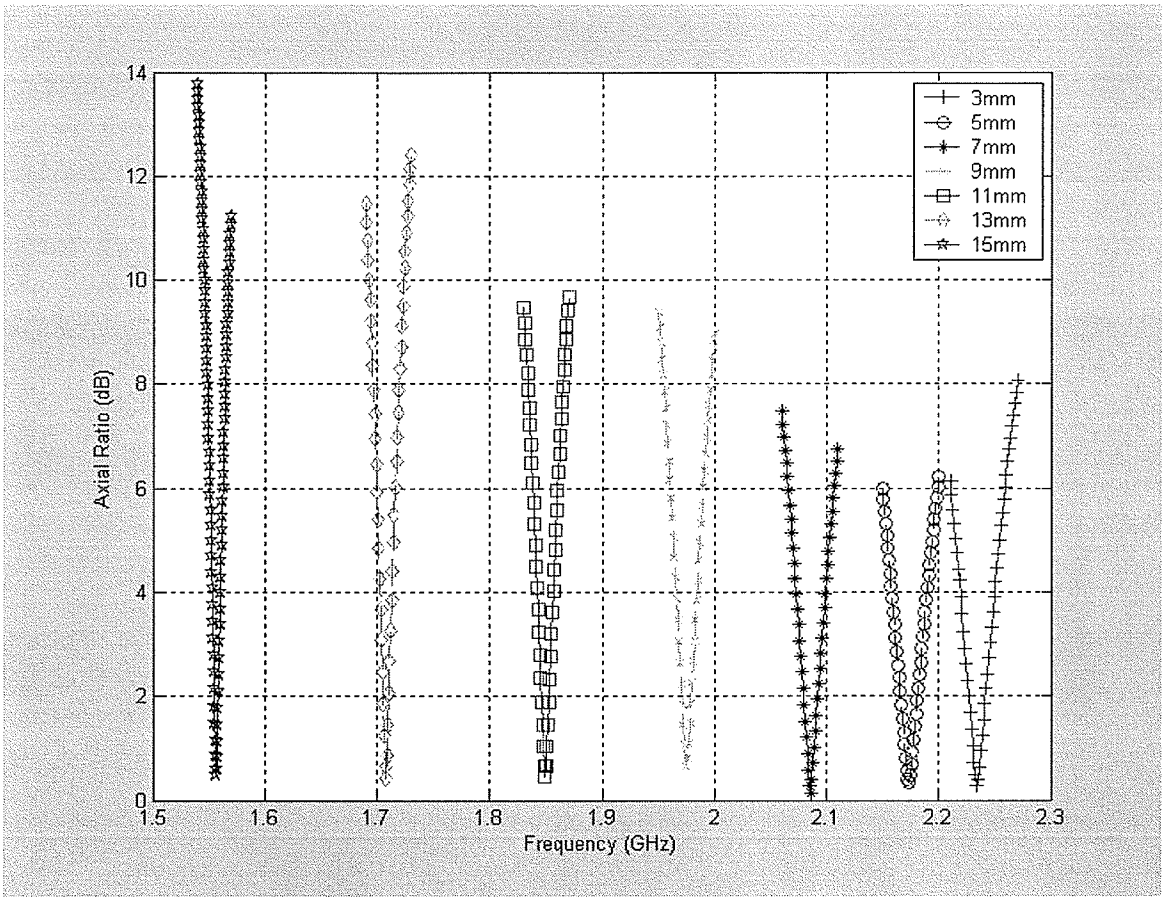

Fig. 3.11: Axial ratio versus frequency of modified Koch Island patches at $l_x/2$ = 3, 5, 7, 9, 11, 13, 15mm, while keeping w = 2mm (in regard to Fig. 3.9)

All the parameters of the Fig. 3.10 and Fig. 3.11 are summarized in Table 3.1. The first column shows the slot length $l_x/2$ of the patches and the second column gives the respective length $l_y/2$ in order to maintain circular polarization. The remaining columns show resonant frequency (f_{res}), lowest return loss (S_{11}), 10dB impedance bandwidth (BW), lowest axial ratio response frequency (f_{ar}), and 3dB axial ratio bandwidth (ARBW). The resonant frequency drops from 2.247GHz for $l_x/2$ = 3mm to 1.559GHz for $l_x/2$ = 15mm (31% reduction). Moreover, the 3dB axial ratio bandwidths fall within the 10dB impedance bandwidth, so the antennas can maintain their circular polarized

operation within reasonable return losses. The impedance bandwidth of the antennas decrease from 2% for $l_x/2$ = 3mm to 0.45% for $l_x/2$ = 15mm. The 3dB axial ratio bandwidth is within the 10dB impedance bandwidth and also decreases as the slot length extend. It decreases from 1% for $l_x/2$ = 3mm to 0.45% for $l_x/2$ = 15mm. As slot length extend further, the 3dB axial ratio bandwidth is closer to the 10dB impedance bandwidth. Furthermore, the lowest axial ratio frequency also approaches the resonant frequency as slot length expand, 1.557GHz and 1.559GHz for $l_x/2$ = 15mm. However, when the slots approach the centre of the patch, it is more difficult to choose the feeding point for the antennas (more sensitive to feed locations).

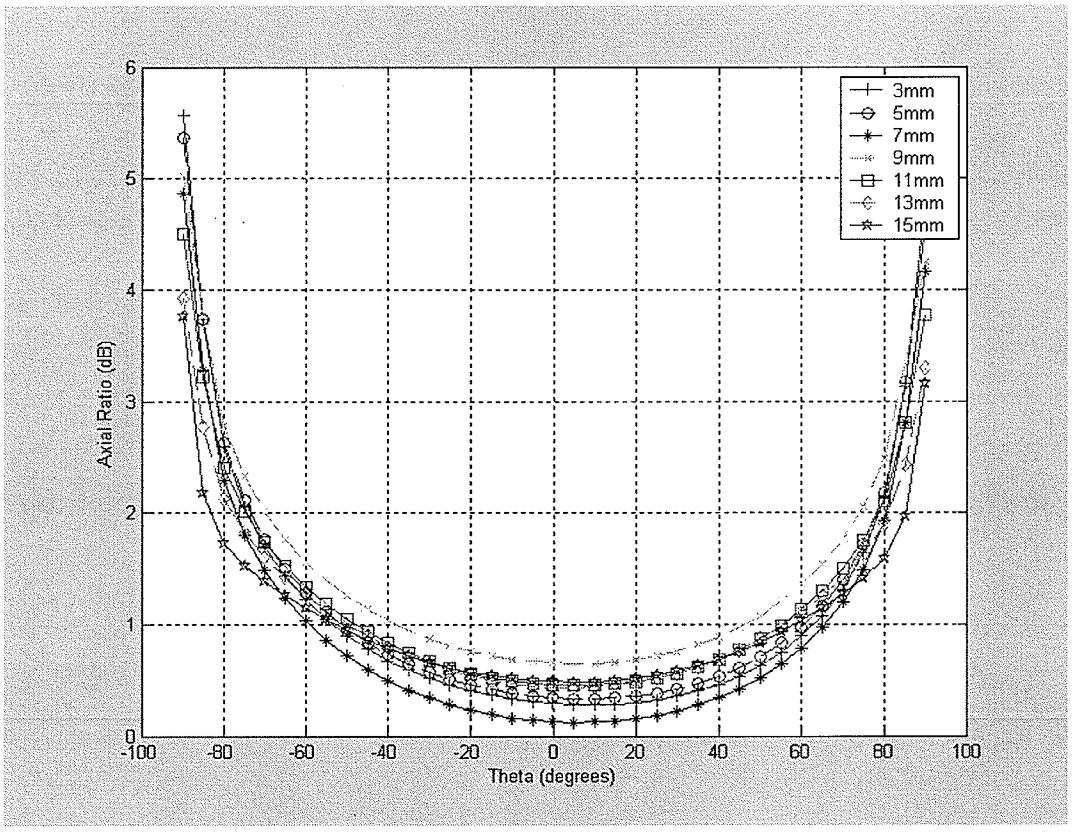

Fig. 3.12: Axial ratio versus angle θ of modified Koch Island patches at $l_x/2$ = 3, 5, 7, 9, 11, 13, 15mm, while keeping w = 2mm (in regard to Fig. 3.9)

Table 3.1: Relationships between slot length ($l_x/2$) and resonant frequency (f_{res}), -10dB impedance bandwidth (BW), lowest response axial ratio frequency (f_{ar}), 3dB axial ratio bandwidth (ARBW) of antenna in Fig. 3.9

$l_x/2$ (mm)	$l_y/2$ (mm)	f_{res} (GHz)	S_{11min} (dB)	BW (GHz)	f_{ar} (GHz)	ARBW (GHz)
3	4	2.247	-25.44	2.218 – 2.264	2.234	2.223 – 2.246
5	5.75	2.182	-37.63	2.154 – 2.185	2.174	2.162 – 2.185
7	7.50	2.085	-23.31	2.070 – 2.106	2.086	2.076 – 2.096
9	9.30	1.980	-24.96	1.964 – 1.992	1.975	1.968 – 1.982
11	11.20	1.853	-29.52	1.841 – 1.862	1.849	1.844 – 1.854
13	13.15	1.709	-27.21	1.702 – 1.716	1.708	1.705 – 1.712
15	15.10	1.559	-22.20	1.553 – 1.560	1.557	1.554 – 1.560

3.2.2 Effect of Slot Width

This section deals with the effects of the slot width of the proposed modified Koch Island patches. The slot's length is kept constant at $l_x/2$ = 7mm, then the slot width w is varied from 1mm to 12mm. The return losses and axial ratios are recorded similarly to the previous section. Fig. 3.13 shows the return losses of the modified Koch Island patch antennas with varying slot widths. The resonant frequency does not change much as the slot's width expands in compare to slot's length expansion. The resonant frequency is

2.122GHz for w = 1mm and 2.037GHz for w = 12mm. Moreover, the resonant frequency does not seem to change, when the slot's width w expands beyond 9mm. Therefore, the antenna slot width does contribute much to the process of miniaturization.

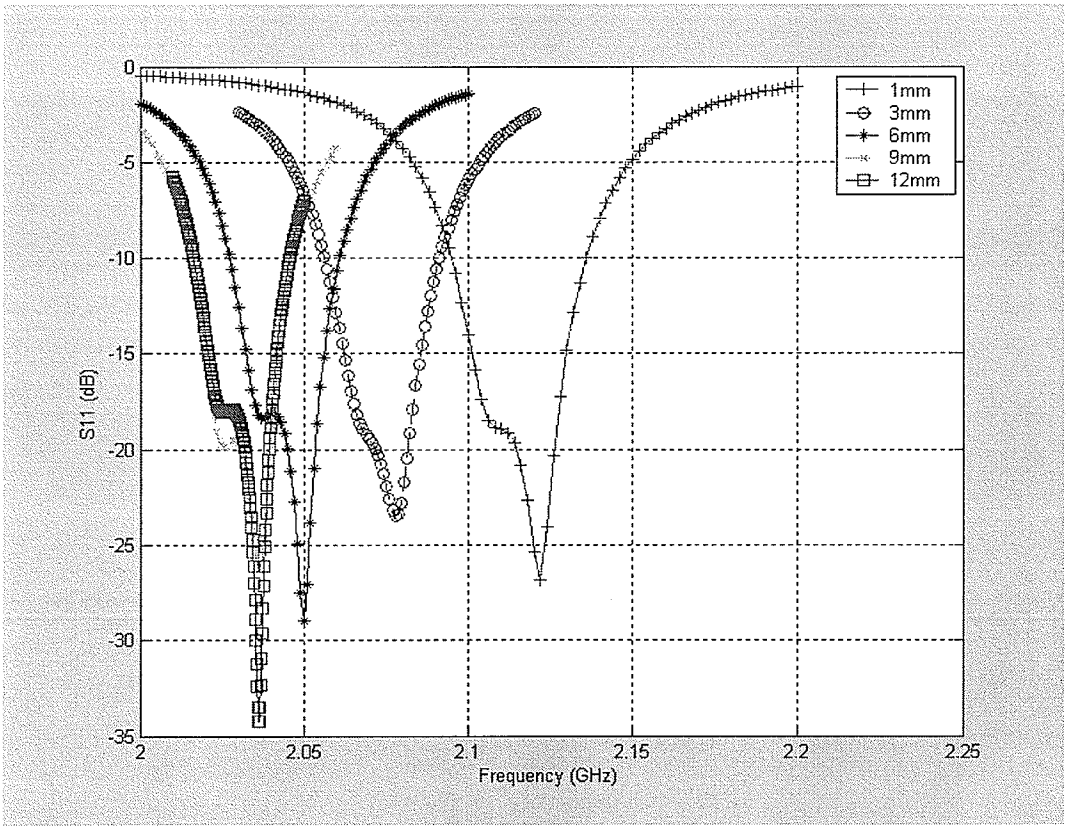

Fig. 3.13: Return losses of modified Koch Island patches at w = 1, 3, 6, 9, 12mm, while keeping $l_x/2$ = 7mm (in regard to Fig. 3.9)

The relationship between axial ratio and frequency of the proposed antennas is shown in the Fig. 3.14 below. The axial ratio is measured at boresight of the antenna. Similarly, the slot's width does not have much effect on the axial ratios of the antennas. The lowest axial ratio frequency shifts only from f_{ar} = 2.111GHz for w = 1mm to f_{ar} = 2.028GHz for w = 12mm.

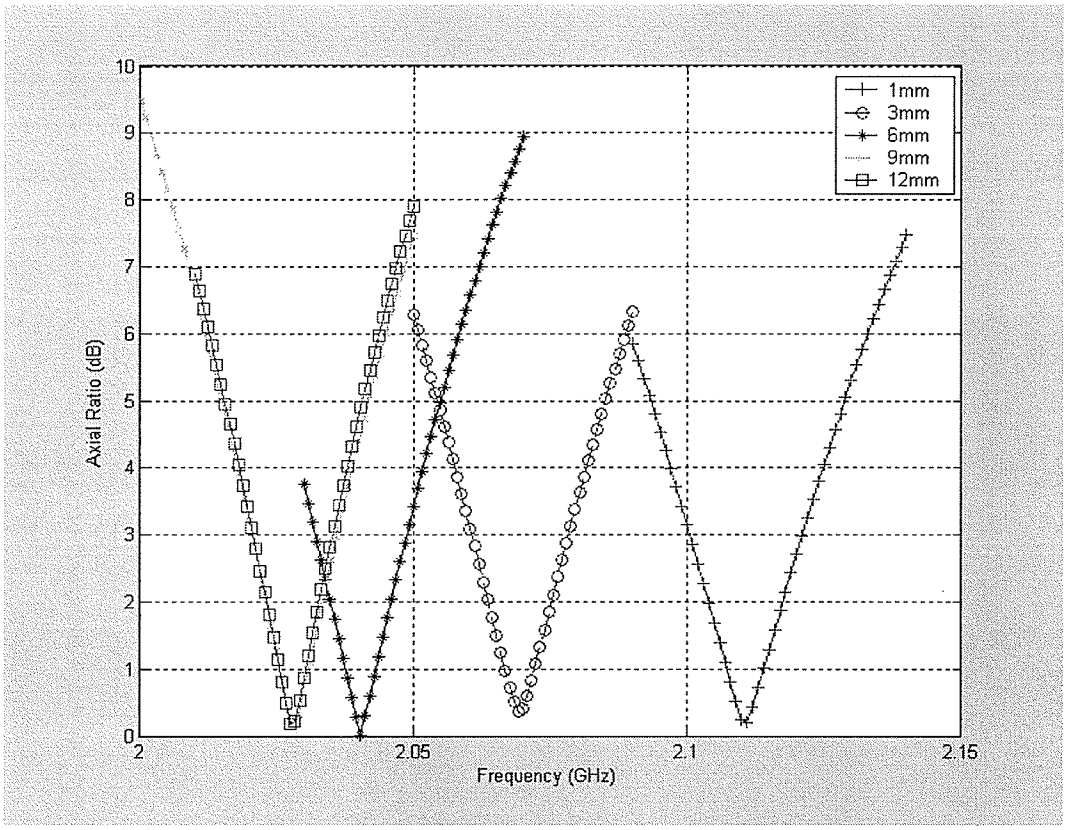

Fig. 3.14: Axial ratio versus frequency of modified Koch Island patches at w = 1, 3, 6, 9, 12mm, while keeping $l_x/2$ = 7mm (in regard to Fig. 3.9)

Fig. 3.15 shows the relationship between the axial ratio and angle θ of the modified Koch Island patches at the frequencies that gave the lowest axial ratio response, and ϕ is set at 0 degree. The plots show only the axial ratio at $\phi = 0$ degrees because the axial ratio at $\phi = 90$ degree is very similar. In these cases, the 3dB axial ratio beamwidths are also around 165 degrees, and a very broad beam. Therefore, changing the slot's width does not affect the circular polarized beamwidth of the antenna.

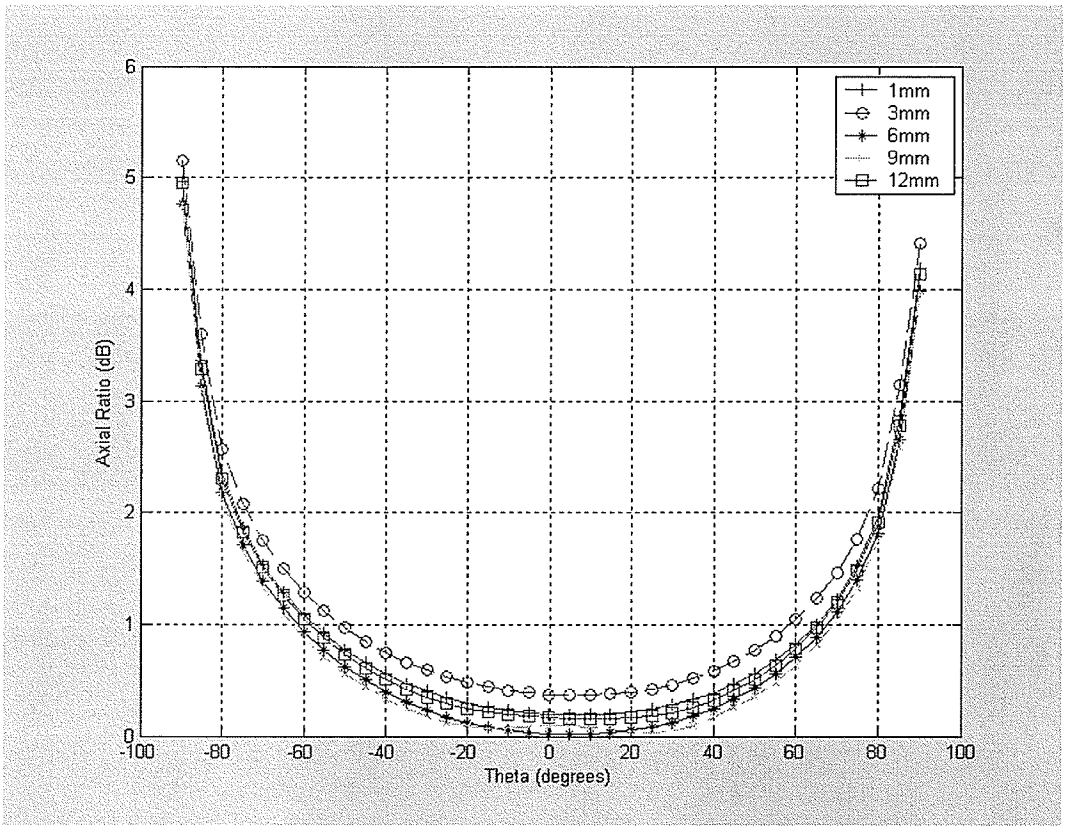

Fig. 3.15: Axial ratio versus angle θ of modified Koch Island patches at w = 1, 3, 6, 9, 12mm, while keeping $l_x/2$ = 7mm (in regard to Fig. 3.9)

The resonant frequency, 10dB impedance bandwidths and 3dB axial ratio bandwidths of the modified Koch Island patches, for varying slots widths, are given in Table 3.2. As shown, the 3dB axial ratio bandwidth still falls within the 10dB impedance bandwidth. The resonant frequency and the lowest axial ratio frequency response decrease as the slot width increases. However, the variation of the slot's width does not have much effect on the operation of the antenna.

Table 3.2: Relationships between slot width (w) and resonant frequency (f_{res}), -10dB impedance bandwidth (BW), lowest axial ratio frequency (f_{ar}), 3dB axial ratio bandwidth (ARBW) of antenna in Fig. 3.9

w (mm)	f_{res} (GHz)	S_{11min} (dB)	BW (GHz)	f_{ar} (GHz)	ARBW(GHz)
1	2.122	-26.84	2.095 – 2.136	2.111	2.101 – 2.121
3	2.078	-23.49	2.056 – 2.092	2.069	2.060 – 2.078
6	2.044	-28.96	2.023 – 2.062	2.040	2.032 – 2.049
9	2.036	-26.32	2.015 – 2.047	2.028	2.020 – 2.036
12	2.036	-34.22	2.016 – 2.046	2.028	2.021 – 2.035

In order to see the effect of the slot sizes on the resonant frequency and axial ratio of the modified Koch Island patch antenna, several more cases will be investigated. At first, the substrate permittivity is fixed at 2.5 but the height of the substrate is varied through h = 0.78mm, 1.6mm, and 3.2mm. On the other hand, the substrate height will be kept at constant h = 1.6mm while varying its permittivity through ε_r = 1.01, 2.5, and 9.8, in the second set of cases. Table 3.3 – Table 3.12 show the relationship between slots sizes and resonant frequency (f_{res}), -10dB impedance bandwidths (BW), lowest axial ratio frequency (f_{ar}), 3dB axial ratio bandwidths (ARBW) of antenna in Fig. 3.9. Once again, it is very clear that only the slot length ($l_x/2$) has a significant effect on the resonant frequency of the nearly Koch Island microstrip patch antenna. Longer slot lengths give lower resonant frequencies. In all the cases, the 3dB axial ratio bandwidth (ARBW) falls

within the -10dB impedance bandwidth (BW) of the antenna. Moreover, ARBW is around 50% of the BW. The effect of substrate parameters (height and permittivity) on the antenna resonant frequency is also significant. The substrate height mostly affects the antenna impedance bandwidth. As shown in the Tables, a higher substrate thickness (h) results in a broader impedance bandwidth. For example, by comparing Table 3.3 and Table 3.5, one can see that the impedance bandwidth when h = 3.2mm is more than three times larger than the one with h = 0.78mm. On the other hand, the antenna resonant frequency can be reduced by increasing its substrate permittivity. For example, the resonant frequency for the antenna with permittivity of 9.8 is about three times lower than the one with permittivity of 1.01 (compare Table 3.9 and Table 3.11). However, the slot length ($l_x/2$) has less effect on the resonant frequency in the case of high permittivity. As in Table 3.11, the resonant frequency does not change much as the slot length increases. Fig. 3.16 and Fig. 3.18 show the plots of the relationship between resonant frequency and the slot length of the nearly Koch Island patch antenna for circular polarization. In addition, the relationships between the lowest axial ratio frequency and the slot length are shown in Fig. 3.17 and Fig. 3.19.

Table 3.3: Relationships between slot length ($l_x/2$) and resonant frequency (f_{res}), -10dB impedance bandwidth (BW), lowest axial ratio frequency (f_{ar}), 3dB axial ratio bandwidth (ARBW) of antenna in Fig. 3.9

h = 0.78mm, ε_r = 2.5, w = 2mm				
$l_x/2$ (mm)	f_{res} (GHz)	BW (%)	f_{ar} (GHz)	ARBW (%)
3	2.27	1.32	2.275	0.70
5	2.20	1.23	2.198	0.64
7	2.09	1.24	2.094	0.57
9	1.97	0.92	1.965	0.46
11	1.83	0.66	1.823	0.33

Table 3.4: Relationships between slot width (w) and resonant frequency (f_{res}), -10dB impedance bandwidth (BW), lowest axial ratio frequency (f_{ar}), 3dB axial ratio bandwidth (ARBW) of antenna in Fig. 3.9

h = 0.78mm, ε_r = 2.5, $l_x/2$ = 7mm				
w (mm)	f_{res} (GHz)	BW (%)	f_{ar} (GHz)	ARBW (%)
1	2.120	0.94	2.116	0.47
3	2.080	0.96	2.082	0.43
6	2.050	0.97	2.051	0.49
9	2.040	0.93	2.041	0.44
12	2.040	0.98	2.036	0.49

Table 3.5: Relationships between slot length ($l_x/2$) and resonant frequency (f_{res}), -10dB impedance bandwidth (BW), lowest axial ratio frequency (f_{ar}), 3dB axial ratio bandwidth (ARBW) of antenna in Fig. 3.9

h = 3.2mm, ε_r = 2.5, w = 2mm				
$l_x/2$ (mm)	f_{res} (GHz)	BW (%)	f_{ar} (GHz)	ARBW (%)
3	2.190	4.61	2.152	2.56
5	2.140	4.24	2.105	2.14
7	2.080	3.88	2.040	1.86
9	1.990	2.53	1.962	1.32
11	1.880	2.14	1.862	1.13

Table 3.6: Relationships between slot width (w) and resonant frequency (f_{res}), -10dB impedance bandwidth (BW), lowest axial ratio frequency (f_{ar}), 3dB axial ratio bandwidth (ARBW) of antenna in Fig. 3.9

h = 3.2mm, ε_r = 2.5, $l_x/2$ = 7mm				
w (mm)	f_{res} (GHz)	BW (%)	f_{ar} (GHz)	ARBW (%)
1	2.100	3.37	2.065	1.94
3	2.060	3.42	2.028	1.68
6	2.030	2.97	2.004	1.45
9	2.010	3.00	1.988	1.51
12	2.010	2.49	1.990	1.20

Table 3.7: Relationships between slot length ($l_x/2$) and resonant frequency (f_{res}), -10dB impedance bandwidth (BW), lowest axial ratio frequency (f_{ar}), 3dB axial ratio bandwidth (ARBW) of antenna in Fig. 3.9

h = 1.6mm, ε_r = 2.5, w = 2mm				
$l_x/2$ (mm)	f_{res} (GHz)	BW (%)	f_{ar} (GHz)	BW (%)
3	2.25	2.32	2.23	1.17
5	2.18	2.07	2.17	1.01
7	2.09	1.91	2.08	0.86
9	1.98	1.41	1.99	0.71
11	1.85	1.08	1.85	0.54

Table 3.8: Relationships between slot width (w) and resonant frequency (f_{res}), -10dB impedance bandwidth (BW), lowest axial ratio frequency (f_{ar}), 3dB axial ratio bandwidth (ARBW) of antenna in Fig. 3.9

h = 1.6mm, ε_r = 2.5, $l_x/2$ = 7mm				
w (mm)	f_{res} (GHz)	BW (%)	f_{ar} (GHz)	ARBW (%)
1	2.12	1.84	2.11	0.95
3	2.08	1.64	2.07	0.82
6	2.05	1.61	2.04	0.78
9	2.04	1.48	2.03	0.79
12	2.03	1.33	2.03	0.74

Table 3.9: Relationships between slot length ($l_x/2$) and resonant frequency (f_{res}), -10dB impedance bandwidth (BW), lowest axial ratio frequency (f_{ar}), 3dB axial ratio bandwidth (ARBW) of antenna in Fig. 3.9

h = 1.6mm, ε_r = 1.01, w = 2mm				
$l_x/2$ (mm)	f_{res} (GHz)	BW (%)	f_{ar} (GHz)	BW (%)
3	3.38	3.27	3.34	1.65
5	3.28	3.06	3.24	1.54
7	3.14	2.56	3.11	1.35
9	2.96	2.03	2.94	1.02
11	2.76	1.45	2.74	0.80

Table 3.10: Relationships between slot width (w) and resonant frequency (f_{res}), -10dB impedance bandwidth (BW), lowest axial ratio frequency (f_{ar}), 3dB axial ratio bandwidth (ARBW) of antenna in Fig. 3.9

h = 1.6mm, ε_r = 1.01, $l_x/2$ = 7mm				
w (mm)	f_{res} (GHz)	BW (%)	f_{ar} (GHz)	ARBW (%)
1	3.18	2.92	3.15	1.40
3	3.11	2.84	3.08	1.33
6	3.06	2.63	3.03	1.25
9	3.03	2.32	3.01	1.06
12	3.02	2.00	2.99	1.00

Table 3.11: Relationships between slot length ($l_x/2$) and resonant frequency (f_{res}), -10dB impedance bandwidth (BW), lowest axial ratio frequency (f_{ar}), 3dB axial ratio bandwidth (ARBW) of antenna in Fig. 3.9

h = 1.6mm, ε_r = 9.8, w = 2mm				
$l_x/2$ (mm)	f_{res} (GHz)	BW (%)	f_{ar} (GHz)	ARBW (%)
3	1.165	0.86	1.165	0.43
5	1.135	0.70	1.135	0.44
7	1.092	0.73	1.093	0.37
9	1.036	0.77	1.036	0.39
11	0.972	0.82	0.970	0.41

Table 3.12: Relationships between slot width (w) and resonant frequency (f_{res}), -10dB impedance bandwidth (BW), lowest axial ratio frequency (f_{ar}), 3dB axial ratio bandwidth (ARBW) of antenna in Fig. 3.9

h = 1.6mm, ε_r = 9.8, $l_x/2$ = 7mm				
w (mm)	f_{res} (GHz)	BW (%)	f_{ar} (GHz)	ARBW (%)
1	1.104	0.81	1.104	0.36
3	1.084	0.74	1.084	0.37
6	1.071	0.65	1.071	0.37
9	1.068	0.56	1.068	0.37
12	1.067	0.75	1.067	0.37

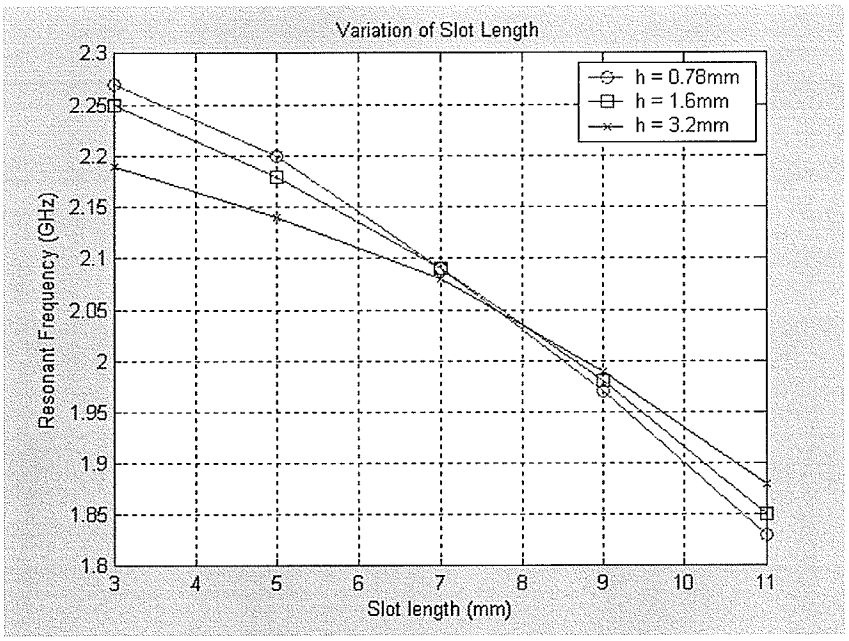

Fig. 3.16: Resonant frequency (f_{res}) versus slot length ($l_x/2$), with ε_r = 2.5 and different substrate height h = 0.78mm, 1.6mm, and 3.2mm

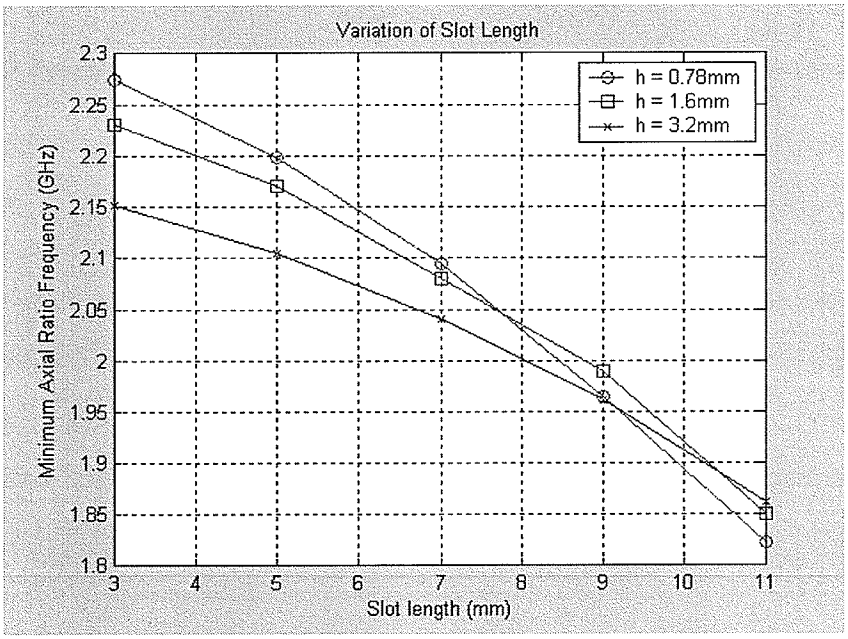

Fig. 3.17: Minimum axial ratio frequency (f_{ar}) versus slot length ($l_x/2$) with ε_r = 2.5 and different substrate heights h = 0.78mm, 1.6mm, and 3.2mm

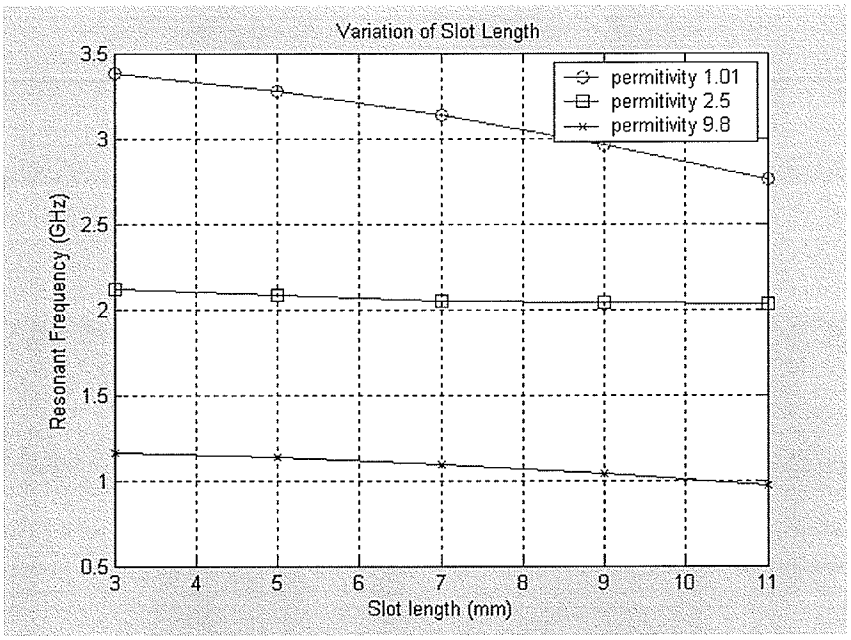

Fig. 3.18: Resonant frequency (f_{res}) versus slot length ($l_x/2$), with h = 1.6mm and different substrate permittivities ε_r = 1.01, 2.5, and 9.8

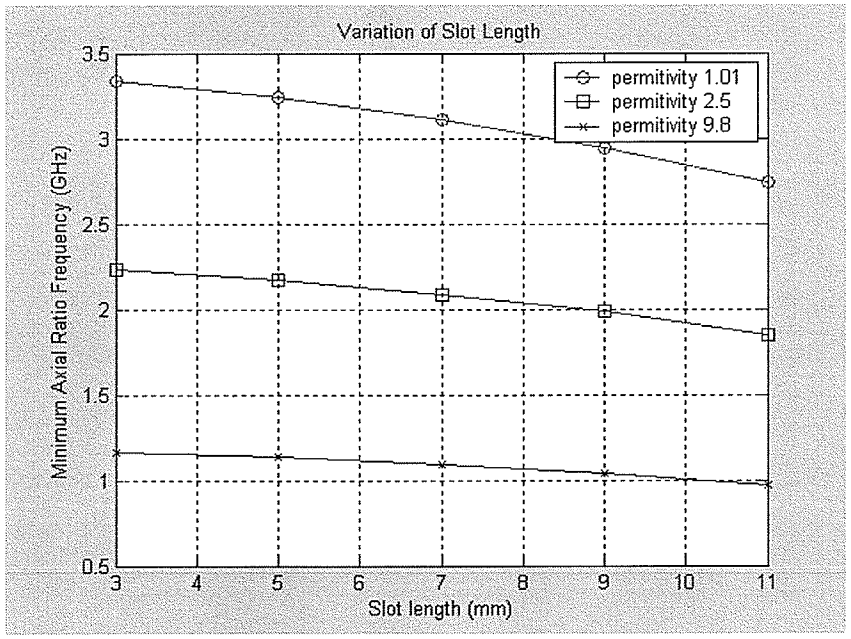

Fig. 3.19: Minimum axial ratio frequency (f_{ar}) versus slot length ($l_x/2$), with h=1.6mm and different substrate permittivities ε_r = 1.01, 2.5, and 9.8

3.3 Summary

In this chapter, background of antenna polarization and circular polarization was presented. The fundamental techniques to construct circularly polarized microstrip patch antennas also were reviewed. The proposed modified Koch Island microstrip patch antenna for circularly polarized operation was studied. The results show that the modified Koch Island microstrip antenna is a good candidate for compact circularly polarized application. However, this antenna also has the limitation of narrow bandwidth like other miniaturized antennas. Therefore, bandwidth enhancement for miniaturized antennas is essential. The next chapter will be dealing with the bandwidth enhancement for microstrip patch antennas.

Chapter 4

Bandwidth Enhancement by Slots Loading Ground Plane

4.1 Introduction

Although microstrip antennas have many advantages, they also suffer from serious limitations, such as low gain, low power handling capability and narrow bandwidth. Furthermore, antenna miniaturization will bring the antenna bandwidth further down from conventional antennas. Therefore, bandwidth enhancement techniques are necessary to overcome this limitation. Over the years, antenna researchers have proposed a large number of methods in order to enhance microstrip antenna bandwidth. However, the most popular techniques are: changing the substrate parameters, choosing a suitable patch shape, using aperture coupled feeding technique, multi-mode operation, impedance matching, and resistive loading. The bandwidth of microstrip antenna can be expressed in term of its voltage standing wave ratio (VSWR) and quality factor (Q) as in equation (1.6).

Therefore, antenna impedance bandwidth is inversely proportional to the quality factor (Q_t). It means lower quality factor will result a broader bandwidth.

4.1.1 Changing Substrate Parameters for Broadband Operation

As stated in [6], the impedance bandwidth of the patch antenna increases monotonically with substrate thickness and it decreases with increase in relative

permittivity ε_r. By changing these two parameters, the quality factor (Q_t) will be varied. The quality factor (Q_t) is expressed by:

$$Q = \frac{Energy\_stored}{Power\_lost}$$

In [6], the patch antenna was modeled as a lossy capacitor. When the substrate thickness is increases, the stored energy decreases; therefore, the quality factor Q_t decreases. On the other hand, the stored energy increases by increasing the relative permittivity ε_r of the substrate. The relationship between the quality factor Q_t and the substrate thickness or value of relative permittivity are shown in Fig. 4.1 and Fig. 4.2.

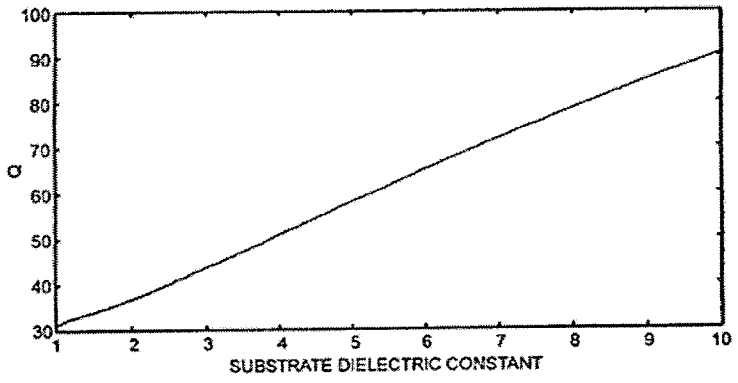

Fig. 4.1: Variation of Q for a rectangular patch antenna as a function of substrate dielectric constant; h = 1.59mm; W = 0.9L, f = 3GHz [6]

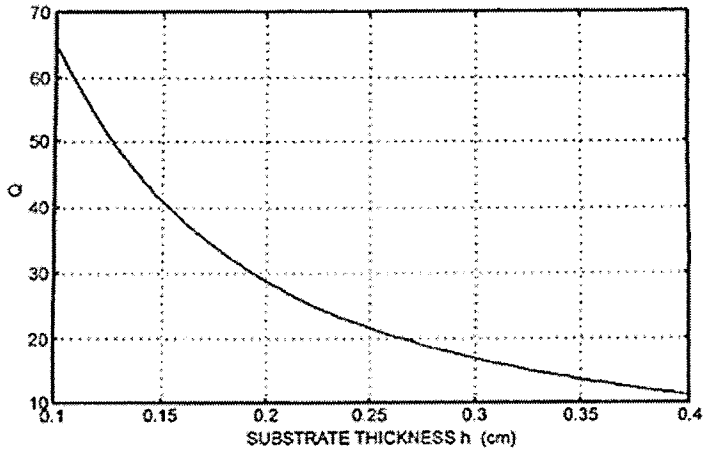

Fig. 4.2: Variation of Q for a rectangular patch antenna as a function of substrate thickness; $\varepsilon_r = 2.2$, $W = 0.9L$, $f = 3GHz$ *[6]*

4.1.2 Suitable Patch Shapes for Broadband Operation

There have been many approaches for bandwidth enhancement by changing the geometry of the conventional patch. The patch shapes can be annular ring, rectangular/square ring, quarter-wave (shorted) patch [6], or other possible geometries. In [25] Huynh and Lee have proposed one of the most popular designs, the U-slot patch antenna, which can give the factional impedance bandwidth of 40% (Fig. 4.3 and Fig. 4.4).

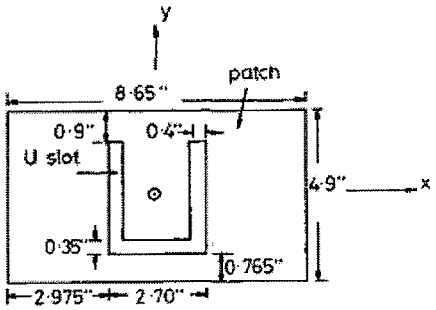

Fig. 4.3: Geometry of a broadband U-slot microstrip patch antenna [25]

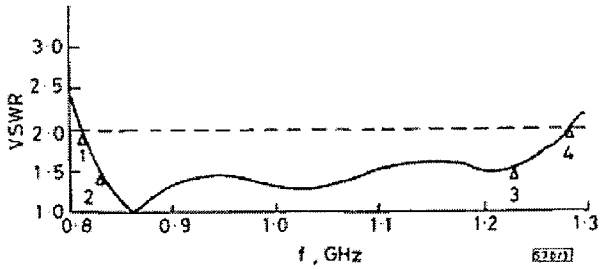

Fig. 4.4: Measured VSWR versus frequency for the above U-slot antenna[25]

4.1.3 Aperture Coupled Feed for Broadband Operation

The aperture coupling method has been used to enhance the bandwidths of the conventional microstrip patch antenna. This feeding technique uses thick layers of substrate which give a large number of parameters that can be adjusted. The parameters included aperture length, width and shape. The stub dimensions are also adjustable in order to optimize the bandwidth enhancement. A 70% bandwidth antenna has been proposed by using this feeding technique [6]. Fig 4.5 shows a typical aperture coupled feed microstrip antenna.

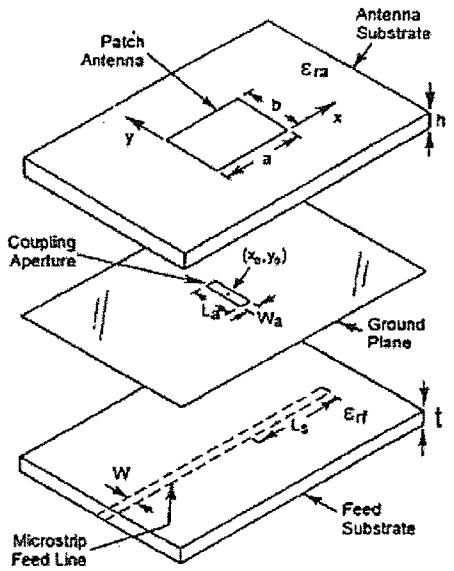

Fig. 4.5: Exploded view of an aperture coupled microstrip antenna [6]

The shape of the aperture that is used in this technique can be in many forms. Fig. 4.6 shows some of the popular aperture shapes that have been proposed for wideband application.

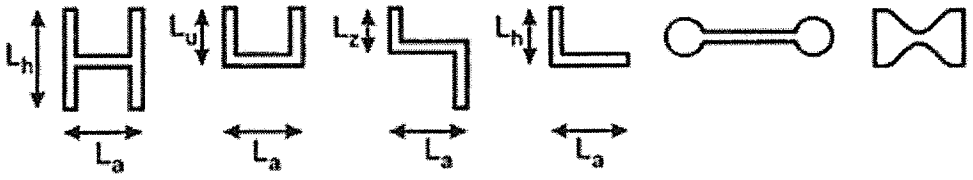

Fig. 4.6: Various aperture shapes used in aperture coupled microstrip antennas[6]

4.1.4 Multi-Modes for Broadband Operation

In this technique, a number of resonant modes are excited on a single patch or on several different patches which are closely coupled to each other but resonating at slightly different frequencies [26]. The single element technique is very much the same as using suitable patch geometry, so that it can resonate at several close frequencies. The U-slot patch antenna in [27] is a good example of this technique. For two or more elements, the elements can be located on the same level (parasitic coupling) or on top of each other (stacked patches). Fig. 4.7 shows the exploded view of a typical aperture coupled stacked microstrip antenna. Impedance bandwidths of 10% to 67% have been achieved by using this technique. Fig. 4.8 demonstrates some coplanar parasitically coupled configurations for wideband application [6].

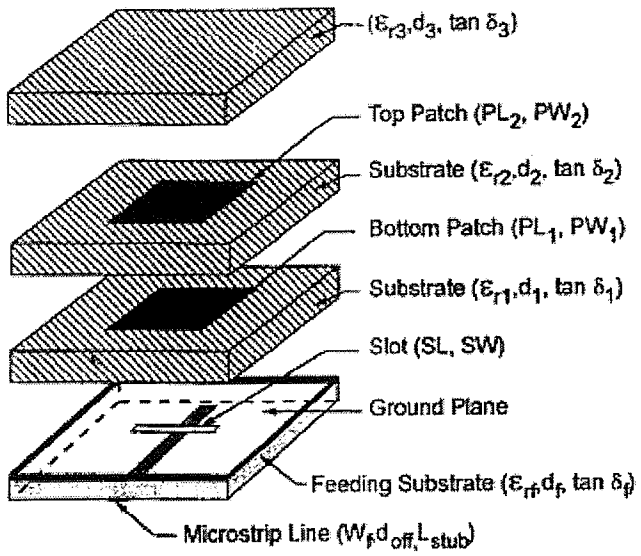

Fig. 4.7: Exploded view of a typical aperture coupled stacked microstrip antenna[6]

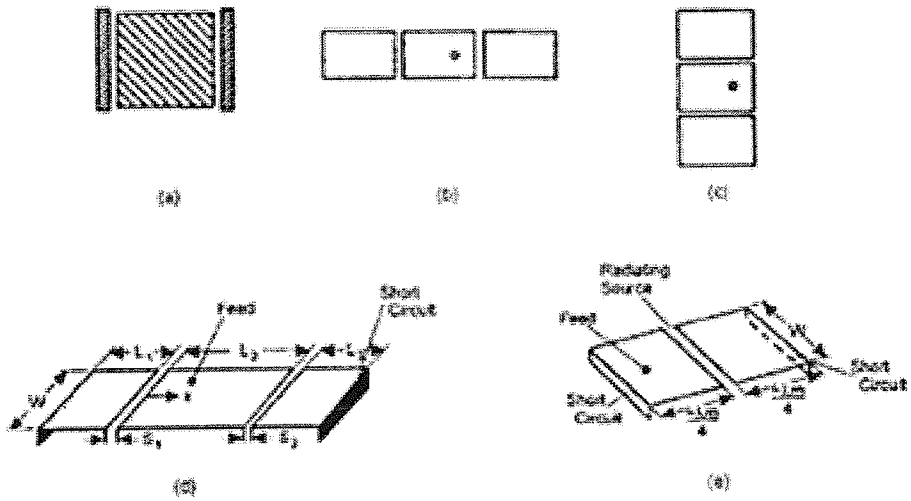

Fig. 4.8: Some configurations of broadband microstrip antennas using coplanar gap-coupled resonators [6]

4.1.5 Impedance Matching for Broadband Operation

It has been found that, except for a single-feed circular polarized element, the microstrip antenna impedance bandwidth is limited only by the resonant behavior of the input impedance and not by their radiation pattern or gain variations [28]. Therefore, impedance matching is one of the most direct techniques that has been used to increase the antenna bandwidth. This technique uses an impedance matching network, which can be stubs and quarter-wave transformers, in the feed part of the microstrip antenna. In reference [28], a simple matching network of stubs and quarter-wave transformers, which gives 10% to 20% bandwidth, has been proposed (Fig. 4.9). By using a more complicated impedance matching technique, a 90% impedance bandwidth has been achieved in [29] by Herscovici.

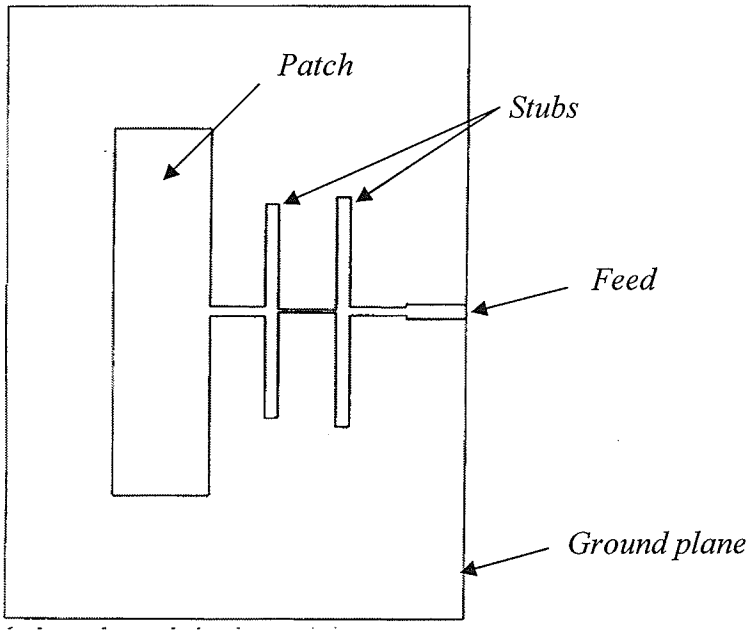

Fig. 4.9: Layout of rectangular impedance-matched antenna [28]

4.1.6 Resistive Loading for Broadband Operation

As stated in [6], the impedance bandwidth of a patch antenna can be increased by introducing losses in the antenna. The losses can be in many different forms such as lossy substrate material, layer of lossy film, or a discrete chip resistor. However, a drawback of this technique is the reduction in antenna radiation efficiency. In [30], Wong has proposed a study on chip resistor loading at the edge of a rectangular patch antenna (Fig. 4.10). In this microstrip antenna, a 9.3% bandwidth has been achieved, which is almost 5 times the original bandwidth of the patch without chip resistor loading.

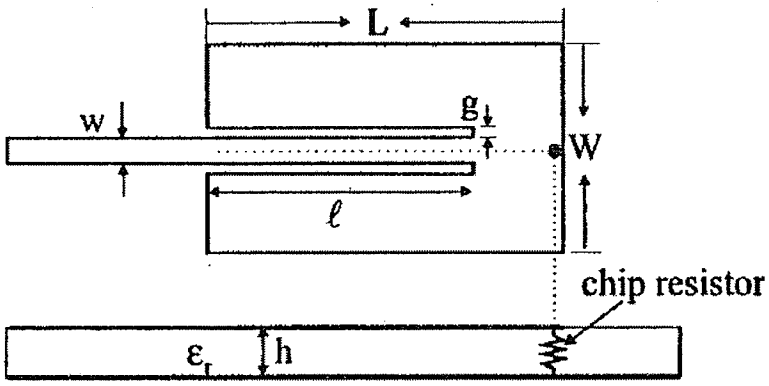

Fig. 4.10: Geometry of a compact broadband rectangular microstrip antenna with chip-resistor loading [30]

4.2 Slot Loading of Ground Plane for Broadband Operation

In previous sections, an overview of popular techniques for bandwidth enhancement in microstrip antenna was presented. However, there is another less popular broadband technique that has been proposed by Chiou and Wong in [31]. In this technique, a pair of narrow slots was embedded along the centerline of the ground plane which is perpendicular to the antenna's resonant direction. The slots will cause the surface current paths to meander on the ground plane, which leads to antenna miniaturization, the back radiation increases the losses and thus, broaden the bandwidths. However, a drawback of this technique is the increase of the back lobe radiation which causes the antenna gain reduction. This can be considered as a trade off for this technique.

In this section, the ground plane of the antenna is loaded with slots to make it H-shaped. The antenna impedance bandwidth is recorded and reported. Furthermore, an H-shaped ground plane will be applied to the H-shaped patch in order to enhance its bandwidth. In the last part of this section, a Koch Island slotted ground plane is implemented with an attempt of increasing the bandwidth of one circularly polarized modified Koch Island microstrip antenna of section 3.2.

The study starts with a square patch antenna which has dimensions of 55mm by 55mm, dielectric constant ε_r= 1 as air is used, the distance between the patch and its ground is 2mm. The ground plane is chosen at sizes of 90mm by 90mm in these simulations. The patch and ground plane were made out of copper. The patch was excited by a 50Ω coaxial probe feed at a location 9mm from the center of the patch.

4.2.1 H-shaped Ground Plane for Broadband Operation

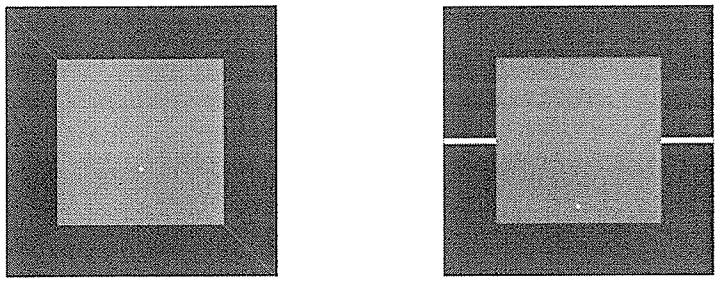

a) b)

Fig. 4.11: Microstrip antennas with patch sizes of 55mm by 55mm; ground plane of 90mm by 90mm; and substrate permittivity of 1: a) A regular square patch antenna; and b) A square patch antenna with H-shaped ground plane with slot sizes of 25mm by 2mm

At the beginning of this section, a study on resonant frequency, impedance bandwidth, and radiation patterns of a square patch and a square patch with H-shaped ground plane is performed in order to understand the effects of an H-shaped ground plane on the square patch antenna. The same square patch antenna as above is used to perform the first set of simulations. Then two slots of size 25mm by 2 mm are embedded to the ground plane in form an H-shaped ground. As studied in [31], the longer slots will cause some reduction in the resonant frequency. However, the slots can be made much longer in this case due to the location of the feed. The feed location moves further to the edge of the patch as the slots are extending. For the slot length of 25mm, the feed location is at 22mm from the center of the patch. This means, the feed location is less sensitive for the H-shaped ground plane microstrip patch antenna. Therefore, it will be a good application

for reducing the sensitivity of feed location in miniature antenna. Fig. 4.11 shows the geometries of a square patch antenna and a square patch antenna with an H-shaped ground plane.

The return losses of the two antennas in Fig. 4.11 are presented in Fig. 4.12. The resonant frequency of the regular square patch antenna is 2.526GHz and its impedance bandwidth is about 2%. After applying the two slots to the ground plane, the resonant frequency of the H-shaped ground plane antenna is shifted to 2.45GHz, which is not very far from the resonant frequency of the regular square patch antenna. However, the impedance bandwidth of the H-shaped ground antenna, which is 9%, is much broader than the original square patch antenna.

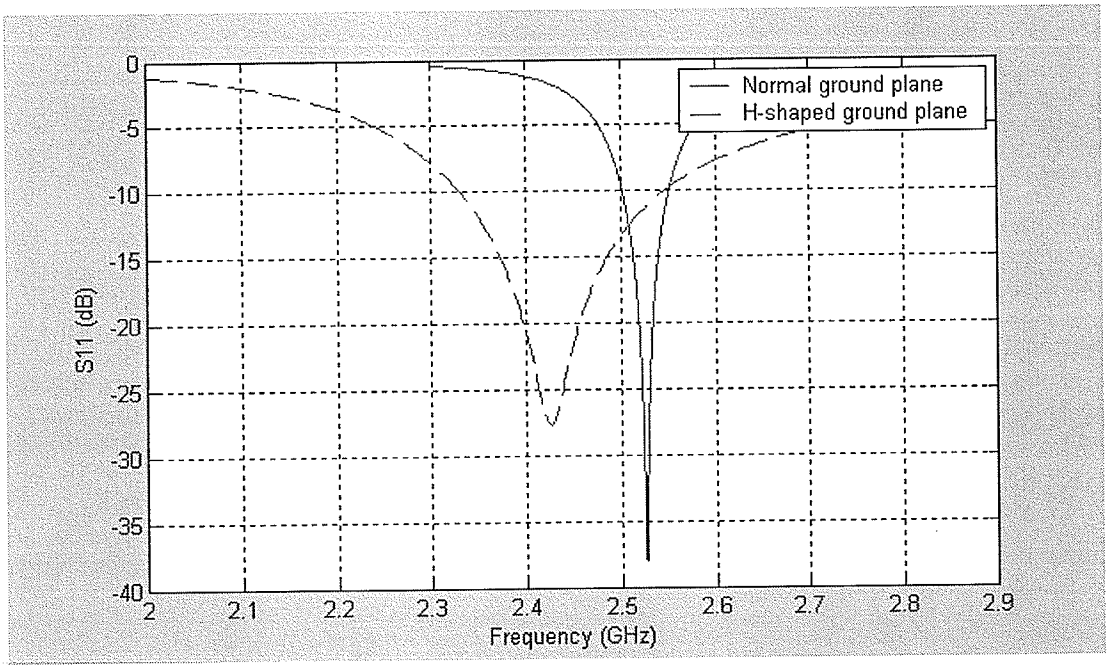

Fig. 4.12: Return losses of regular square patch and H-shaped ground plane antennas shown in Fig. 4.11

As stated earlier, ground plane slot loading of a microstrip antenna will reduce the front-to-back radiation ratio. Therefore, the directivity of the antenna will be also reduced. Fig. 4.13 presents the radiation patterns of the two antennas in Fig. 4.11. The plots show the accepted gains of the two antennas, which can be considered as co-polarizations. One can see that the back lobe of the H-shaped ground plane patch antenna is much higher than the back lobe of the original square patch antenna (2.65dB in compare to -8.07dB). As a result, the directivity of the H-shaped ground plane antenna drops to 6.07dB in comparison to 9.06dB of the original square microstrip patch antenna. Both of these antennas give relatively broad 3dB beamwidth of about 80 degrees. Because the H-shaped ground plane patch antenna has symmetrical geometrically, the cross-polarization is very low (below -25dB) so that it does not affect the radiation of the patch. The summary of the two above antennas' parameters are given in Table 4.1

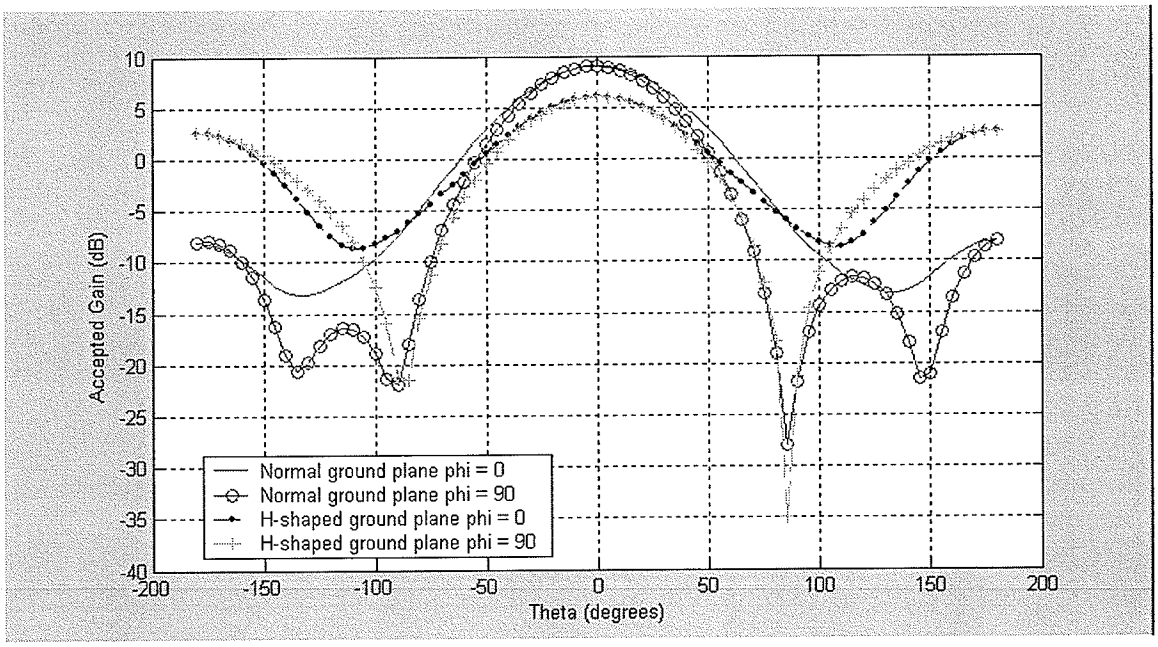

Fig. 4.13: Radiation pattern of original square patch and H-shaped ground plane patch antennas in Fig. 4.11

Table 4.1: Resonant frequency (f_{res}), minimum reflection coefficient (S_{11min}), -10dB impedance bandwidth (BW), 3dB axial ratio bandwidth (ARBW), and back-lobe level of the two antennas in Fig. 4.11

	Regular square patch	H-shaped ground patch
f_{res} (GHz)	2.526	2.45
S_{11} (dB)	-37.7	-27.8
Impedance BW (%)	2	9
Directivity (dB)	9.06	6.07
Back-lobe level (dB)	-8.07	2.65

From the above study on the H-shaped ground plane antennas, one can see that the H-shaped ground plane will result in a broader impedance bandwidth for microstrip patch antennas but with a reduction in the gain. Therefore, the H-shaped ground plane can be implemented in the miniaturized microstrip antennas in order to overcome their limitation of very narrow impedance bandwidth. However, this technique can only be used in certain applications which do not require high gain.

In order to study the effects of an H-shaped ground plane on miniature microstrip antennas, the H-shaped ground plane will be applied to the regular H-shaped patch antenna. Comparisons in the resonant frequency, impedance bandwidth, radiation patterns of regular square patch, regular H-shaped patch and H-shaped patch with H-shaped ground plane are performed. All three antennas in Fig. 4.14 have the same

properties as the square patch antenna at the beginning of this section. The H-shaped patch in Fig. 4.14(b) has slot dimensions of 20mm by 2mm. The antenna in Fig. 4.14(c) has the same H-shaped patch dimension as the antenna in Fig. 4.14b, but two slots of 35mm by 2mm were embedded in the ground plane. The feed location for the regular H-shaped patch antenna is at 2.7mm from the center of the patch, and the feed point for the H-shaped patch with the H-shaped ground is 10mm from patch-center. The H-shaped ground plane has overcome the sensitivity of the feed location in miniaturized H-shaped patch antennas. The return losses of the three antennas are shown in Fig. 4.15. The resonant frequency has shifted from 2.526GHz for the square patch to 1.755GHz for the H-shaped patch. The resonant frequency of the H-shaped patch with H-shaped ground plane is reduced further to 1.735GHz. The impedance bandwidth of the H-shaped patch antenna has been reduced to 0.34% from 2% for the original square patch antenna. However, when the H-shaped ground plane was implemented to the H-shaped patch, the impedance bandwidth of the antenna has increased dramatically to 3.5% (10 times that of H-shaped patch). Once again, the radiation pattern of the H-shaped patch antenna will be affected by the slots in the ground plane. The same effect of directivity reduction for the H-shaped patch with H-shaped ground occurred due to the increase of the back-lobe radiation. The directivity is reduced from 9.06dB, for the regular square patch, to 6.81dB for the H-shaped patch. The back-lobe levels of these two antennas are -8.07dB and -1.16dB, respectively. When the H-shaped ground plane is embedded, the directivity of the antenna decreases further to 4.48dB and its back-lobe level is 1.9dB. Therefore, the trade off of antenna directivity for its miniaturized broadband characteristic has been shown. Table 4.2 will summarize the parameters of all three antennas in Fig. 4.14.

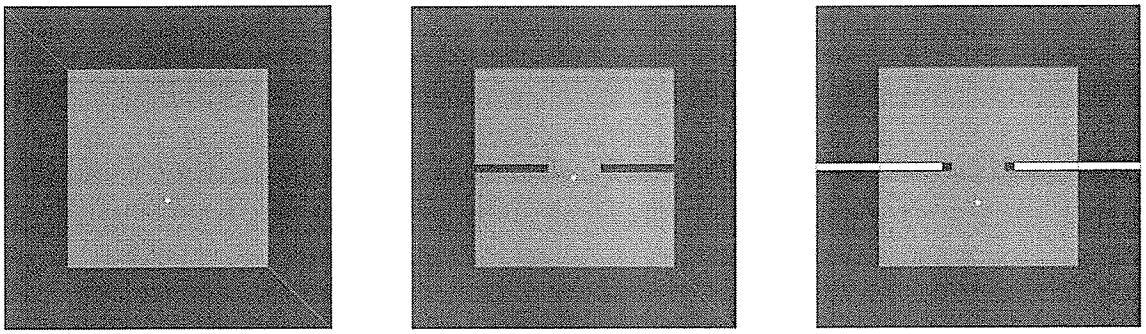

a) b) c)

Fig. 4.14: Microstrip antennas with patch sizes of 55mm by 55mm; ground plane sizes of 90mm by 90mm; and substrate permittivity of 1: a) Regular square patch antenna; b) H-shaped patch antenna with slot sizes of 20mm by 2mm; and c) H-shaped patch antenna (same as patch in (b)) with H-shaped ground plane (ground slot size of 35mm by 2mm)

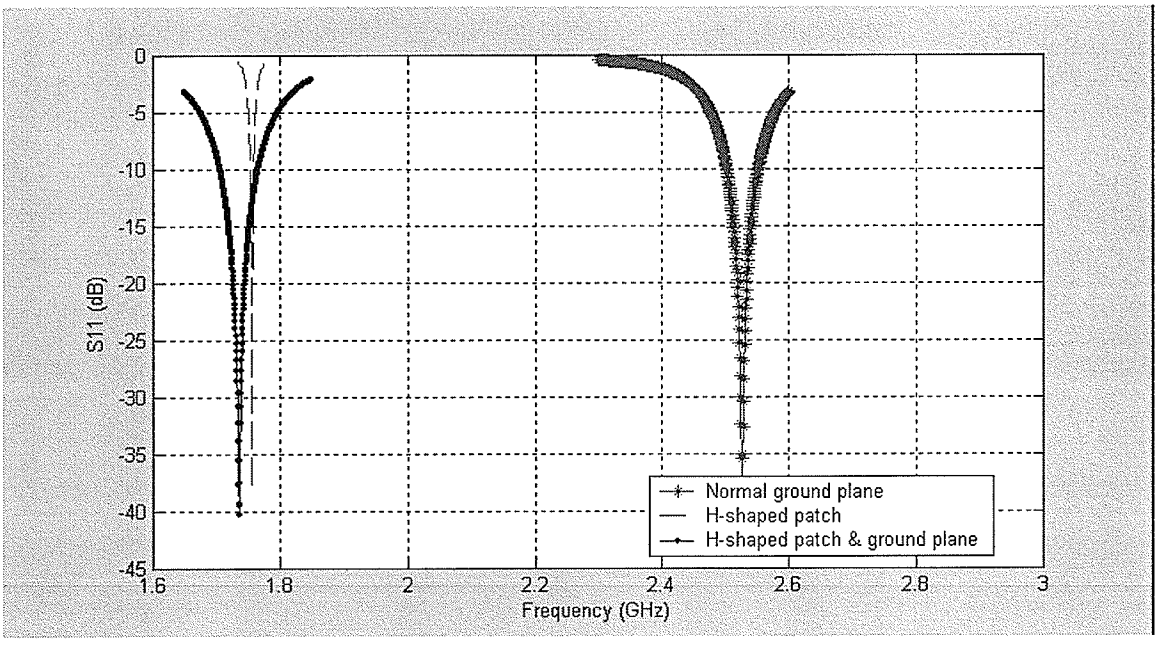

Fig. 4.15: Return losses for antennas in Fig. 4.14

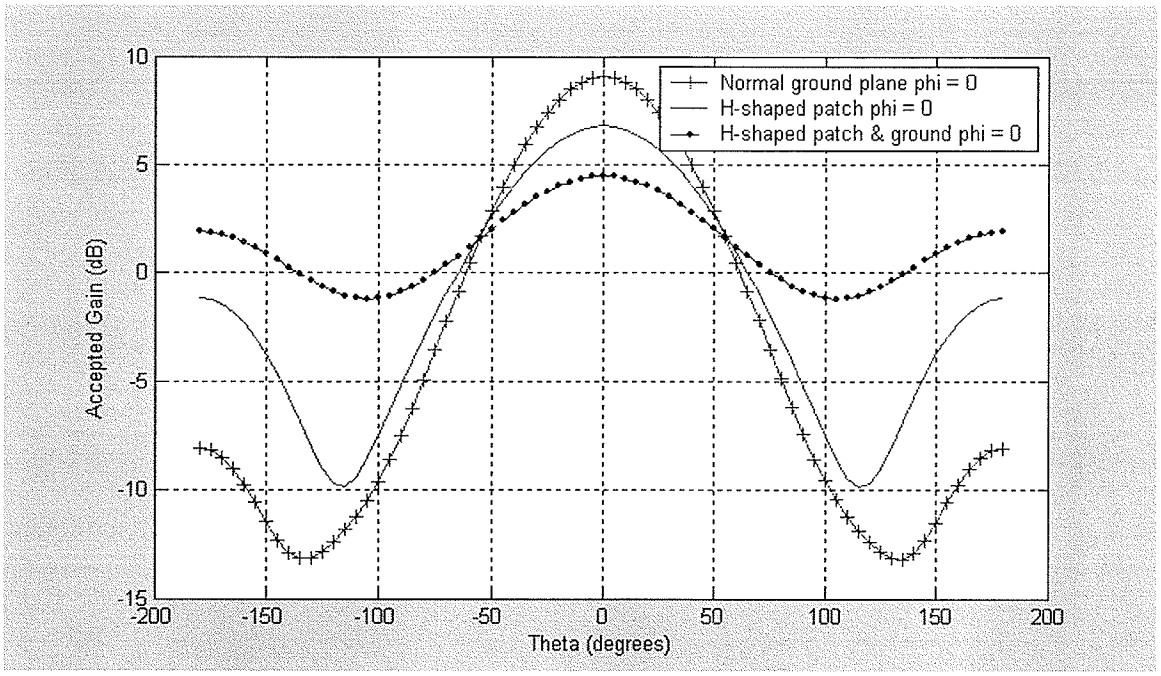

a)

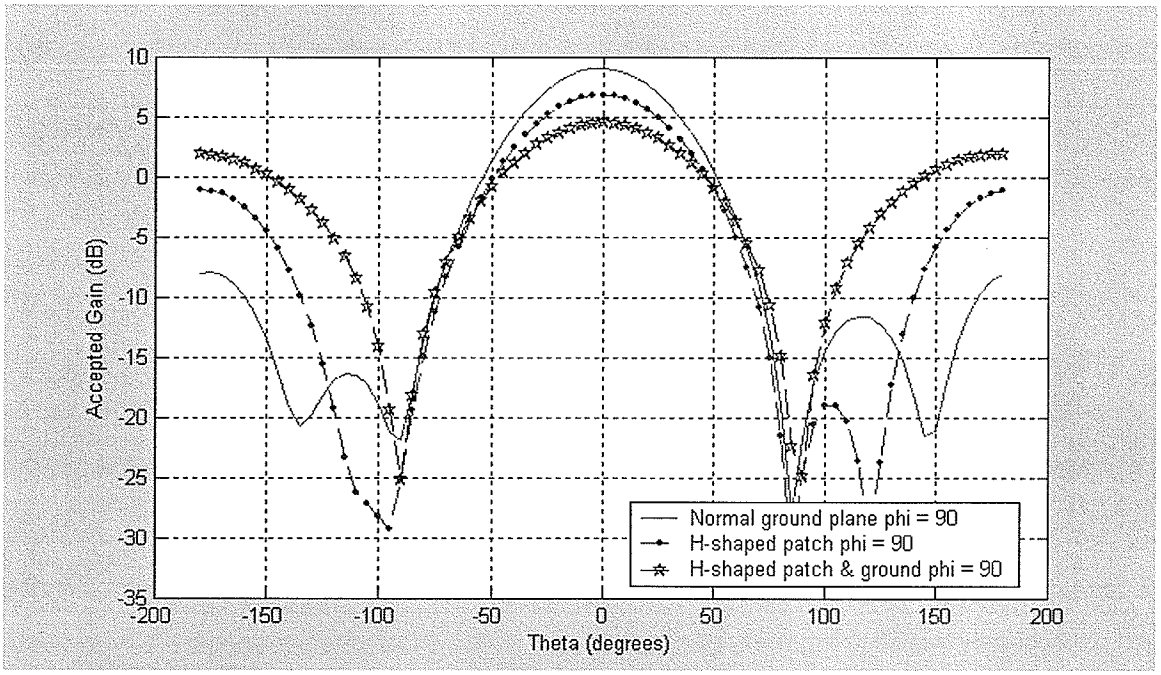

b)

Fig. 4.16: Accepted gain with a) $\phi = 0^o$; and b) $\phi = 90^o$ for the three antennas in Fig. 4.14

Table 4.2: Resonant frequency (f_{res}), minimum reflection coefficient (S_{11min}), -10dB impedance bandwidth (BW), 3dB axial ratio bandwidth (ARBW), and back-lobe level of the three antennas in Fig. 4.14

	Square patch	H-shaped patch	H-shaped patch with H-shaped ground
f_{res} (GHz)	2.526	1.755	1.735
S_{11} (dB)	-37.7	-38.0	-40.3
Impedance BW (%)	2	0.34	3.5
Directivity (dB)	9.06	6.81	4.48
Back-lobe level (dB)	-8.07	-1.16	1.90

4.2.2 Koch Island Ground Plane for Broadband Operation

In the previous section, the slotted ground has shown its effects on the impedance bandwidth of the microstrip antennas. In this section, the slotted ground will be implemented in order to improve the impedance bandwidth and axial ratio bandwidth of the modified Koch Island microstrip antenna in Chapter 3. The modified Koch Island microstrip antenna with $l_x/2$ = 9mm from Chapter 3 is chosen to perform the bandwidth enhancement by slot loading of the ground plane. This microstrip patch has dimensions of 40mm by 40mm and the ground plane dimensions of 80mm by 80mm. The feed location is 3.8mm away from the patch center along the diagonal axis of the patch. The Koch Island ground plane then will be applied to the original modified Koch Island microstrip antenna with four slots of 25mm by 2mm. The feed location is moved away to 6.5mm from the patch center in the effect of Koch Island ground plane. This again will

overcome the limitation of feed location sensitivity in the miniature modified Koch Island patch antenna. These two antennas are shown in Fig. 4.17 below.

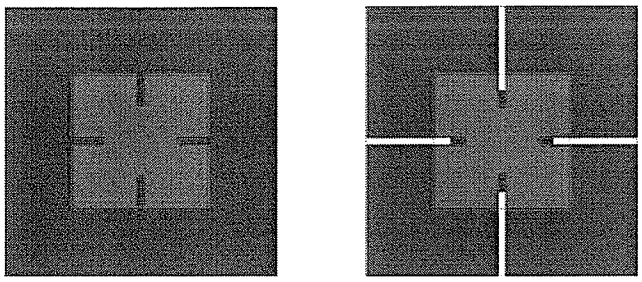

a) b)

Fig. 4.17: Square microstrip antennas with patch sizes of 40mm by 40mm, ground plane sizes of 80mm by 80mm, ε_r= 2.5; a) Modified Koch Island patch antenna for circularly polarized operation with the slot sizes $l_x/2$ = 9mm from Chapter 3; b) Modified Koch Island patch antenna with slotted ground plane for circularly polarized operation with ground slot sizes of 25mm by 2mm

The return losses of the two antennas in Fig. 4.17 are reported in Fig. 4.18. One can see that the impedance bandwidth of the modified Koch Island patch is significantly improved after applying the Koch Island ground plane. The original modified Koch Island patch antenna has the resonant frequency of 1.98GHz and an impedance bandwidth of 1.42%. On the other hand, after Koch Island ground plane has been applied to the antenna, the modified patch antenna has resonant frequency of 1.96GHz, but much larger impedance bandwidth of 4.6%. Moreover, the Koch Island ground plane not only improves the impedance bandwidth of the original antenna, it also increases the 3dB axial ratio bandwidths of the modified Koch Island patch antenna from 0.71% to 2.31% as

shown in Fig. 4.19. The 3dB axial ratio bandwidth of the new slotted ground antenna also lies in its 10dB impedance bandwidth. A summary of the important parameters of Fig. 4.18 and Fig. 4.19 is recorded in Table 4.3.

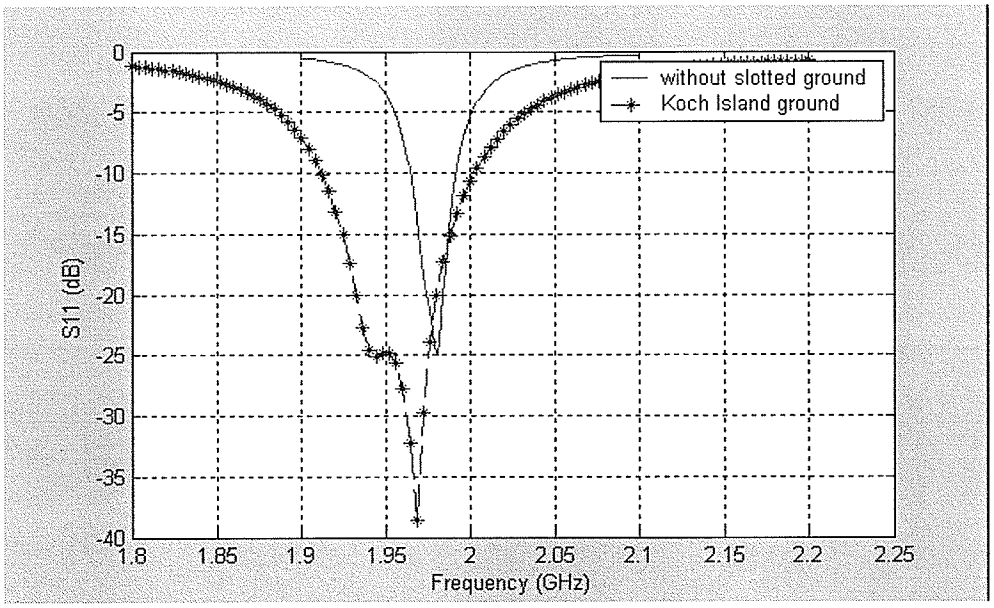

Fig. 4.18: Return losses of the two antennas in Fig. 4.17

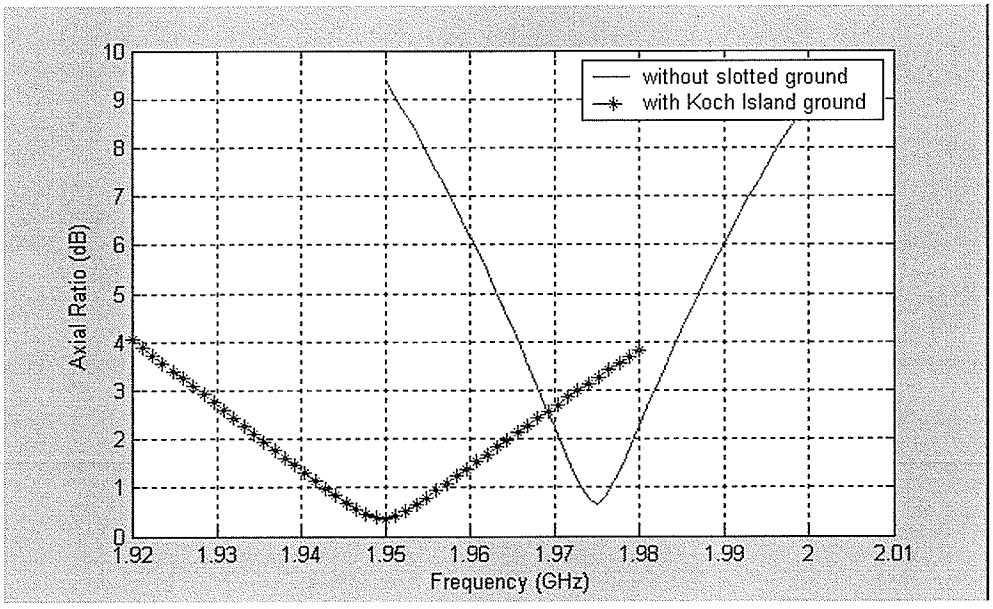

Fig. 4.19: Axial ratios for the two antennas in Fig. 4.17

Table 4.3: Resonant frequency (f_{res}), minimum reflection coefficient (S_{11min}), -10dB impedance bandwidth (BW), and 3dB axial ratio bandwidth (ARBW) of the two antennas in Fig. 4.17

	Modified Koch Island patch without slotted ground	Modified Koch Island patch with slotted ground
f_{res} (GHz)	1.98	1.96
S_{11min} (dB)	-25	-30
BW (%)	1.42	4.6
ARBW (%)	0.71	2.31

4.3 Gain Enhancement by Using Reflector Ground Plane

Due to the effect of back radiation, the gain of the antennas that used slot loaded ground plane had dropped. Therefore, a reflector layer, that is simply a metal layer, is placed directly below the slotted ground plane in an attempt to reduce the back radiation. Fig. 4.20 shows the reflector added modified Koch Island patch antenna. The distance between the reflector and the slotted ground plane is varied to investigate the effect of the reflector on the gain of the antenna. The size of the reflector is chosen equal to the size of the slotted ground plane. The distance between reflector and slotted ground plane is *t*. Table 4.4 gives the resonance frequency (f_{res}), impedance bandwidth (BW), and gain of the reflector backed antennas.

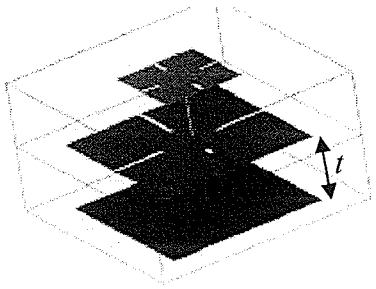

Fig. 4.20: Reflector backed ground for modified Koch Island patch

Table 4.4: Resonance frequency (f_{res}), impedance bandwidth (BW), and gain of the reflector backed antenna in Fig. 4.20 (t is the distance between reflector and slotted ground plane)

	f_{res} (GHz)	BW (%)	Gain (dB)
Without Reflector	1.96	4.6	3.96
t = 1mm	1.97	1.5	5.98
t = 2mm	1.97	1.8	6.45
t = 4mm	1.97	2.2	6.78

4.4 Summary

In this chapter, an overview of bandwidth enhancement in microstrip patch antennas was presented. These techniques included: changing substrate parameters, choosing suitable patch shapes, using aperture coupled feeding, multi-modes operation, impedance matching, resistive loading, and slot loaded ground plane. The slot loaded ground plane technique was implemented by using an H-shaped ground plane for a

regular square patch or H-shaped patch antennas in section 4.2.1. The results showed that after applying the H-shaped ground plane, the impedance bandwidth of the antenna was increased significantly. However, the antenna gain was reduced. Furthermore, the Koch Island ground plane was embedded into the modified Koch Island patch antenna in order to improve both its impedance bandwidth and axial ratio bandwidth in section 4.2.2. In addition, the reflector backed improved the antenna gain, but the impedance bandwidth was reduced.

Chapter 5

Conclusions

5.1 Summary

In this thesis, the results of studies on slot loading of microstrip antennas were presented. At first, the slots were cut on the signal layer of a square microstrip patch antenna, so that the surface currents will meander on a longer path; thus, its resonant frequency will be reduced, which means antenna miniaturization. The Koch Island and H-shaped patch antennas were investigated in order to understand the effects of the slots on the process of miniaturizing microstrip antennas. It has been found that the top and bottom slots of the Koch Island patch antenna do not contribute to the reduction of the resonant frequency of the square patch. For the H-shaped patch antennas, the longer and wider slots will further decrease the patch resonant frequency. The lowest resonant frequency of the H-shaped patch antenna that has been achieved in the designs is 56% f_0, where f_0 is the resonant frequency of the original square patch antenna. In order to further reduce the patch resonant frequency, more slots were added to the H-shaped patch by using fractal geometry. This new type of antenna was called multi-slot (or modified H-shaped) patch antenna, which can resonate at as low as 38% f_0. The limitation of sensitivity on feeding location was overcome by using 100Ω probe feed instead of the conventional 50Ω ones. However, these miniaturized antennas have suffered from gain reductions, due to higher surface current density on the patch, which introduced more ohmic losses. The square patch, H-shaped patch and multi-slot patch antennas were

fabricated and tested in the Antenna Laboratory at The University of Manitoba. The measurement results were in good agreement with the simulated results, which were created from the Ansoft Designer software package. Furthermore, the different patch shapes were placed in Yagi configurations for the purpose of steering the antennas main beam. A 50 degrees tilt angle has been achieved for H-shaped patches Yagi antenna.

It has been realized that if two opposite slots of the Koch Island patch antenna were slightly extended and the feed location was placed on the diagonal axis of the patch, circular polarization can be achieved. The study on the effects of the slot's length and width on resonant frequency, impedance bandwidth, and axial ratio bandwidth of this nearly Koch Island patch antenna was performed. Similarly to the H-shaped patch antenna, with the longer slot lengths, a lower resonant frequency is achieved but with price of narrower impedance bandwidth.

It also has been found that the patch antenna impedance bandwidth can be enhanced by slot loading of its ground plane. An H-shaped ground plane was applied to the ground plane of the above linear polarized antennas in order to improve their narrow bandwidth characteristic. On the other hand, a Koch Island ground plane was used to enhance both impedance and axial ratio bandwidth of the nearly Koch Island microstrip patch antenna. However, this bandwidth enhancement technique has suffered from the increase in antenna's back-lobe radiations.

With all the above characteristics, these miniaturized microstrip patch antennas will be good candidates for certain mobile communication applications, which require small antenna systems.

5.2 Future Works

Even though this thesis carried an extensive parametric study on slot loading of microstrip antennas for miniaturization, there are still needs for the future research. The future research can be suggested as follows:

- Develop mathematical equations to predict the resonant frequency of the H-shaped patch antenna depending on its dimensions.
- Optimize the sizes and positions of the slots, on multi-slot patches in order to achieve minimum resonant frequency and maximum gain.
- Improve gain for all miniaturized antennas.
- Optimized spacing between patches in the Yagi configurations in order to achieve maximum tilt angles.
- Investigate the effects of slot length and width in the Koch Island ground plane.

References:

[1] D. Pozar, "Microstrip Antennas", *Proceeding of the IEEE,* vol. 80, No. 1, January 1992, pp. 79-91.

[2] D. Pozar and D. Schaubert, "*Microstrip Antennas – The Analysis and Design of Microstrip Antennas and Arrays*", IEEE Press, NY, 1995.

[3] L. Shafai, "24.427 Antennas", *Course notes,* The University of Manitoba, Winnipeg, Canada, 2005.

[4] Y. Yoshimura, "A Microstrip Slot Antenna", *IEEE Trans. On Microwave Theory and Techniques*, Vol. 20, No. 11, November 1972, pp. 760 – 762.

[5] G. Kumar, K. P. Ray, "*Broadband Microstrip Antennas*", Artech House, Boston, MA, 2003.

[6] R. Garg, I. J. Bhal, P. Bhatia, P. Ittipibon, "*Microstrip Antenna Design Handbook*", Artech House, Boston, MA, USA, 2001.

[7] A. K. Skivervik, J. F. Zurcher, O. Staub and J. R. Mosig, "PCS Antenna Design: The Challenge of Miniaturization", *IEEE Antennas and Propagations Magazine*, Vol. 43, No. 4, Aug 2001, pp. 12 – 27.

[8] K. Hirasawa and M. Haneishi, "*Analysis, Design and Measurement of Small and Low-Profile Antennas*", Artech House, Boston, MA, USA, 1992.

[9] Y. Hwang, Y. P. Zhang, T. K. C. Lo, K. M. Luk and E. K. N. Yung, "Miniaturization of Planar Antennas with Very High Permittivity Materials", *1997 Asia-Pacific Microwave Conference Proceedings, APMC'97,* Vol. 1, December 1997, pp. 217 – 220.

[10] K. L. Wong, "*Compact and Broadband Microstrip Antennas*", John Wiley and Sons Inc., NY, USA, 2001.

[11] D. Werner and S. Ganguly, "An Overview of Fractal Antenna Engineering Research", *IEEE Antennas and Propagation Magazine*, vol. 45, No. 1, Feb. 2003, pp. 38-57.

[12] I. Kim, J. Yook and H. Park, "Fractal-Shape Small Size Microstrip Patch Antenna", *Microwave and Optical Technology Letter*, vol. 34, No. 1, July 2002, pp. 15-17.

[13] J. Anguera, C. Puente and J. Soler, "Miniature Monopole Antenna Based on the Fractal Hilbert Curve", *IEEE Antennas and Propagation Inter. Symp. Digest*, vol. 4, Texas, 2002, pp. 546-549.

[14] J. P. Gianvittorio and Y. Rahmat-Samii, "Fractal Antennas: A Novel Antenna miniaturization Technique, and Applications", *IEEE Antennas and Propagation Magazine*, vol. 44, Feb. 2002, pp. 20-35.

[15] D. H. Werner, R. L. Haupt, P. L. Werner, "Fractal Antenna Engineering: The Theory and Design of Fractal Antenna Arrays", *IEEE Antennas and Propagation Magazine*, Vol. 41, No. 5, Oct. 1999, pp. 37-59.

[16] D. H. Werner, R. Mittra, "*Frontiers in Electromagnetics*", The IEEE Press, New York 2000.

[17] J. P. Gianvittorio, J. Romeu, S. Blanch, Y. Rahmat-Samii, "Self-Similar Prefractal Frequency Selective Surfaces for Multiband and Dual-Polarized Application", *IEEE Transaction on Antennas and Propagation*, Vol. 51, No. 11, Nov. 2003, pp. 3088 - 3096.

[18] B. B. Mandelbrot, "*The Fractal Geometry of Nature*", San Francisco: W.H. Freeman, 1983.

[19] C. A. Balanis, "*Antenna theory: Analysis and Design*", John Wiley and Sons Inc., NY, USA, 1997.

[20] T. A. Milligan, "*Modern Antenna Design*", John Wiley and Sons Inc., NY, USA, 2005.

[21] B. Y. Toh, R. Cahill, V. F. Fusco, "Understanding and Measuring Circular Polarization", *IEEE Transactions On Education*, Vol. 46, No. 3, Aug. 2003, pp. 313 – 318.

[22] A. C. Ludwig, "The Definition of Cross Polarization", *IEEE Transactions on Antennas and Propagation*, Jan. 1973, pp. 116 – 119.

[23] J. Huang, "A Technique for an Array to Generate Circular Polarization with Linearly Polarized Elements", *IEEE Transactions on Antennas and Propagation*, Vol. 34, No. 9, Sept. 1986, pp. 1113 – 1124.

[24] K. L. Wong and J. Y. Wu, "Single-feed Small Circularly Polarized Square Microstrip Antenna", *Electronics Letters*, Vol. 33, No. 22, Oct. 1997, pp. 1833 – 1834.

[25] T. Huynh and K. F. Lee, "Single-layer Single-patch Wideband Microstrip Antenna", *Electronics Letters*, Vol. 31, No. 16, Aug. 1995, pp. 1310 – 1312.

[26] J. F. Zurcher and F. E. Gardiol, "*Broadband Patch Antennas*", Artech House, Boston, MA, USA, 1995.

[27] R. Bhalla and L. Shafai, "Resonance Behavior of Single U-slot and Double U-slot antenna", *IEEE Antennas and Propagation Inter. Symp. Digest*, Vol. 2, July 2001, pp. 700 – 703.

[28] H. F. Pues and A. R. Van De Capelle, "An Impedance-Matching Technique for Increasing the Bandwidth of Microstrip Antennas", *IEEE Transactions on Antennas and Propagation*, Vol. 37, No. 11, Nov. 1989, pp. 1345 – 1354.

[29] N. Herscovici, "A Wide-Band Single-Layer Patch Antenna", *IEEE Transactions on Antennas and Propagation*, Vol. 46, No. 4, Apr. 1998, pp. 471 – 474.

[30] K. L. Wong and Y. F. Lin, "Microstrip-Line-Fed Compact Microstrip Antenna with Broadband Operation", *IEEE Antennas and Propagation Inter. Symp. Digest*, Vol. 2, June 1998, pp. 1120 – 1123.

[31] T. W. Chiou and K. L. Wong, "Design of Compact Microstrip Antennas with a Slotted Ground Plane", *IEEE Antennas and Propagation Inter. Symp. Digest*, Vol. 2, July 2001, pp. 732 – 735.

[32] H. T. Nguyen, S. Noghanian, L. Shafai, "Miniature Microstrip Patch Antennas by Slots Loading", *IEEE Antennas and Propagation International Symposium,* Washington D.C., USA, July 2005.

[33] H. T. Nguyen, S. Noghanian, L. Shafai, "Feed Location Effects on Miniature Microstrip Patch Antennas Bandwidth", *Symposium on Antenna Technology and Applied Electromagnetics,* Saint- Malo, France, June 2005.